Global paleogeography since the late Paleozoic: integrating geological databases, plate tectonic models and reconstructions of past mantle flow

Wenchao Cao
2019

Submitted in fulfilment of the requirements
for the degree of Doctor of Philosophy

School of Geosciences, Faculty of Science
The University of Sydney, NSW, 2006
Australia

Declaration

I declare that this thesis is less than 80 000 words in length, and that the work contained in this thesis has not been submitted for a higher degree at any other university or institution.

Wenchao Cao
January, 2019

Preface

This thesis consists of three articles, two published in international peer-reviewed journals and one manuscript in revision for an international peer-reviewed journal. All the articles are appropriate to the discipline of geology and geophysics, and are produced during my candidature. This thesis contains an introductory chapter that outlines the background, data and methodology and that provides an overview of the thesis. The significance of this work, broader implications, remaining challenges and future work are discussed in the Discussion chapter. The main findings from this work are summarised in the Conclusion chapter. All the chapters are inter-connected to form a coherent and unified whole.

No animal or ethical approvals were needed during the completion of this study.

Acknowledgements

I thank my supervisor Dietmar Müller for giving me the opportunity to pursue a PhD degree in EarthByte Group at the University of Sydney. Without him, it would be not possible for me to study in this university. Undoubtedly, his guidance, support and encouragement greatly helped me throughout the course of this thesis. His passion for Earth Sciences and enthusiasm for learning new techniques have always inspired me to keep learning and stay being curious. I also thank him for all the support he provided me to attend conferences, workshops and field trips both inland and overseas.

I am very grateful to my co-supervisors Sabin Zahirovic, Nicolas Flament and Simon Williams for their guidance, support and help over the past three and a half years. I feel extremely lucky to have them as my supervisors. Without any of them, this thesis would not be possible. The numberless meetings and discussions with them and the countless hours of help and guidance from them made my project advance smoothly and finally form this thesis. Their hardworking, responsibility and intelligence have always inspired me to work harder and learn faster. In addition, I am indebted to Nicolas Flament for the arrangement for my visiting to the University of Wollongong in my last year of PhD. It was a very pleasant and productive period indeed.

I thank Patrice Rey, Adriana Dutkiewicz, Maria Seton, Clarie Mallard, Tristan Salles, Gilles Brocard, Kara Matthews and Gregory Houseman for their discussions and comments about my studies and presentations. I am thankful to my officemates Rhiannon Garrett, Ömer Bodur, Luke Mondy, Ruken Alac, Sarah McLeod, Andrew Merdith, Qiuge Wang and Xiaozhi Cao. Their company makes my journey easy and very enjoyable. I thank Mandi Thran, Maelis Arnould, Xuesong Ding, Amy l'Anson and all other fellow members of the EarthByte group for their friendship, goodwill and support over the years.

I wish to thank my collaborators Jan Golonka and Christopher Scotese for their constructive discussions and for their highly important contributions to this thesis. I thank Sally Cripps and Rohitash Chandra for their help in the second article of this thesis and for sharing all resources and knowledge about machine learning.

I express my heartfelt thanks to my family. Without their continued support, none of this would be possible. My parents give me unfailing love, support and trust. They have always encouraged me to make decisions by myself and motivated me to pursue my dreams. My old brother has always given me very helpful advice that made me think the bigger picture. His support and positive attitude encouraged me to challenge myself and explore my potential much further.

Abstract

This thesis comprises three studies exploring the connections between Earth's surface paleoenvironments, paleoclimate, eustatic sea-level change and deep mantle processes by integrating geological observations with numerical Earth models over the last ~400 Myr.

I obtained flexible time-dependent global paleogeographic reconstructions since the late Paleozoic by building on a set of published paleogeographic maps, and tested and revised them using paleoenvironmental information indicated by marine fossil collections from the Paleobiology Database. As a result, the consistency ratio between the paleogeography and the paleoenvironments is increased from an average of 75% to nearly full consistency.

I analysed the latitudinal distribution patterns of a global-scale database of lithologic indicators of climate over the last ~400 Myr. The results suggest that the paleolatitudinal distributions of the lithologies have changed through deep time, notably a pronounced pole-ward shift in the distribution of coals in early Permian. The distribution of evaporites indicate a predominantly bimodal pattern, as opposed to previously proposed bimodal or unimodal patterns. The distribution of glacial deposits is consistent with previous interpretations of the main icehouse and greenhouse periods during the last ~400 Myr.

The comparison between flooding of continents, modelled dynamic topography and published eustatic curves in the late Paleozoic indicates that the first-order flooding history of North America correlates with eustasy. South American flooding history during the Carboniferous are at odds with estimates of eustasy and can be explained by dynamic topography. The reference districts used to reconstruct eustatic curves which are most affected by dynamic topography are those in South China and North America. Therefore, the interpretation of stratigraphic data gathered from these regions should be treated with caution when used to estimate global sea level variations.

This thesis is based on the following three articles:

Article 1: Cao, W., Zahirovic, S., Flament, N., Williams, S., Golonka, J., and Müller, R. D., 2017: Improving global paleogeography since the late Paleozoic using paleobiology, *Biogeosciences*, 14, 5425-5439. https://doi.org/10.5194/bg-14-5425-2017.

I designed this study in collaboration with S.Z., N.F., S.W., J.G. and R.D.M. I restored paleogeographic maps to their present-day coordinates and attached them to an alternative reconstruction, and collected and processed paleobiology data sets. I conducted paleobiology tests on paleogeographic maps and modified the paleogeography based on the test results. I analysed and interpreted the results, considering the advice given by all the co-authors. I produced all the figures and tables, wrote the manuscript and revised it based on feedback from co-authors and reviewers. I did the revisions in collaboration with all the co-authors. I handled correspondence at all stages of refereeing, publication and post-publication.

Article 2: Cao, W., Williams, S., Flament, N., Zahirovic, S., Scotese, C., and Müller, R. D., 2018. Paleolatitudinal distribution of lithologic indicators of climate in a paleogeographic framework. *Geological Magazine*, 1-24. doi:10.1017/S0016756818000110.

I designed this study in collaboration with S.W., N.F., S.Z., C.S. and R.D.M. I conducted all data analysis. I analysed and interpreted the results, considering the advice given by all the co-authors. I produced all the figures and tables, wrote the manuscript and revised it based on feedback from co-authors and reviewers. I did the revisions in collaboration with the co-authors. I handled correspondence at all stages of refereeing, publication and post-publication.

Article 3: Cao, W., Flament, N., Zahirovic, S., Williams, S., and Müller, R. D., 2019. The interplay of dynamic topography and eustasy on continental flooding in the late Paleozoic. *Tectonophysics, in revision*.

I designed this study in collaboration with N.F., S.Z., S.W. and R.D.M. I calculated continental flooding ratios using paleogeographic maps, described and analysed the continental flooding results and dynamic topography modelling results. I compared these results with published global sea level curves. I interpreted the results, considering the advice given from all the co-authors. I produced all the figures and tables, wrote the manuscript and revised it based on feedback from co-authors.

Wenchao Cao		28/01/2019
Student name	Signature	Date

As supervisor for the candidature upon which this thesis is based, I can confirm that the statements above are correct.

R. Dietmar Müller		28/01/2019
Supervisor name	Signature	Date

Co-author contribution form

Statement identifying co-author contributions to published works

The University of Sydney policy stated that candidates must provide evidence to identify the sections of work for which the candidate is responsible. The work and interpretations in the following articles are the work of the author except where stated below:

Article 1
Cao, W., Zahirovic, S., Flament, N., Williams, S., Golonka, J., and Müller, R. D., 2017: Improving global paleogeography since the late Paleozoic using paleobiology, *Biogeosciences*, 14, 5425-5439.

Sabin Zahirovic: Initial ideas of methods, discussion and advice on the development of the study; guidance and feedback to develop and write the manuscript

Signature:

Nicolas Flament: Discussion and advice on the development of the study and manuscript; guidance and feedback to develop and write the manuscript

Signature:

Simon Williams: Discussion and advice on the development of the study and manuscript; guidance and feedback to develop and write the manuscript

Signature:

Jan Golonka: Discussion of methodology and results, and advice

Signature:

Dietmar Müller: Discussion and advice on the development of the study and manuscript; guidance and feedback to develop and write the manuscript

Signature:

Article 2:
Cao, W., Williams, S., Flament, N., Zahirovic, S., Scotese, C., and Müller, R. D., 2018. Paleolatitudinal distribution of lithologic indicators of climate in a paleogeographic framework. *Geological Magazine*, 1-24.

Simon Williams: Initial ideas of methods, discussion and advice on the development of the study and manuscript; guidance and feedback to develop and write the manuscript

Signature:

Nicolas Flament: Discussion and advice on the development of the study and manuscript; guidance and feedback to develop and write the manuscript

Signature:

Sabin Zahirovic: Discussion and advice on the development of the study and manuscript; guidance and feedback to develop and write the manuscript

Signature:

Christopher Scotese: Discussion, advice and review of manuscript, and provided lithologic data set

Signature:

Dietmar Müller: Discussion and advice on the development of the study and manuscript; guidance and feedback to develop and write the manuscript

Signature:

Contents

Introduction

1. Background

The dynamics of the Earth system are reflected in surface paleogeographic evolution, flooding of continents, climate change, long-term sea level variations, biological evolution and deep Earth mantle flow. Combining geological observations and virtual Earth models is important to explore the connections between surface and deep Earth processes.

Paleogeography documents the distributions of land and ocean over time and is important for understanding plate tectonic evolution, paleoclimate and ocean circulation, past eustatic and regional sea level change, resource exploration and geodynamics. Several global-scale paleogeographic compilations, estimated from paleoenvironmental and paleo-lithofacies data, have been published (e.g. Blakey, 2008; Golonka et al., 2006; Ronov, et al., 1984, 1989; Scotese, 2001, 2004; Smith et al., 1994). However, they are generally presented as static paleogeographic snapshots with varying map projections and different time intervals represented by the maps, and are tied to different plate motion models. This makes it difficult to convert the maps into a digital form, link them to alternative digital plate tectonic reconstructions and and update them when plate motion models are improved. Building flexible time-dependent global paleogeographic reconstructions is therefore important. Digital paleogeographic reconstructions can also be tested and improved with incorporation of new data (Wright et al., 2013).

The paleolatitudinal distribution of climate-sensitive lithologic deposits is important for reconstructing paleogeographies (Ronov et al., 1984, 1989; Scotese 2001, 2004; Golonka et al., 2006; Blakey, 2008), understanding past climate (Gordon, 1975; Evans, 2006; Boucot et al., 2013) and providing constraints for climate modelling (Boucot and Gray, 2001; Craggs et al., 2011) and plate motion histories (Scotese and Barrett, 1990; Witzke, 1990). However, whether the latitudinal distribution of climate-sensitive lithologies is stable through greenhouse and icehouse regimes remains unclear. Previous studies suggest that the paleolatitudinal distribution of palaeoclimate indicators, including coals, evaporites, reefs and carbonates, has remained broadly similar since the Permian period, leading to the conclusion that atmospheric and oceanic circulation control their distribution rather than the latitudinal temperature gradient (Ziegler et al., 2003). However, a global paleomagnetic compilation of Earth's basin-scale evaporite records suggests that evaporite paleolatitudes have varied to some degree over the past 2 billion years (Evans, 2006). In addition, previous studies have rarely considered the effect of the uneven distribution of continental areas through time (Vilhena and Smith, 2013) and the implications of applying different global tectonic reconstruction models (Scotese and Barrett, 1990; Ziegler et al. 2003) on latitudinal distribution of climate indicators. Advances in global plate motion models (e.g. Matthews et al., 2016), modern data analysis approaches (e.g., Chaudhuri and Marron, 1999; Hyndman, 1996) and paleoclimate studies (e.g. Hay, 2016; Foster et al., 2017) made it possible to re-evaluate the latitudinal distribution patterns of climate-sensitive lithologies in deeper geological time and re-investigate how they respond to changes in plate motion, orogenesis, biological evolution and greenhouse/icehouse conditions over the last ~400 Myr.

The mechanisms driving late Paleozoic continental flooding are not fully understood. Tectonics, eustasy and/or dynamic topography are thought to drive the marine inundation of continents. Eustatic sea level changes during the Paleozoic have been reconstructed by interpreting sequence stratigraphy (e.g. Vail et a., 1977; Hallam,

1992; Haq and Schutter, 2008; Snedden and Liu, 2010). Sequence stratigraphy is a semi-quantitative method that makes it possible to reconstruct relative variations in sea level from stratigraphic sections in pericratonic and cratonic basins. Correlations between sea level events recorded in sedimentary strata across several basins are used to build short-term eustatic sea level curves (Haq et al., 1987; Haq and Schutter, 2008). A key assumption in the sequence stratigraphic approach to reconstruct past sea levels is that these chosen regions used as reference districts to establish the chronology of Paleozoic sea level changes are assumed to be tectonically stable. However, it has long been known that long-wavelength vertical deflections of the solid Earth's surface as a result of mantle flow, called dynamic topography, may occur without any crustal thickening or thinning (Gurnis et al., 1990; Gurnis, 1993; Liu et al., 2008; Moucha et al., 2008; Spasojević et al., 2012; Flament et al., 2013). This issue has been recognised by stratigraphers who are aware of the effect of dynamic topography on long-term sea level change (Haq, 2014; Kominz et al., 2008). Recent developments in global tectonic reconstructions of the late Paleozoic (Matthews et al., 2016 ; Young et al., 2018) indicate that some of the regions (e.g. the Yangtze platform of South China during the Permian) used to reconstructed global sea level change could be affected by tectonic activity and mantle flow. Therefore, whether the estimated sea level change using this method can truly represent global sea level change is debated (Hallam et al., 1992; Cloetingh and Haq, 2015).

2. Data and Methodology

In this thesis, I used a set of published global paleogeographic maps for times since the late Paleozoic (Golonka et al., 2006), two geological data sets: paleoenvironmental data set indicated by the marine fossil collections from the Paleobiology Database (PBDB, paleobiodb.org) and a global data set of lithologic indicators of climate (Boucot et al., 2013) for the last ~400 million years (Myr), four global plate tectonic reconstructions (Golonka, 2007; Scotese, 2008; Matthews et al., 2016; Young et al., 2018) and two sets of time-dependent mantle flow models based on two tectonic reconstructions (Matthews et al., 2016; Young et al., 2018) as time-dependent boundary conditions.

I presented a workflow to obtain flexible global paleogeographic reconstructions since the late Paleozoic by building on a set of published static global paleogeographic maps (Golonka et al., 2006). I developed an approach to test and improve the maximum inundation paleo-coastline locations and paleogeographic geometries using paleo-environmental data indicated by the marine fossil collections from the PBDB. This workflow and approach can be applied to any other global paleogeographic maps. The details are described in the Methods section of Article 1.

I revisited a global-scale comprehensive database of lithologic indicators of climate, including coals, evaporites and glacial deposits, back to the Devonian (Boucot et al., 2013). I quantified the paleolatitudinal distributions of these lithologies with corrections for sampling- and area-biases, and used statistical methods to fit these distributions with probability density functions (Chaudhuri and Marron, 1999) and estimate high-probability latitudinal belts (Hyndman, 1996). I also tested the sensitivity of their latitudinal distributions to the uneven distribution of continental areas through time and to three distinct global tectonic models (Golonka, 2007; Scotese, 2008; Matthews et al., 2016). The details are described in the Methods section of Article 2.

I estimated the inundation history of the North and South American continents individually, and of all continents combined, from my digital time-dependent paleogeographic reconstructions for the late Paleozoic. I analysed the dynamic topography for the continents predicted by

two forward mantle flow models based on time-dependent boundary conditions from two distinct tectonic reconstructions by Matthews et al. (2016) and Young et al. (2018). I then compared the resulting continental flooding ratios with trends in modelled dynamic topography and published global long-term sea level curves (Algeo and Seslavinsky, 1995; Hallam, 1992; Haq and Schutter, 2008). I mapped the temporal evolution of mantle temperature along cross sections to identify the origin of changes in dynamic topography. I predicted the evolution of dynamic topography at the reference districts used to reconstruct the late Paleozoic eustatic curves to examine whether these reference districts were affected by dynamic topography. The details are described in the Methods section of Article 3.

3. Thesis Overview

This thesis comprises three interconnected studies. The digital time-varying paleogeographic reconstructions with modifications by paleoenvironmental data from the PBDB since the Early Devonian in the first study (Article 1) formed the fundamental data set for discussing how paleolatitudinal distributions of shallow marine basins, mountains and ice sheets contribute to the paleolatitudinal distributions of climate-sensitive lithologies in the second study (Article 2) and for quantifying continental flooding history in the third study (Article 3).

The first study presents a workflow that I applied to transfer paleogeographic geometries from one plate motion model to another and then using paleoenvironmental information indicated by marine fossil collections from the PBDB to improve the paleo-coastline locations and paleogeographic geometries. The second study highlights that combining tectonic reconstructions with a comprehensive lithologic database and modern data analysis approaches provides insights into the nature and causes of shifting climatic zones through deep time. The third study highlights that combining digital paleogeographic reconstructions, geological observations, plate reconstruction models and models of past mantle flow provides insights into understanding mechanisms of continental inundation and distinguish global or regional sea level change over deep time.

Plate tectonic reconstruction models were used throughout all these three studies. They provided basic plate kinematic framework for reconstructing paleogeography and lithologic indicators of climate back in time, and for mantle flow models as time-dependent boundary constraints. This thesis explored the connections between Earth's surface paleogeography, paleoclimate, long-term sea level variations and mantle flow processes for the last ~400 Myr by integrating geological observations with numerical Earth models.

Article 1

Improving global paleogeography since the late Paleozoic using paleobiology

Biogeosciences, 14, 5425–5439, 2017
https://doi.org/10.5194/bg-14-5425-2017

Biogeosciences Open Access EGU

Improving global paleogeography since the late Paleozoic using paleobiology

Wenchao Cao[1], Sabin Zahirovic[1], Nicolas Flament[1,a], Simon Williams[1], Jan Golonka[2], and R. Dietmar Müller[1,3]

[1]EarthByte Group and Basin GENESIS Hub, School of Geosciences, The University of Sydney, Sydney, NSW 2006, Australia
[2]Faculty of Geology, Geophysics and Environmental Protection, AGH University of Science and Technology, Mickiewicza 30, 30-059 Kraków, Poland
[3]Sydney Informatics Hub, The University of Sydney, Sydney, NSW 2006, Australia
[a]current address: School of Earth and Environmental Sciences, University of Wollongong, Northfields Avenue, Wollongong, NSW 2522, Australia

Correspondence to: Wenchao Cao (wenchao.cao@sydney.edu.au)

Received: 16 March 2017 – Discussion started: 18 April 2017
Revised: 10 October 2017 – Accepted: 21 October 2017 – Published: 4 December 2017

Abstract. Paleogeographic reconstructions are important to understand Earth's tectonic evolution, past eustatic and regional sea level change, paleoclimate and ocean circulation, deep Earth resources and to constrain and interpret the dynamic topography predicted by mantle convection models. Global paleogeographic maps have been compiled and published, but they are generally presented as static maps with varying map projections, different time intervals represented by the maps and different plate motion models that underlie the paleogeographic reconstructions. This makes it difficult to convert the maps into a digital form and link them to alternative digital plate tectonic reconstructions. To address this limitation, we develop a workflow to restore global paleogeographic maps to their present-day coordinates and enable them to be linked to a different tectonic reconstruction. We use marine fossil collections from the Paleobiology Database to identify inconsistencies between their indicative paleoenvironments and published paleogeographic maps, and revise the locations of inferred paleo-coastlines that represent the estimated maximum transgression surfaces by resolving these inconsistencies. As a result, the consistency ratio between the paleogeography and the paleoenvironments indicated by the marine fossil collections is increased from an average of 75 % to nearly full consistency (100 %). The paleogeography in the main regions of North America, South America, Europe and Africa is significantly revised, especially in the Late Carboniferous, Middle Permian, Triassic, Jurassic, Late Cretaceous and most of the Cenozoic. The global flooded continental areas since the Early Devonian calculated from the revised paleogeography in this study are generally consistent with results derived from other paleoenvironment and paleo-lithofacies data and with the strontium isotope record in marine carbonates. We also estimate the terrestrial areal change over time associated with transferring reconstruction, filling gaps and modifying the paleogeographic geometries based on the paleobiology test. This indicates that the variation of the underlying plate reconstruction is the main factor that contributes to the terrestrial areal change, and the effect of revising paleogeographic geometries based on paleobiology is secondary.

1 Introduction

Paleogeography, describing the ancient distribution of highlands, lowlands, shallow seas and deep ocean basins, is widely used in a range of fields including paleoclimatology, plate tectonic reconstructions, paleobiogeography, resource exploration and geodynamics. Global deep-time paleogeographic compilations have been published (e.g., Blakey, 2008; Golonka et al., 2006; Ronov, et al., 1984, 1989; Scotese, 2001, 2004; Smith et al., 1994). However, they are generally presented as static paleogeographic snapshots with varying map projections and different time intervals represented by the maps, and are tied to different plate motion

models. This makes it difficult to convert the maps into a digital format, link them to alternative digital plate tectonic reconstructions and update them when plate motion models are improved. It is therefore challenging to use paleogeographic maps to help constrain or interpret numerical models of mantle convection that predict long-wavelength topography (Gurnis et al., 1998; Spasojevic and Gurnis, 2012) based on different tectonic reconstructions, or as an input to models of past ocean and atmosphere circulation/climate (Goddéris et al., 2014; Golonka et al., 1994) and models of past erosion/sedimentation (Salles et al., 2017).

In order to address these issues, we develop a workflow to restore the ancient paleogeographic geometries back to their modern coordinates so that the geometries can be attached to a different plate motion model. This is the first step towards the construction of paleogeographic maps with flexible spatial and temporal resolutions that are more easily testable and expandable with the incorporation of new paleoenvironmental data sets (e.g., Wright et al., 2013). In this study, we use a set of global paleogeographic maps (Golonka et al., 2006) covering the entire Phanerozoic time period as the base paleogeographic model. Coastlines on these paleogeographic maps represent estimated maximum marine transgression surfaces (Kiessling et al., 2003). We first restore the global paleogeographic geometries of Golonka et al. (2006) to their present-day coordinates by reversing the sign of the rotation angle, and then reconstruct them to geological times using a different plate motion model of Matthews et al. (2016). We then use paleoenvironmental information from marine fossil collections from the Paleobiology Database to modify the inferred paleo-coastline locations and paleogeographic geometries. Next, we use the revised paleogeography to estimate the surface areas of global paleogeographic features including deep oceans, shallow marine environments, landmasses, mountains and ice sheets. In addition, we compare the global flooded continental areas since the Devonian calculated from the revised paleogeography with other results derived from other paleoenvironment and paleo-lithofacies maps (Ronov, 1994; Smith et al., 1994; Walker et al., 2002; Blakey, 2003, 2008; Golonka, 2007b, 2009, 2012) or from the strontium isotope record (van der Meer et al., 2017). We estimate the terrestrial areal change over time associated with transferring reconstruction, filling gaps and modifying the paleogeographic geometries based on consistency test. Finally, we test the marine fossil collection data set used in this study for fossil abundances over time using different timescales of the International Commission on Stratigraphy (ICS2016; Cohen et al., 2013, updated) and of Golonka (2000) and discuss the limitations of the workflow we develop in this study.

2 Data and paleogeographic model

The data used in this study are global paleogeographic maps and paleoenvironmental data for the last 402 million years (Myr), which originate from the set of paleogeographic maps produced by Golonka et al. (2006) and the Paleobiology Database (PBDB, https://paleobiodb.org), respectively. The global paleogeographic compilation extending back to the Early Devonian of Golonka et al. (2006) is divided into 24 time-interval maps using the timescale of Golonka (2000) which is based on the original timescale of Sloss (1988; Table 1). Each map is a compilation of paleo-lithofacies and paleoenvironments for each geological time interval. These paleogeographic reconstructions illustrate the changing configuration of ice sheets, mountains, landmasses, shallow marine environments (inclusive of shallow seas and continental slopes) and deep oceans over the last $\sim$400 Myr.

The paleogeographic maps of Golonka et al. (2006) are constructed using a plate tectonic model available in the supplement of Golonka (2007a), where relative plate motions are described. In this rotation model, paleomagnetic data are used to constrain the paleolatitudinal positions of continents and rotation of plates, and hotspots, where applicable, are used as reference points to calculate paleolongtitudes (Golonka, 2007a). This rotation model is necessary to restore these paleogeographic geometries (Golonka et al., 2006) to their present-day coordinates so that they can be attached to a different plate motion model. The relative plate motions of Golonka (2006, 2007a) are based on the reconstruction of Scotese (1997, 2004).

Here, we use a global plate kinematic model to reconstruct paleogeographies back in time from present-day locations. The global tectonic reconstruction of Matthews et al. (2016), with continuously closing plate boundaries from 410–0 Ma, is primarily constructed from a Mesozoic and Cenozoic plate model (230–0 Ma; Müller et al., 2016) and a Paleozoic model (410–250 Ma; Domeier and Torsvik, 2014). This model is a relative plate motion model that is ultimately tied to Earth's spin axis through a paleomagnetic reference frame for times before 70 Ma, and a moving hotspot reference frame for younger times (Matthews et al., 2016).

The PBDB is a compilation of global fossil data covering deep geological time. All fossil collections in the database contain detailed metadata, including on the time range (typically biostratigraphic age), present-day geographic coordinates, host lithology and paleoenvironment. Figure 1 represents distributions of the global fossil collections at present-day coordinates and shows their numbers since the Devonian. The recorded fossil collections are unevenly distributed both spatially and temporally, largely due to the differences in fossil preservation, the spatial sampling biases of fossil localities and the uneven entry of fossil data to the PBDB (Alroy, 2010). For this study, a total of 57 854 fossil collections with temporal and paleoenvironmental assignments from 402 to 2 Ma were downloaded from the database on 7 September 2016.

Table 1. Timescale since the Early Devonian (Golonka, 2000) used in the paleogeographic maps of Golonka et al. (2006), the original timescale of Sloss (1988) and of the International Commission on Stratigraphy (ICS2016). Ages in italics are obtained by linear interpolation between subdivisions.

	Sloss (1988)			Golonka (2000)					ICS2016	
Era	Subsequence	Start (Ma)	End (Ma)	Time slice	Epoch/age	Start (Ma)	End (Ma)	Reconstruction time (Ma)	Start (Ma)	End (Ma)
Cenozoic	Tejas III	29	0	late Tejas III	Tortonian–Gelasian	11	2	6	11.63	1.80
				late Tejas II	Burdigalian–Serravallian	20	11	14	20.44	11.63
				late Tejas I	Chattian–Aquitanian	29	20	22	28.1	20.44
	Tejas II	39	29	early Tejas III	Priabonian–Rupelian	37	29	33	37.8	28.1
	Tejas I	60	39	early Tejas II	Lutetian–Bartonian	49	37	45	47.8	37.8
				early Tejas I	Thanetian–Ypresian	58	49	53	59.2	47.8
Mesozoic	Zuni III	96	60	late Zuni IV	middle Campanian–Selandian (Late Cretaceous–earliest Paleogene)	81	58	76	*79.8*	59.2
				late Zuni III	late Cenomanian–early Campanian (Late Cretaceous)	94	81	90	*96.1*	*79.8*
	Zuni II	134	96	late Zuni II	late Aptian–middle Cenomanian (Early Cretaceous–earliest Late Cretaceous)	117	94	105	*119.0*	*96.1*
				late Zuni I	late Valanginian–early Aptian (Early Cretaceous)	135	117	126	*136.4*	*119.0*
	Zuni I	186	134	early Zuni III	late Tithonian–early Valanginian (latest Late Jurassic–earliest Early Cretaceous)	146	135	140	*147.4*	*136.4*
				early Zuni II	late Bathonian–middle Tithonian (earliest Middle Jurassic–Late Jurassic)	166	146	152	*166.8*	*147.4*
				early Zuni I	middle Aalenian–middle Bathonian (Middle Jurassic)	179	166	169	*172.8*	*166.8*
	Absaroka III	245	186	late Absaroka III	late Hettangian–early Aalenian (Early Jurassic–earliest Middle Jurassic)	203	179	195	*200.0*	*172.8*
				late Absaroka II	late Carnian–middle Hettangian (Late Triassic–earliest Jurassic)	224	203	218	*232*	*200.0*
				late Absaroka I	Induan–early Carnian (Early–earliest Late Triassic)	248	224	232	252.17	*232*
Paleozoic	Absaroka II	268	245	early Absaroka IV	Roadian–Changhsingian (Late Permian)	269	248	255	272.3	252.17
				early Absaroka III	Sakmarian–Kungurian (Early Permian)	285	269	277	295.0	272.3
	Absaroka I	330	268	early Absaroka II	Gzhelian–Asselian (latest Carboniferous–earliest Permian)	296	285	287	303.7	295.0
				early Absaroka I	Bashkirian–Kasimovian (Late Carboniferous)	323	296	302	323.2	303.7
	Kaskaskia II	362	330	Kaskaskia IV	middle Visean–Serpukhovian (Lower Carboniferous)	338	323	328	*341.4*	323.2
				Kaskaskia III	late Famennian–early Visean (latest Devonian–Early Carboniferous)	359	338	348	*365.6*	*341.4*
	Kaskaskia I	401	362	Kaskaskia II	Givetian–early Famennian (Middle–Late Devonian)	380	359	368	387.7	*365.6*
				Kaskaskia I	late Pragian–Eifelian (Early–Middle Devonian)	402	380	396	*408.7*	387.7

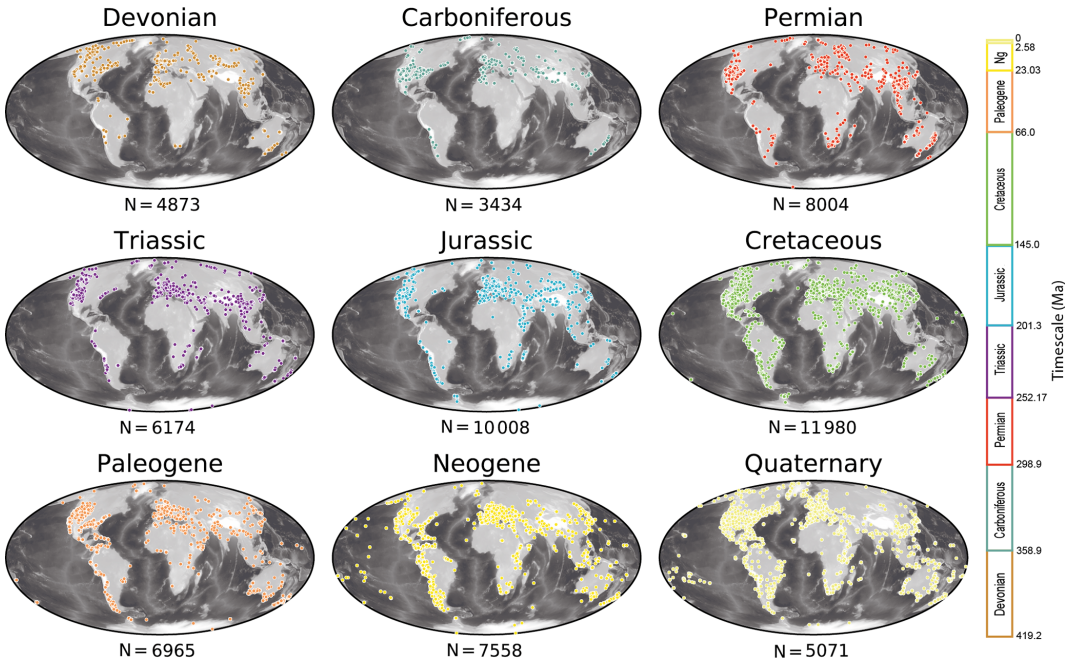

Figure 1. Global distributions and number of fossil collections since the Devonian. The greyscale background shows global present-day topography ETOPO1 (Amante and Eakins, 2009) with lighter shades corresponding to increasing elevation. Fossil collections from the PBDB are colored following the standard used by the International Commission on Stratigraphy.

3 Methods

The methodology can be divided into three main steps: (1) the original paleogeographic geometries are restored to present-day coordinates by applying the inverse of the rotations used to make the reconstruction, (2) these restored geometries are then rotated to new locations using the plate tectonic model of Matthews et al. (2016) and (3) the paleocoastline locations and paleogeographic geometries are adjusted using paleoenvironmental data from the PBDB. Figure 2 illustrates the generalized workflow that can be applied to a different paleogeography model. In order to represent the paleogeographic maps as digital geographic geometries, they are first georeferenced using the original projection and coordinate system (global Mollweide in Golonka et al., 2006), and then re-projected into the WGS84 geographic coordinate system. The resulting maps are then attached to the original rotation model using the open-source and cross-platform plate reconstruction software *GPlates* (http://gplates.org). Every plate is then assigned a unique plate ID that defines the rotation of the tectonic elements so that the paleogeographic geometries can be rotated back to their present-day coordinates (see example in Fig. 3a, b). We use present-day coastlines and terrane boundaries with the plate IDs of Golonka (2007a) as a reference to refine the rotations and ensure that the paleogeographic geometries are restored accurately to their present-day locations.

When the paleogeographic geometries in present-day coordinates are attached to a new reconstruction model, as

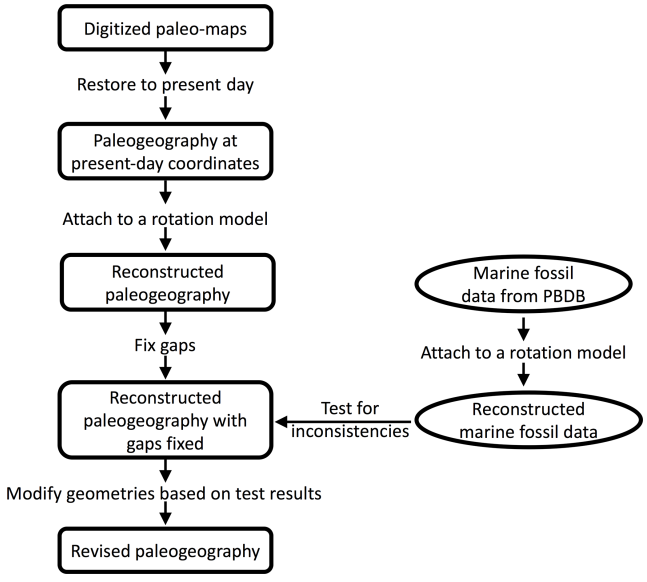

Figure 2. Workflow used to transfer a set of paleogeographic geometries from one reconstruction to another, followed by revision using paleoenvironmental information indicated by marine fossil collections from the Paleobiology Database (PBDB).

Matthews et al. (2016) used in this study, the resulting paleogeographies result in gaps (Fig. 3c, pink) and overlaps between neighboring polygons, when compared to the original reconstruction (Fig. 3a). These gaps and overlaps essentially

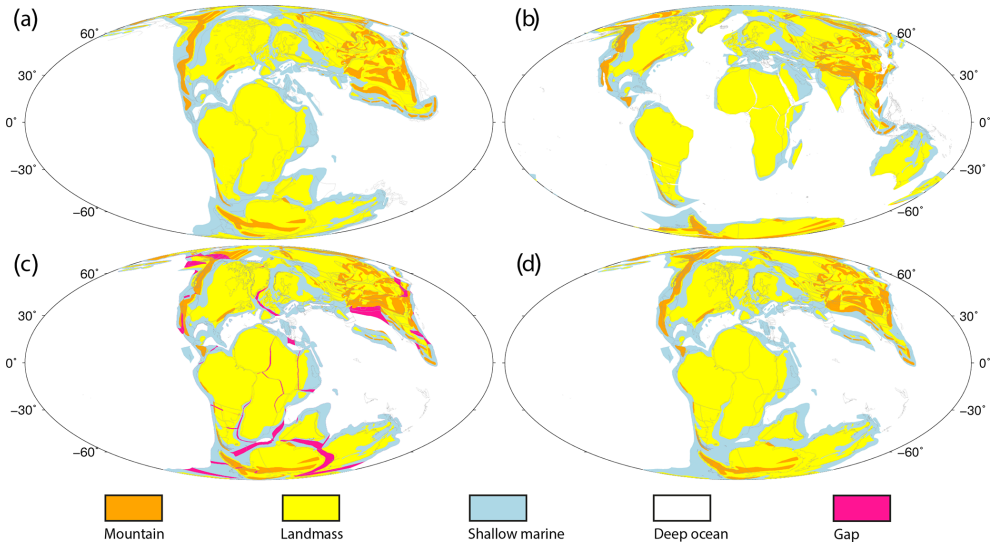

Figure 3. (a) Original global paleogeographic map from Golonka et al. (2006) at 126 Ma. **(b)** Global paleogeographic geometries at 126 Ma in present-day coordinates. **(c)** Global paleogeography at 126 Ma reconstructed using the plate motion model of Matthews et al. (2016). Gaps are highlighted in pink. **(d)** Global paleogeography at 126 Ma reconstructed using the reconstruction of Matthews et al. (2016) with gaps fixed by filling with adjacent paleoenvironment attributes. Grey lines indicate reconstructed present-day coastlines and terrane boundaries. Mollweide projection with 0° E central meridian.

Table 2. Lookup table to classify fossil data indicating different paleoenvironments into marine or terrestrial settings and their corresponding paleogeographic types presented in Golonka et al. (2006). Terrestrial fossil paleoenvironments correspond to paleogeographic features of landmasses, mountains or ice sheets and marine fossil paleoenvironments to shallow marine environments or deep oceans.

Marine			Terrestrial/transitional zone		
Paleogeography	Fossil paleoenvironments		Paleogeography	Fossil paleoenvironments	
shallow marine environments/deep oceans	marine indet.	slope	Landmasses/mountains	terrestrial indet.	pond
	carbonate indet.	basinal (carbonate)		fluvial indet.	crater lake
	peritidal	basinal (siliceous)		alluvial fan	lacustrine delta plain
	shallow subtidal indet.	marginal marine indet.		channel lag	lacustrine interdistributary bay
	open shallow subtidal	coastal indet.		coarse channel fill	lacustrine delta front
	lagoonal/restricted shallow subtidal	estuary/bay		fine channel fill	lacustrine prodelta
	sand shoal	lagoonal		channel	lacustrine deltaic indet.
	reef, buildup or bioherm	paralic indet.		wet floodplain	lacustrine indet.
	peri-reef or sub-reef	interdistributary bay		dry floodplain	dune
	intra-shelf/intraplatform reef	delta front		floodplain	inter-dune
	platform/shelf-margin reef	prodelta		crevasse splay	loess
	slope/ramp reef	deltaic indet.		levee	eolian indet.
	basin reef	foreshore		mire/swamp	cave
	deep subtidal ramp	shore face		fluvial–lacustrine indet.	fissure fill
	deep subtidal shelf	transition zone/lower shore face		delta plain	sinkhole
	deep subtidal indet.	offshore		fluvial–deltaic indet.	karst indet.
	offshore ramp	submarine fan		lacustrine – large	tar
	offshore shelf	basinal (siliciclastic)		lacustrine – small	spring
	offshore indet.	deep-water indet.	ice sheets	glacial	

arise from the differences in the reconstructions described in Matthews et al. (2016) and Golonka et al. (2006). The reconstruction of Golonka et al. (2006) has a tighter fit of the major continents within Pangea prior to the supercontinent breakup. In addition, this reconstruction contains a different plate motion history and block boundary definitions in regions of complex continental deformation, for example along active continental margins (e.g., Himalayas, western North America; Fig. 3c).

The gaps and overlaps cause changes in the total terrestrial or oceanic paleogeographic areas at different time intervals, becoming larger or smaller, when compared with the original paleogeographic maps (Golonka et al., 2006). The gaps can be fixed by interactively extending the outlines of the polygons in a GIS platform to make the plates connect as in

the original paleogeographic maps (Fig. 3a, c, d). Changes in the extent of total terrestrial or oceanic area of the paleogeographies with filled gaps are compared with the original paleogeographies in Fig. 3d (Golonka et al., 2006).

Once the gaps are filled, the reconstructed paleogeographic features are compared with the paleoenvironments indicated by the marine fossil collections from the PBDB. These comparisons aim to identify the differences between the mapped paleogeography and the marine fossil collection environments in order to revise the paleo-coastline locations and paleogeographic geometries. Fossil collections belonging to each time interval (Table 1; Golonka, 2000) are first extracted from the data set downloaded from the PBDB. Only the fossil collections with temporal ranges lying entirely within the corresponding time intervals are selected, as opposed to including the fossil collections that have larger temporal ranges. Fossil collections with temporal ranges crossing any time-interval boundary are not taken into consideration. As a result, a minimum number of fossil collections are selected for each time interval. The selected fossil collections are classified into either the terrestrial or marine setting category, according to a lookup table (Table 2).

Marine fossil collections are then attached to the plate motion model of Matthews et al. (2016) so they can be reconstructed at each time interval. Subsequently, a point-in-polygon test is used to determine whether or not the indicated marine fossil collection is within the appropriate marine paleogeographic polygon. The results of these tests are discussed in the following section.

In the next step, we modify the paleo-coastline locations and paleogeographic geometries based on the test (Figs. 4, 5 and Supplement). Modifications are made according to the following rules. (1) Marine fossil collections from the PBDB are presumed to be well dated, constrained geographically, not reworked and representative of their broader paleoenvironments. Their indicative environments are assumed to be correct. (2) Only marine fossil collections within 500 km of the nearest paleo-coastlines are taken into account as most marine fossil collections used in this study are located within 500 km from the paleo-coastlines (see Fig. S1 in the Supplement). (3) The paleo-coastlines and paleogeographic geometries are modified until they are consistent with the marine fossil collection environments and at the same time remain about 30 km distance from the fossil points used (Fig. 5c, f, l). (4) The adjacent paleo-coastlines are accordingly adjusted and smoothed (Figs. 4, 5). (5) The modified area (Fig. 5b, e, k, blue) resulting from shifting the coastline is filled using the shallow marine environment. These rules are designed to maximize the use of the paleoenvironmental information obtained from the marine fossil collections to improve the coastline locations and paleogeography while attempting to minimize spurious modifications.

However, in some rare cases, outlier marine fossil data may be a deceptive recorder of paleogeography. For instance, Wichura et al. (2015) discussed the discovery of a ∼ 17 Myr old beaked whale fossil 740 km inland from the present-day coastline of the Indian Ocean in east Africa. The authors found evidence to suggest that this whale could have traveled inland from the Indian Ocean along an eastward-directed fluvial (terrestrial) drainage system and was stranded there, rather than representing a marine setting that would be implied under our assumptions. Therefore, theoretically, when using the fossil collections to improve paleogeography, additional concerns about living habits of fossils and associated geological settings should be taken into account. In this study, we have removed this misleading fossil whale from the data set. Such instances of deceptive fossil data are a potential limitation within our workflow, which we seek to minimize by excluding inconsistent fossils more than 500 km away from previously interpreted paleo-coastlines described above.

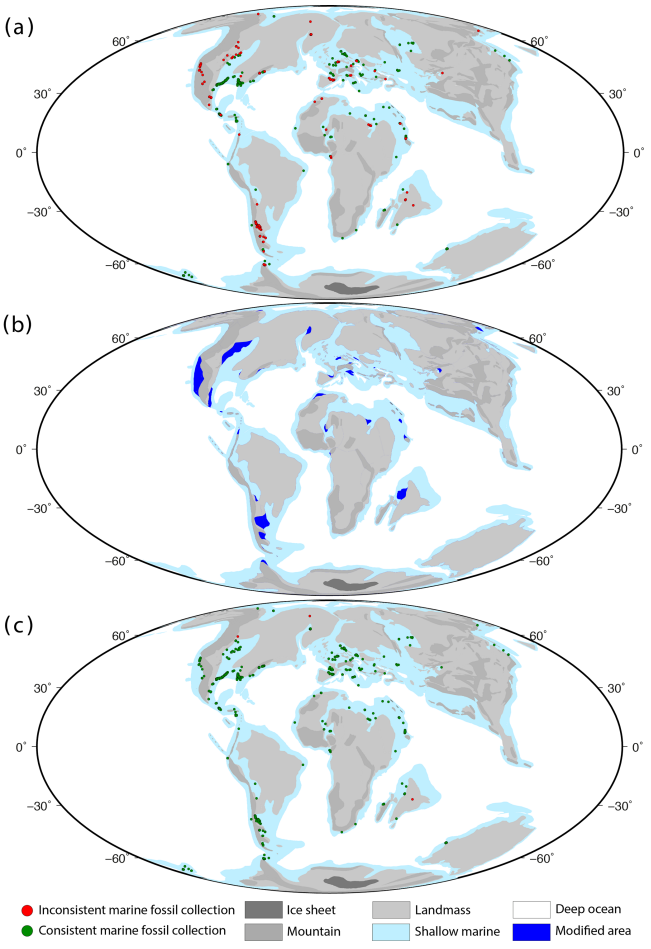

Figure 4. (a) Test between the global paleogeography at 76 Ma reconstructed using the plate motion model of Matthews et al. (2016) with gaps fixed and the paleoenvironments indicated by the marine fossil collections from the PBDB. **(b)** Area modified (blue) to resolve the test inconsistencies. **(c)** Test between the revised paleogeography at 76 Ma and the same marine fossil collections. Mollweide projection with 0° E central meridian.

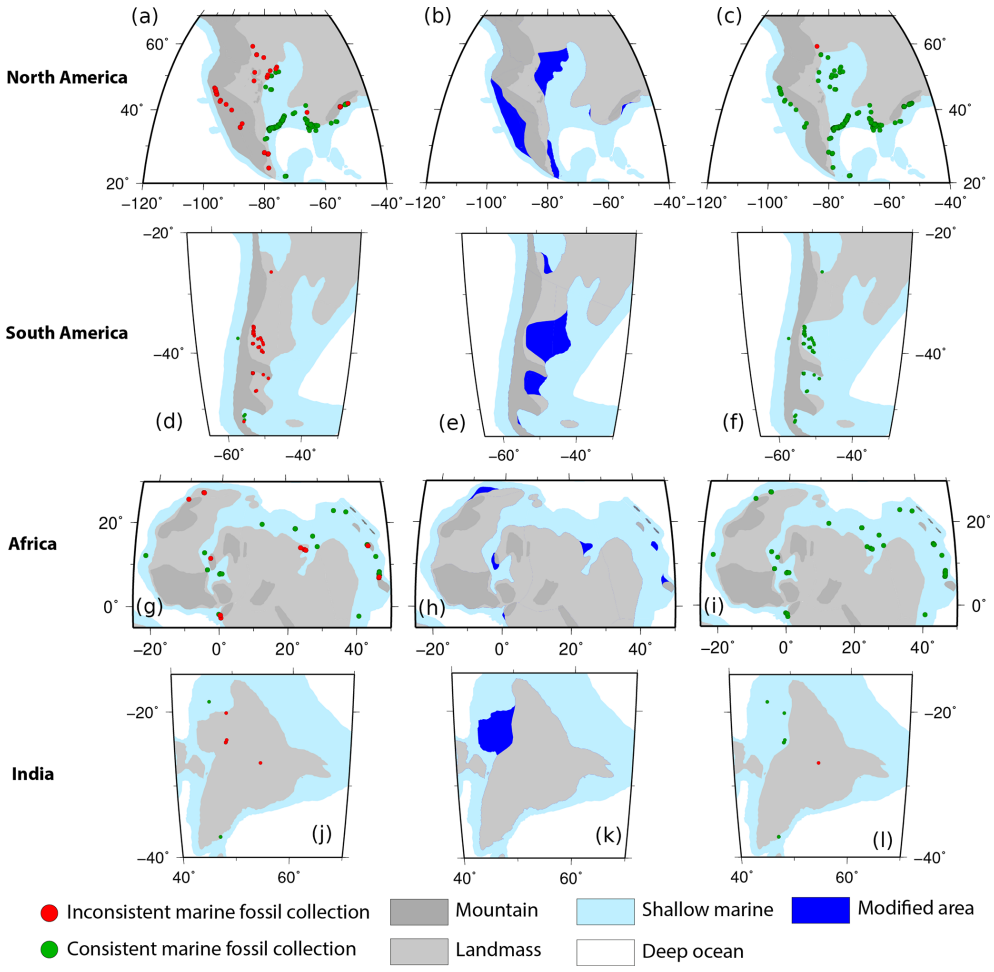

Figure 5. Test between unrevised and revised paleogeography at 76 Ma, respectively, and paleoenvironments indicated by the marine fossil collections from the PBDB, and revision of the paleo-coastlines and paleogeographic geometries based on the test results, for southern North America **(a, b, c)**, southern South America **(d, e, f)**, northern Africa **(g, h, i)** and India **(j, k, l)**. Regional Mollweide projection.

4 Results

4.1 Paleoenvironmental tests

Global reconstructed paleogeographic maps from 402 to 2 Ma are tested against paleoenvironments indicated by the marine fossil collections that are reconstructed in the same rotation model (Matthews et al., 2016). The consistency ratio is defined by the marine fossil collections within shallow marine or deep ocean paleogeographic polygons as a percentage of all marine fossil collections at the time interval, and in contrast, the inconsistency ratio is defined by the marine fossil collections not within shallow marine or deep ocean paleogeography as a percentage of all marine fossil collections. Heine et al. (2015) used a similar metric to evaluate global paleo-coastline models since the Cretaceous.

The inconsistent marine fossil collections are used to modify coastlines and paleogeographic geometries according to the rules outlined in the Methods section. The consistency ratios of marine fossil collections during 402–2 Ma are all over 55 %, with an average of 75 % (Fig. 6a, shaded area) although with large fluctuations over time (Fig. 6). This indicates that the paleogeography of Golonka et al. (2006) has relatively high consistency with the fossil records. However, 52 fossil collections over all time intervals cannot be resolved as they are over 500 km distant from the nearest coastline (for example, red points in Fig. 5c, l). Therefore, in some cases, the paleogeography cannot be fully reconciled with the paleobiology (see Supplement). The results since the Cretaceous are similar to that of Heine et al. (2015).

The sums of marine fossil collections change significantly over time (Fig. 6b); for example, there are more than 4000 in total within 269–248 Ma but only 20 during 37–29 Ma. These variations are due to the spatiotemporal sampling bias and incompleteness of the fossil record (Benton et al., 2000; Benson and Upchurch, 2013; Smith et al., 2012; Valentine et al., 2006; Wright et al., 2013), biota extinction and recovery (Hallam and Wignall, 1997; Hart, 1996), the uneven entry of

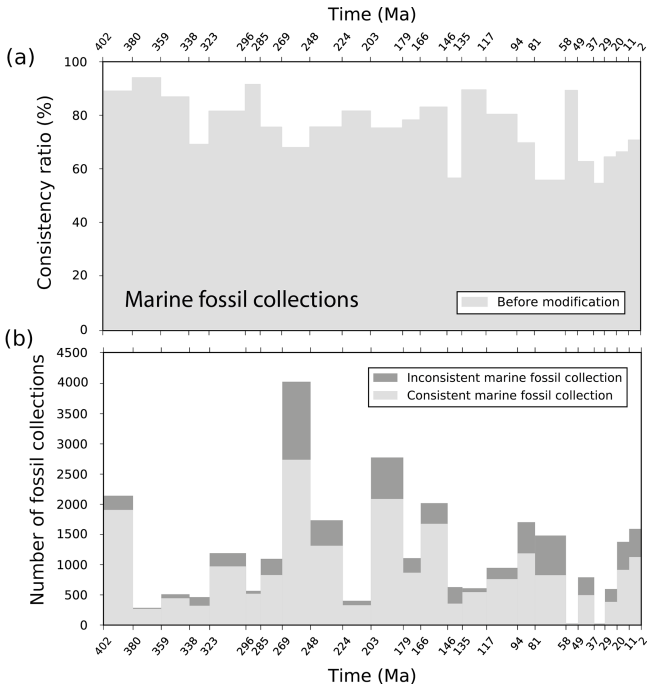

Figure 6. (a) Consistency ratios between global paleogeography with gap filled, but before PBDB test for the period 402–2 Ma, reconstructed using the plate motion model of Matthews et al. (2016) and the paleoenvironments indicated by the marine fossil collections from the PBDB. **(b)** Numbers of consistent (light grey) and inconsistent (dark grey) marine fossil collections used in the tests for each time interval from 402 to 2 Ma.

fossil data to the PBDB (Alroy, 2010) and our temporal selection criterion. In addition, the differences in the duration of geological time subdivisions lead to some time intervals having shorter time spans that contain fewer fossil records, which we discuss in a later section. As for the time intervals during which fossil data are scarce, the fossil collections are of limited use in improving paleogeography. However, additional records in the future will increase the usefulness of the PBDB in such instances.

4.2 Revised global reconstructed paleogeography

Based on the PBDB test results at all the time intervals, we can revise the inferred paleo-coastlines and paleogeographic geometries using the approach described in the Methods section. As a result, the revised paleo-coastlines and paleogeographies are significantly improved, mainly in the regions of North America, South America, Europe and Africa during the Late Carboniferous, Middle Permian, Triassic, Jurassic, Late Cretaceous and most of Cenozoic (Figs. 4, 5, 6 and Supplement). The resulting improved global paleogeographic maps since the Devonian are presented in Fig. 7. They provide improved paleo-coastlines that are important to constrain past changes in sea level and long-wavelength dynamic topography.

We subsequently calculate the area covered by each paleogeographic feature as a percentage of Earth's total surface area at each time interval from 402 to 2 Ma (Fig. 8), using the HEALPix pixelization method that results in equal sampling of data on a sphere (Górski et al., 2005) and therefore equal sampling of surface areas. This method effectively excludes the effect of overlaps between paleogeographic geometries.

As a result, the areas of landmass, mountain and ice sheet generally indicate increasing trends, while shallow marine and deep ocean areas show decreasing trends through geological time (Fig. 8). Overall, the computed areas increase in the following order: ice sheet (average 1.0 % of Earth surface), mountain belts (3.4 %), shallow marine (14.3 %), landmass (21.3 %) and deep ocean (60.1 %). Only during the time interval of 323–296 Ma are landmass and shallow marine areas nearly equal at about 14.0 %, and only during 359–285 Ma do ice sheet areas exceed mountain areas, but ice sheets only exist during 380–285, 81–58 and 37–2 Ma. With Pangea formation during the latest Carboniferous or the Early Permian and breakup initiation in the Early Jurassic (Blakey, 2003; Domeier et al., 2012; Lenardic, 2016; Stampfli et al., 2013; Vai, 2003; Veevers, 2004; Yeh and Shellnutt, 2016), these paleogeographic feature areas significantly change over time (Fig. 8). During 323–296 Ma (Late Carboniferous–earliest Permian), the landmass extent reaches its smallest area (13.6 %) and subsequently undergoes a rapid increase until peaking at 26.6 % between 224 and 203 Ma (Late Triassic). In contrast, ice sheets reach their largest area (7.2 %) between 323 and 296 Ma. In the Early Jurassic of Pangea breakup, landmass area rapidly decreases from 26.6 % between 224 and 203 Ma to 23.5 % between 203 and 179 Ma, but shallow marine area increases by 3.7 %.

5 Discussions

5.1 Global flooded continental areas

We estimate the global flooded continental areas since the Early Devonian from the revised paleogeography in this study (Fig. 9, pink solid line) and from the original paleogeographic maps of Golonka et al. (2006; Fig. 9, grey solid line). Both sets of results are similar, with a decrease during Pangea amalgamation from the Late Devonian until the Late Carboniferous, increase from the Early Jurassic with the breakup of Pangea until the Late Cretaceous and then a decrease again until the Pleistocene. We compare the two curves (pink solid line, grey solid line; Fig. 9) to the results of other studies (Fig. 9; Ronov, 1994; Smith et al., 1994; Walker et al., 2002; Blakey, 2003, 2008; Golonka, 2007b, 2009, 2012) derived from independent paleoenvironment and paleo-lithofacies data. The results are generally consistent, except for the periods 338–269 Ma and 248–203 Ma, during which the flooded continental areas for this study and Golonka et al. (2006) are smaller, reflecting smaller extent

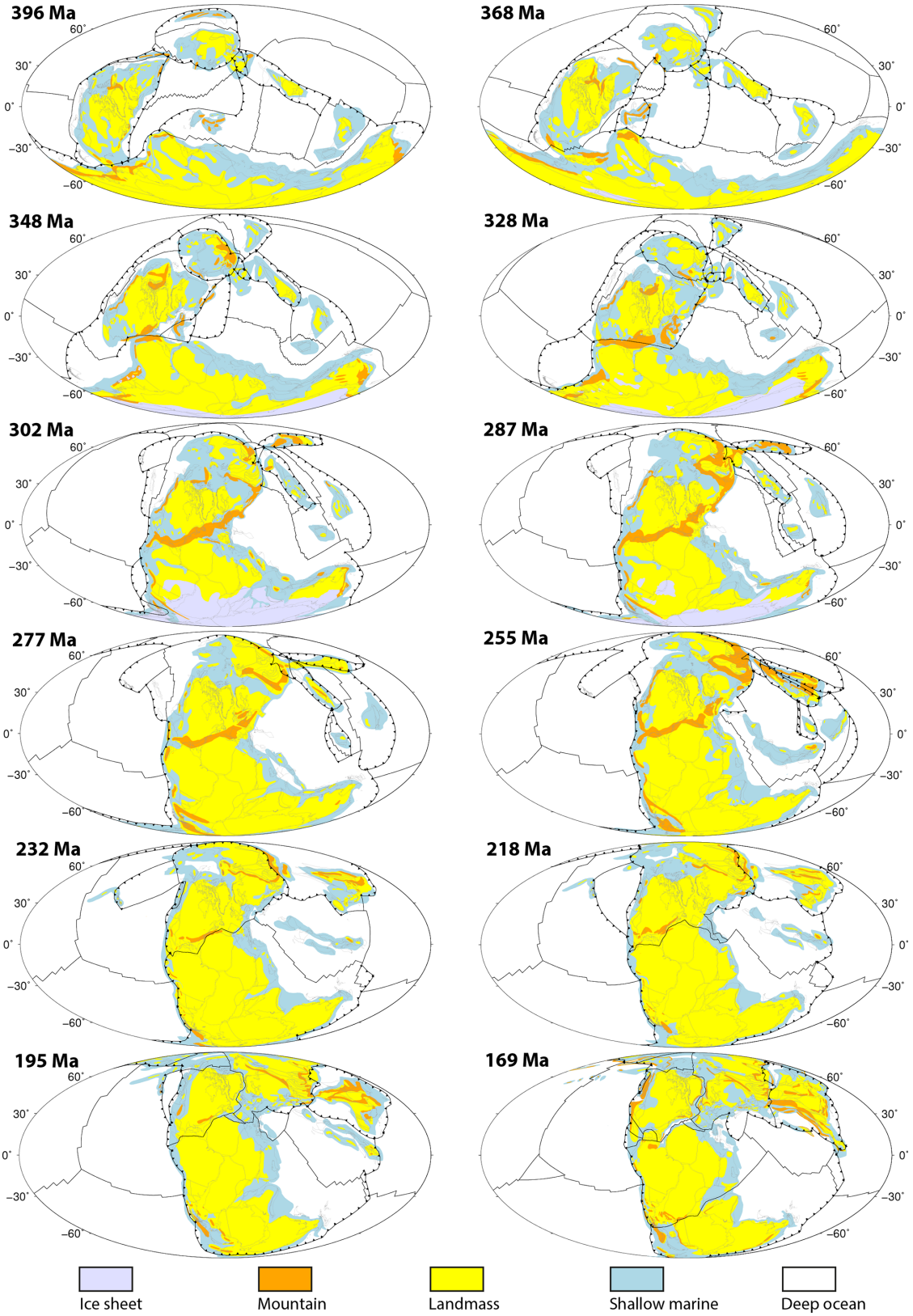

Figure 7. Global paleogeography from 402 to 2 Ma reconstructed using the plate motion model of Matthews et al. (2016) and revised using paleoenvironmental data from the PBDB. Black dotted lines indicate subduction zones, and other black lines denote mid-ocean ridges and transforms. Grey outlines delineate reconstructed present-day coastlines and terranes. Mollweide projection with 0° E central meridian.

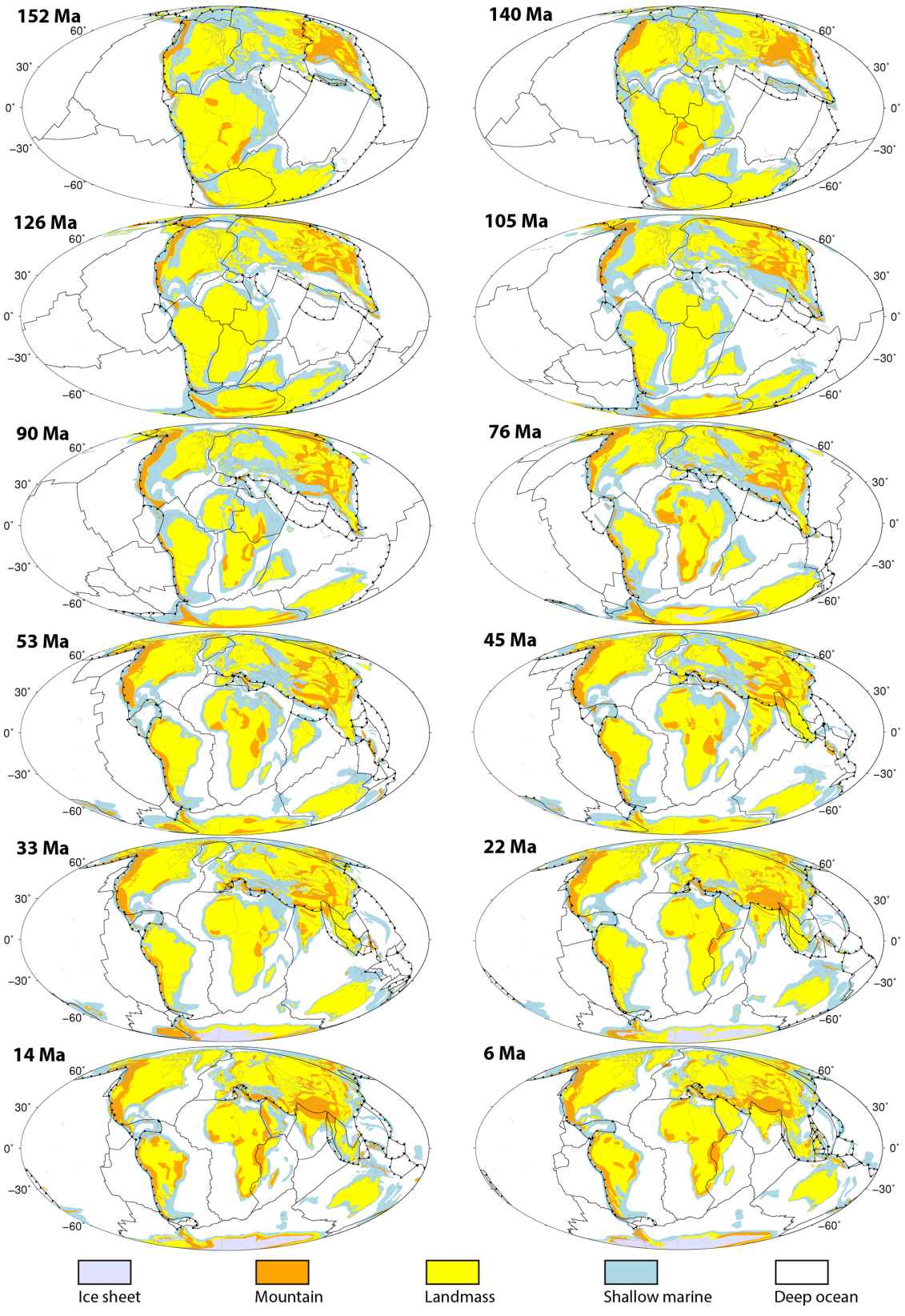

Figure 7. (continued)

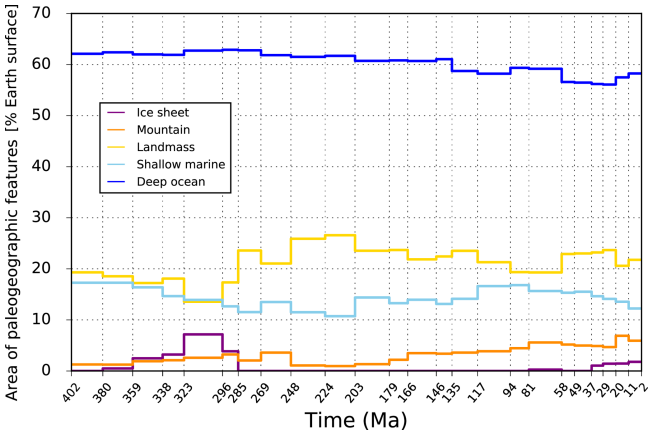

Figure 8. Global paleogeographic feature areas as percentages of Earth's total surface area estimated from the revised paleogeographic maps from 402 Ma to 2 Ma.

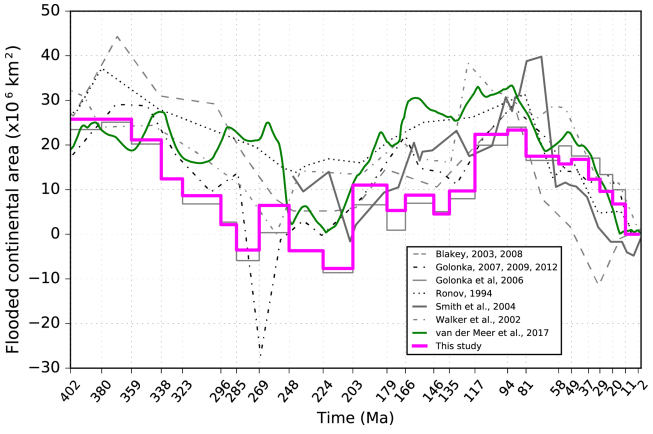

Figure 9. Global flooded continental area since the Early Devonian from the original paleogeographic maps of Golonka et al. (2006; grey solid line) and from the revised paleogeography in this study (pink line). Results for Blakey (2003, 2008), Golonka (2007b, 2009, 2012), Ronov (1994), Smith et al. (2004) and Walker et al. (2002) are as in van der Meer et al. (2017). The van der Meer et al. (2017) curve (green line) is derived from the strontium isotope record of marine carbonates.

of transgression in these times. Van der Meer et al. (2017, green line in Fig. 9) derived sea level and continental flooding from the strontium isotope record of marine carbonates. These results are generally consistent with the estimates from paleoenvironment and paleo-lithofacies data, except during the Permian and the Late Jurassic–early Cretaceous, during which van der Meer et al. (2017) predict larger extent of flooding than others (Fig. 9). This could indicate that the evolution of $^{87}Sr/^{86}Sr$ reflects variations in the composition of emergent continental crust (Bataille et al., 2017; Flament et al., 2013) as well as global weathering rates (e.g., Flament et al., 2013; Vérard et al., 2015; van der Meer et al., 2017).

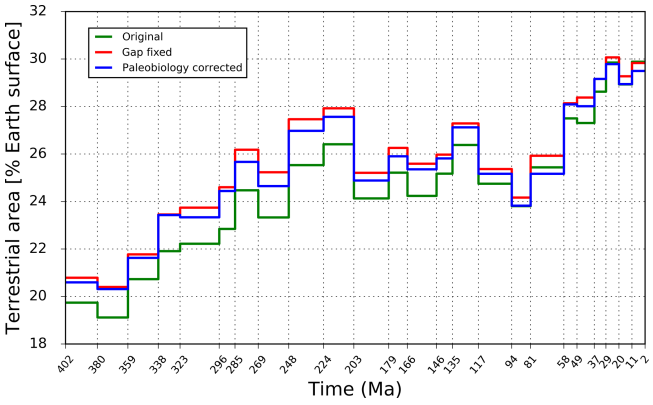

Figure 10. Terrestrial areal change due to filling gaps and modifying the paleo-coastlines and paleogeographic geometries over time. Green: based on the original paleogeographic maps of Golonka et al. (2006); red: based on paleogeography reconstructed using a different plate motion model of Matthews et al. (2016) and gaps filled; blue: based on paleogeography with gaps fixed and revised using the paleoenvironments indicated by marine fossil collections from the PBDB.

5.2 Terrestrial areal change associated with transferring reconstruction, filling gaps and revising paleogeography

We estimate the terrestrial areas, including ice sheets, mountains and landmasses, as percentages of Earth's surface area, from the original paleogeography of Golonka et al. (2006; Fig. 10, green), from the paleogeography reconstructed using a different plate motion model of Matthews et al. (2016) and gaps filled (Fig. 10, red) and from the paleogeography with gaps fixed and revised using the paleoenvironmental information indicated by marine fossil collections from the PBDB (Fig. 10, blue). These three curves are similar and generally indicate a reverse changing trend to the flooded continental areal curves over time (Fig. 9), as expected. We also calculate the areas of the terrestrial paleogeographic geometries after transferring the reconstruction but before filling gaps and the results are nearly identical to the original terrestrial paleogeographic areas of Golonka et al. (2006). This is because the reconstruction of Golonka et al. (2006) has a tighter fit of the major continents within Pangea prior to the supercontinent breakup than the reconstruction of Matthews et al. (2016), so that transferring the paleogeographic geometries mainly produces gaps rather than overlaps. Comparing between the three curves (Fig. 10), filling gaps results in a larger terrestrial areal change than revising paleogeographic geometries based on PBDB test. Therefore, variation of the underlying plate reconstruction is the main factor that contributes to the terrestrial areal change (Fig. 10, red and green), and the effect of revising paleogeographic geometries based on paleobiology is secondary (Fig. 10, blue).

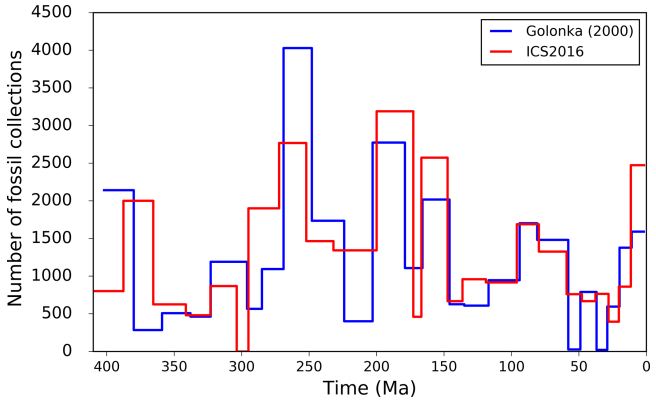

Figure 11. Fossil abundance test on the marine fossil collection data set used in this study with two different timescales: Golonka (2000) and ICS2016 (Table 1).

5.3 Marine fossil collection abundances in two different timescales

We test the marine fossil collection data set used in this study for fossil abundances over time with two different timescales: ICS2016 and Golonka (2000; Table 1). The results indicate the abundances of the data set in the two timescales are significantly different in most time intervals (Fig. 11). Generally, shorter time spans contain fewer data; for instance, there are about 400 marine fossil collections between 224 and 203 Ma using the Golonka (2000) timescale (Fig. 11, red), while there are over 1300 collections during 232–200 Ma using the ICS2016 timescale (Fig. 11, blue). In addition, the difference of the start age and end age of the time interval could remarkably affect the fossil abundance, so that there are over 2000 marine fossil collections between 387.7 and 365.6 Ma in ICS2016 but fewer than 300 collections between 380 and 359 Ma using the Golonka (2000) timescale. As a result, the timescale applied to the paleobiology could significantly affect the fossil collection abundance being assigned to paleogeographic time intervals.

5.4 Limitations of the workflow

The workflow we develop in this study illustrates transferring paleogeographic geometries from one plate motion model to another and then using paleoenvironmental information indicated by marine fossil collections from the PBDB to improve the paleo-coastline locations and paleogeographic geometries. However, the methodology still has some limitations. Transferring paleogeographic geometries to a different reconstruction inevitably results in gaps and/or overlaps, which can only be addressed using presently laborious methods. In addition, revising the coastlines and paleogeographic geometries based on the PBDB test is also currently achieved manually, and could be automated in the future.

Paleogeographic maps such as those considered here typically represent discrete time periods of many millions of years, whereas global plate motion models, even though also based on tectonic stages, provide a somewhat more continuous description of evolving plate configurations. A remaining question is how to provide a continuous representation of paleogeographic change that combines continuous plate motion models with paleogeographic maps that do not explicitly capture changes at the same temporal resolution. In addition, it is currently difficult to apply a timescale to the raw paleobiology data from the PBDB that are currently not tied to any timescale. The paleoenvironmental data used here have variable temporal resolutions, but the paleo-coastlines representing maximum transgressions are presented in a location at specific times. However, due to the inaccessibility of the original data that were used to build the paleogeographic maps, we are not in a position to estimate the temporal resolution of the original coastlines and paleogeographic maps.

The PBDB is a widely used resource (e.g., Wright et al., 2013; Finnegan et al., 2015; Heim et al., 2015; Mannion et al., 2015; Nicolson et al., 2015; Fischer et al., 2016; Tennant et al., 2016; Close et al., 2017; Zaffos et al., 2017), yet, the spatial coverage of data is still highly heterogeneous, with relatively few data points across large areas of the globe for some time periods. Hence, it is important to combine it with other geological data, such as stratigraphic data from StratDB Database (http://sil.usask.ca) and Macrostrat Database (https://macrostrat.org/) and other sources of paleoenvironment and paleo-lithofacies data, to further constrain the paleogeographic reconstructions.

6 Conclusions

Our study highlights the flexibility of digital paleogeographic models linked to plate tectonic reconstructions in order to better understand the interplay of continental growth and eustasy, with wider implications for understanding Earth's paleotopography, ocean circulation and the role of mantle convection in shaping long-wavelength topography. We present a workflow that enables the construction of paleogeographic maps with variable spatial and temporal resolutions, while also becoming more testable and expandable with the incorporation of new paleoenvironmental data sets.

We develop an approach to revise the paleo-coastline locations and paleogeographic geometries using paleoenvironmental information indicated by the marine fossil collections from the PBDB. Using this approach, the consistency ratio between the paleogeography and the paleobiology records since the Devonian is increased from an average 75 % to nearly full consistency. The paleogeography in the main regions of North America, South America, Europe and Africa is significantly improved, especially in the Late Carboniferous, Middle Permian, Triassic, Jurassic, Late Cretaceous and most portions of the Cenozoic. The flooded continental ar-

eas since the Late Devonian inferred from the revised global paleogeography in this study are generally consistent with the results derived from other paleoenvironment and paleolithofacies data or from the strontium isotope record in marine carbonates.

Comparing the terrestrial areal change over time associated with transferring the reconstruction and filling gaps, and revising paleogeographic geometries using the paleoenvironmental data from the PBDB, indicates that reconstruction difference is a main factor in paleogeographic areal change when comparing with the original maps, and revising paleogeographic geometries based on PBDB test is secondary.

Information about the supplement

We provide two sets of digital global paleogeographic maps during 402–2 Ma: (1) the paleogeography reconstructed using the plate motion model of Matthews et al. (2016) and revised using paleoenvironmental information indicated by the marine fossil collections from the PBDB and (2) the original paleogeography of Golonka et al. (2006). We also provide the original rotation file of Golonka et al. (2006), a set of paleogeographic maps illustrating the PBDB test and revision of paleo-coastlines and paleogeographic geometries, a set of GeoTiff files of all revised paleogeographic maps, paleobiology data in shapefile used in this study separated into two sets of consistent marine fossil collections and inconsistent marine fossil collections, an animation for the revised global paleogeographic maps, and a README file outlined the workflow of this study.

The Supplement related to this article is available online at https://doi.org/10.5194/bg-14-5425-2017-supplement.

Data availability. No data sets were used in this article.

Competing interests. The authors declare that they have no conflict of interest.

Acknowledgements. This work was supported by Australian Research Council grants IH130200012 (RDM, SZ), DE160101020 (NF) and SIEF RP 04-174 (SW). W. Cao was also supported by a University of Sydney International Scholarship (USydIS). We thank Julia Sheehan and Logan Yeo for digitizing these paleogeographic maps, and John Cannon and Michael Chin for help with GPlates and pyGPlates. We sincerely thank Shanan Peters and three anonymous reviewers for their constructive reviews and suggestions. We thank Natascha Töpfer for editorial support and Tina Treude for editing the manuscript. We are also thankful for the entire PBDB team and all PBDB data contributors. This is Paleobiology Database Publication 296.

Edited by: Tina Treude
Reviewed by: Shanan Peters and three anonymous referees

References

Amante, C. and Eakins, B. W.: ETOPO1 1 arc-minute global relief model: Procedures, data sources and analysis, NOAA Technical Memorandum NESDIS NGDC-24, National Geophysical Data Center, National Oceanic and Atmospheric Administration, 19 pp., 2009.

Alroy, J.: Geographical, environmental and intrinsic biotic controls on Phanerozoic marine diversification, Palaeontology, 53, 1211–1235, 2010.

Bataille, C. P., Willis, A., Yang, X., and Liu, X. M.: Continental igneous rock composition: A major control of past global chemical weathering, Science Advances, 3, 1–16, 2017.

Benson, R. B. J. and Upchurch, P.: Diversity trends in the establishment of terrestrial vertebrate eco-systems: interactions between spatial and temporal sampling biases, Geology, 41, 43–46, 2013.

Benton, M. J., Wills, M. A., and Hitchin, R.: Quality of the fossil record through time, Nature, 403, 534–537, 2000.

Blakey, R. C.: Carboniferous Permian global paleogeography of the assembly of Pangaea, in: Fifteenth International Congress on Carboniferous and Permian Stratigraphy, edited by: Wong, T. E., Royal Netherlands Academy of Arts and Sciences, Utrecht, the Netherlands, 443–465, 2003.

Blakey, R. C.: Gondwana paleogeography from assembly to breakup–A 500 m.y. odyssey, in: Resolving the Late Paleozoic Ice Age in Time and Space, edited by: Christopher R. Fielding, C. R., Frank, T. D., and Isbell, J. L., Geol. S. Am. S., 441, 1–28, https://doi.org/10.1130/2008.2441(01), 2008.

Close, R. A., Benson, R. B. J., Upchurch, P., and Butler, R. J.: Controlling for the species-area effect supports constrained long-term Mesozoic terrestrial vertebrate diversification, Nature Communications, 8, 15381, https://doi.org/10.1038/ncomms15381, 2017.

Cohen, K. M., Finney, S. C., Gibbard, P. L., and Fan, J.-X.: The ICS International Chronostratigraphic Chart, Episodes, 36, 199–204, 2013, updated.

Domeier, M. and Torsvik, T. H.: Plate tectonics in the late Paleozoic, Geosci. Front. 5, 303–350, 2014.

Domeier, M., Van der Voo, R., and Torsvik, T. H.: Paleomagnetism and Pangea: the road to reconciliation, Tectonophysics, 514–517, 14–43, 2012.

Finnegan, S., Anderson, S. C., Harnik, P. G., Simpson, C., Byrnes, J. E., Tittensor, D. P., Finkel, Z. V., Lindberg, D. R., Liow, L. H., Lockwood, R., Lotze, H. K., McClain, C. R., McGuire, J. L., O'Dea, A., and Pandolfi, J. M.: Paleontological baselines for evaluating extinction risk in the modern oceans, Science, 348, 567–570, https://doi.org/10.1126/science.aaa6635, 2015.

Fischer, V., Bardet, N., Benson, R. B. J., Arkhangelsky, M. S., and Friedman, M.: Extinction of fish-shaped marine reptiles associated with reduced evolutionary rates and global environmental volatility, Nature Communications, 7, 10825, https://doi.org/10.1038/ncomms10825, 2016.

Flament, N., Coltice, N., and Rey, P. F.: The evolution of the $^{87}Sr/^{86}Sr$ of marine carbonates does not constrain continental growth, Precambrian Res., 229, 177–188, 2013.

Goddéris, Y., Donnadieu, Y., Le, Hir. G., and Lefebvre, V.: The role of palaeogeography in the Phanerozoic history of atmospheric CO_2 and climate, Earth-Sci. Rev., 128, 122–138, 2014.

Golonka, J.: Cambrian-Neogene Plate Tectonic Maps, Wydawnictwa Uniwersytetu Jagielloñskiego, Kraków, 125 pp., 2000.

Golonka, J.: Late Triassic and Early Jurassic palaeogeography of the world, Palaeogeography, Palaeogeogr. Palaeocl., 244, 297–307, 2007a.

Golonka, J.: Phanerozoic paleoenvironment and paleolithofacies maps: Mesozoic, Geologia / Akad. Gór.-Hut. im. Stanisława Staszica w Krakowie, 33, 211–264, 2007b.

Golonka, J.: Phanerozoic paleoenvironment and paleolithofacies maps: Cenozoic, Geologia / Akad. Gór.-Hut. im. Stanisława Staszica w Krakowie, 35, 507–587, 2009.

Golonka, J.: Paleozoic Paleoenvironment and Paleolithofacies Maps of Gondwana, AGH University of Science and Technology Press, Kraków, 2012.

Golonka, J., Ross, M. I., and Scotese, C. R.: Phanerozoic paleogeographic and paleoclimatic modeling maps, in: Pangea: Global Environment and Resources – Memoir 17, edited by: Embry, A. F., Beauchamp, B., and Glass, D. J., Canadian Society of Petroleum Geologists, Calgary, Alberta, Canada, 1–47, 1994.

Golonka, J., Krobicki, M., Pajak, J., Giang, N. V., and Zuchiewicz, W.: Global Plate Tectonics and Paleogeography of Southeast Asia, Faculty of Geology, Geophysics and Environmental Protection, AGH University of Science and Technology, Arkadia, Krakow, Poland, 2006.

Górski, K. M., Hivon, E., Banday, A. J., Wandelt, B. D., Hansen, F. K., Reinecke, M., and Bartelmann, M.: HEALPix: A Framework for High-Resolution Discretization and Fast Analysis of Data Distributed on the Sphere, Astrophys. J., 622: 759–771, 2005.

Gurnis, M., Müller R. D., and Moresi, L.: Dynamics of Cretaceous to the present vertical motion of Australia and the Origin of the Australian- Antarctic Discordance, Science, 279, 1499–1504, 1998.

Hallam, A. and Wignall, P. B.: Mass extinctions and their aftermath, Oxford University Press, Oxford, UK, 320 pp., 1997.

Hart, M. B.: Biotic recovery from mass extinction events, Geological Society of London, Special Publications, 102, 1996.

Heim, N. A., Knope, M. L., Schaal, E. K., Wang, S. C., and Payne, J. L.: Cope's Rule in the evolution of marine animals, Science, 347, 867–870, https://doi.org/10.1126/science.1260065, 2015.

Heine, C., Yeo, L. G., and Müller, R. D.: Evaluating global paleoshoreline models for the Cretaceous and Cenozoic, Aust. J. Earth Sci., 62, 275–287, 2015.

Kiessling, W., Flügel, E., and Golonka, J.: Patterns of Phanerozoic carbonate platform sedimentation, Lethaia, 36, 195–226, 2003.

Lenardic, A.: Plate tectonics: A supercontinental boost, Nat. Geosc., 10, https://doi.org/10.1038/ngeo2862, 2016.

Mannion, P. D., Benson, R. B. J., Carrano, M. T., Tennant, J. P., Judd, J., and Butler, R. J.: Climate constrains the evolutionary history and biodiversity of crocodylians, Nature Communications, 6, 8438, https://doi.org/10.1038/ncomms9438, 2015.

Matthews, K. J., Maloney, K. T., Zahirovic, S., Williams, S. E., Seton, M., and Müller, R. D.: Global plate boundary evolution and kinematics since the late Paleozoic, Global Planet. Change, 146, 226–250, 2016.

Müller, R. D., Seton, M.; Zahirovic, S.; Williams, S. E., Matthews, K. J., Wright, N. M., Shephard, G. E., Maloney, K. T., Barnett-Moore, N., Hosseinpour, M., Dan, J. B., and John, C.: Ocean basin evolution and global-scale reorganization events since Pangea breakup, Annu. Rev. Earth Pl. Sc., 44, 107–138, 2016.

Nicholson, D. B., Holroyd, P. A., Benson, R. B. J., and Barrett, P. M.: Climate mediated diversification of turtles in the Cretaceous, Nature Communications, 6, 7848, https://doi.org/10.1038/ncomms8848, 2015.

Ronov, A. B.: Phanerozoic transgressions and regressions on the continents; a quantitative approach based on areas flooded by the sea and areas of marine and continental deposition, Am. J. Sci., 294, 777–801, 1994.

Ronov, A., Khain, V., and Seslavinsky, K.: Atlas of Lithological-Paleogeographical Maps of the World, Late Precambrian and Paleozoic of Continents, U.S.S.R. Academy of Sciences, Leningrad, 70 pp., 1984.

Ronov, A., Khain, V., and Balukhovsky, A.: Atlas of Lithological-Paleogeographical Maps of the World, Mesozoic and Cenozoic of Continents and Oceans, U.S.S.R. Academy of Sciences, Leningrad, 79 pp., 1989.

Salles, T., Flament, N., and Müller, D.: Influence of mantle flow on the drainage of eastern Australia since the Jurassic Period, Geochem. Geophy. Geosy., 18, 280–305, https://doi.org/10.1002/2016GC006617, 2017.

Scotese, C. R.: Paleogeographic Atlas, PALEOMAP project, Arlington, Texas, USA, 1997.

Scotese, C. R.: Atlas of Earth History, Volume 1, Paleogeography, PALEOMAP project, Arlington, Texas, 52 pp., 2001.

Scotese, C.: A continental drift flipbook, J. Geol., 112, 729–741, https://doi.org/10.1086/424867, 2004.

Sloss, L. L.: Tectonic evolution of the craton in Phanerozoic time, in: Sedimentary cover–North American craton: U.S., edited by: Sloss, L. L., The Geology of North America, D-2, Geological Society of America, 25–51, 1988.

Smith, A. B., Lloyd, G. T., and McGowan, A. J.: Phanerozoic marine diversity: rock record modelling provides an independent test of large-scale trends, P. Roy. Soc. B-Biol. Sci., 279, 4489–4495, 2012.

Smith, A. G., Smith, D. G., and Funnell, B. M.: Atlas of Mesozoic and Cenozoic Coastlines, Cambridge University Press, Cambridge, 99 pp, 1994.

Spasojevic, S. and Gurnis, M.: Sea level and vertical motion of continents from dynamic Earth models since the Late Cretaceous, AAPG Bull., 96, 2037–2064, https://doi.org/10.1306/03261211121, 2012.

Stampfli, G. M., Hochard, C., Vérard, C., Wilhem, C., and von-Raumer, J.: The formation of Pangea, Tectonophysics, 593, 1–19, 2013.

Tennant, J. P., Mannion, P. D., Upchurch, P.: Sea level regulated tetrapod diversity dynamics through the Jurassic/Cretaceous interval, Nature Communications, 7, 12737, https://doi.org/10.1038/ncomms12737, 2016.

Vai, G. B.: Development of the palaeogeography of Pangaea from Late Carboniferous to Early Permian, Palaeogeogr. Palaeocl., 196, 125–155, 2003.

Valentine, J. W., Jablonski, D., Kidwell, S., and Roy, K.: Assessing the fidelity of the fossil record by using marine bivalves, P. Natl. Acad. Sci. USA, 103, 6599–6604, 2006.

van der Meer, D. G., van den Berg van Saparoea, A. P. H., van Hinsbergen, D. J. J., van de Weg, R. M. B., Godderis, Y., Le Hir, G., and Donnadieu, Y.: Reconstructing first-order changes in sea level during the Phanerozoic and Neoproterozoic using strontium isotopes, Gondwana Res., 44, 22–34, 2017.

Veevers, J. J.: Gondwanaland from 650–500 Ma assembly through 320 Ma merger in Pangea to 185–100 Ma breakup: supercontinental tectonics via stratigraphy and radiometric dating, Earth-Sci. Rev., 68, 1–132, 2004.

Vérard, C., Hochard, C., Baumgartner, P. O., and Stampfli, G. M.: 3D palaeogeographic reconstructions of the Phanerozoic versus sea-level and Sr-ratio variations, Journal of Palaeogeography, 4, 167–188, 2015.

Walker, L. J., Wilkinson, B. H., and Ivany, L. C.: Continental drift and Phanerozoic carbonate accumulation in shallow-shelf and deep-marine settings, J. Geol., 110, 75–87, https://doi.org/10.1086/324318, 2002.

Wichura, H., Jacobs, L. L., Lin, A., Polcyn, M. J., Manthi, F. K., Winkler, D. A., Strecker, M. R., and Clemens, M.: A 17-My-old whale constrains onset of uplift and climate change in east Africa, P. Natl. Acad. Sci. USA, 112, 3910–3915, 2015.

Wright, N., Zahirovic, S., Müller, R. D., and Seton, M.: Towards community-driven paleogeographic reconstructions: integrating open-access paleogeographic and paleobiology data with plate tectonics, Biogeosciences, 10, 1529–1541, https://doi.org/10.5194/bg-10-1529-2013, 2013.

Yeh, M. W. and Shellnutt, J. G.: The initial break-up of Pangæa elicited by Late Palæozoic deglaciation, Scientific Reports, 6, 31442, https://doi.org/10.1038/srep31442, 2016.

Zaffos, A., Finnegan, S., and Peters, S. E.: Plate tectonic regulation of global marine animal diversity, P. Natl. Acad. Sci. USA, 114, 5653–5658, https://doi.org/10.1073/pnas.1702297114, 2017.

Article 2

Paleolatitudinal distribution of lithologic indicators of climate in a paleogeographic framework

Geol. Mag.: page 1 of 24 © Cambridge University Press 2018
doi:10.1017/S0016756818000110

Palaeolatitudinal distribution of lithologic indicators of climate in a palaeogeographic framework

WENCHAO CAO*†, SIMON WILLIAMS*, NICOLAS FLAMENT‡, SABIN ZAHIROVIC*, CHRISTOPHER SCOTESE§ & R. DIETMAR MÜLLER*¶

*EarthByte Group and Basin GENESIS Hub, School of Geosciences, The University of Sydney, Sydney, NSW 2006, Australia
‡School of Earth and Environmental Sciences, University of Wollongong, Wollongong, NSW 2522, Australia
§Department of Earth & Planetary Sciences, Northwestern University, Evanston, IL 60208, USA
¶Sydney Informatics Hub, The University of Sydney, Sydney, NSW 2006, Australia

(*Received* 24 September 2017; *accepted* 22 January 2018)

Abstract – Whether the latitudinal distribution of climate-sensitive lithologies is stable through greenhouse and icehouse regimes remains unclear. Previous studies suggest that the palaeolatitudinal distribution of palaeoclimate indicators, including coals, evaporites, reefs and carbonates, has remained broadly similar since the Permian period, leading to the conclusion that atmospheric and oceanic circulation control their distribution rather than the latitudinal temperature gradient. Here we revisit a global-scale compilation of lithologic indicators of climate, including coals, evaporites and glacial deposits, back to the Devonian period. We test the sensitivity of their latitudinal distributions to the uneven distribution of continental areas through time and to global tectonic models, correct the latitudinal distributions of lithologies for sampling- and continental area-bias, and use statistical methods to fit these distributions with probability density functions and estimate their high-density latitudinal ranges with 50 % and 95 % confidence intervals. The results suggest that the palaeolatitudinal distributions of lithologies have changed through deep geological time, notably a pronounced poleward shift in the distribution of coals at the beginning of the Permian. The distribution of evaporites indicates a clearly bimodal distribution over the past ~400 Ma, except for Early Devonian, Early Carboniferous, the earliest Permian and Middle and Late Jurassic times. We discuss how the patterns indicated by these lithologies change through time in response to plate motion, orography, evolution and greenhouse/icehouse conditions. This study highlights that combining tectonic reconstructions with a comprehensive lithologic database and novel data analysis approaches provide insights into the nature and causes of shifting climatic zones through deep time.

Keywords: palaeolatitudinal distribution, palaeoclimate lithologic indicators, atmospheric CO_2, palaeogeography, plate tectonic reconstructions, statistical analysis

1. Introduction

The palaeolatitudinal distribution of climate-sensitive lithologic deposits is important for understanding past climates (Gordon, 1975; Evans, 2006; Boucot, Chen & Scotese, 2013), reconstructing palaeogeographies (Ronov, Khain & Seslavinsky, 1984; Ronov, Khain & Balukhovsky, 1989; Scotese 2001, 2004; Golonka *et al*. 2006; Blakey, 2008) and providing constraints for climate modelling (Boucot & Gray, 2001; Craggs, Valdes & Widdowson, 2011) and plate motion histories (Scotese & Barrett, 1990; Witzke, 1990). However, the past distribution of climate-sensitive lithologies remains poorly understood, especially in deep geological times. Latitudinal distribution patterns of palaeoclimate indicators have been considered broadly stable since the Permian, leading to an interpretation that atmospheric and oceanic circulation control their distribution rather than equator-to-pole temperature gradients (Ziegler *et al*. 2003). A global palaeomagnetic compilation of Earth's basin-scale evaporite records suggests that evaporite palaeolatitudes have varied to some degree over the past 2 billion years, with a relatively large difference between Cenozoic–Mesozoic times (a mean palaeolatitude of $23 \pm 4°$) and Devonian–Ediacaran times (a mean palaeolatitude of $14 \pm 2°$) (Evans, 2006). In addition, previous studies have rarely considered the effect of the uneven distribution of continental areas through time (Vilhena & Smith, 2013) and the implications of applying different global tectonic reconstruction models (Scotese & Barrett, 1990; Ziegler *et al*. 2003) on latitudinal distribution of climate indicators.

In order to better understand the latitudinal distribution patterns of climate-sensitive lithologies and the associated climate change, we revisit a global-scale lithologic compilation of coals, evaporites and glacial deposits, with our analysis extending back to the Devonian period (~400 Ma ago). We test the sensitivity of their latitudinal distribution to uneven distribution of continental areas through time and to reconstruction models, and then quantify their

†Author for correspondence: wenchao.cao@sydney.edu.au

Table 1. Time division of the climate-sensitive lithologic indicators of Boucot, Chen & Scotese (2013) using the 2016 timescale of the International Commission on Stratigraphy (ICS2016). The reconstruction age is the rounded-off middle age of each time interval.

Era	Period	Epoch/Age	Start (Ma)	End (Ma)	Reconstruction age (Ma)
Cenozoic	Neogene	Miocene	23.0	5.3	14
	Palaeogene	Oligocene	33.9	23.0	28
		Middle and Late Eocene (Lutetian–Priabonian)	47.8	33.9	41
		Early Eocene (Ypresian)	56.0	47.8	52
		Palaeocene	66.0	56.0	61
Mesozoic	Cretaceous	Late Cretaceous (Coniacian–Maastrichtian)	89.8	66.0	78
		Late Cretaceous (Albian–Turonian)	113.0	89.8	101
		Early Cretaceous (Berriasian–Aptian)	145.0	113.0	129
	Jurassic	Late Jurassic	164	145	155
		Early and Middle Jurassic	201	164	183
	Triassic	Late Triassic	237	201	219
		Middle Triassic	247	237	242
		Early Triassic	252	247	250
Late Palaeozoic	Permian	Middle-Late Permian (Artinskian–Lopingian)	290	252	271
		Early Permian (Asselian–Sakmarian)	299	290	295
	Carboniferous	Late Carboniferous (Kasimovian–Gzhelian)	307	299	303
		Late Carboniferous (Bashkirian–Moscovian)	323	307	315
		Early Carboniferous (Serpukhovian)	331	323	327
		Early Carboniferous (Tournaisian–Visean)	359	331	345
	Devonian	Late Devonian	383	359	371
		Middle Devonian (Givetian)	388	383	386
		Middle Devonian (Eifelian)	393	388	391
		Early Devonian	419	393	406

distribution patterns with corrections of sampling- and continental area-bias, using Significant Zero crossings of the derivative (SiZer) of Chaudhuri & Marron (1999) to obtain the best-fitting probability density functions and Highest Density Regions (HDR) of Hyndman (1996) to compute 50 % and 95 % confidence intervals. The shifting latitudinal distribution patterns reflect climate change associated with humid/arid, precipitation/evaporation or cold/warm climatic conditions. To understand the mechanism, we compare the trends of latitudinal distribution patterns of these palaeoclimate deposits with the atmospheric CO_2 evolution (Foster, Royer & Lunt, 2017) and tropic mountain range areas derived from the palaeogeographic maps (Golonka *et al*. 2006; Cao *et al*. 2017) over time, as increased silicate weathering rates associated with tropical mountain uplift lead to a decrease in atmospheric CO_2 concentration and this may initiate glaciation (Tabor & Poulsen, 2008; Montañez & Poulsen, 2013; Goddeŕis *et al*. 2017; Swanson-Hysell & Macdonald, 2017).

2. Data and global plate tectonic models

We use a dataset of climate-sensitive lithologies, including coals, evaporites and glacial deposits (tillites, dropstones and glendonites), based on a comprehensive global-scale compilation (Boucot, Chen & Scotese, 2013). This compilation records and evaluates various types of climatically sensitive lithologic deposits, including coal, cyclothems, laterite, bauxite, lateritic manganese, oolitic ironstone, kaolinite, glendonite, tillites, dropstones, calcretes, evaporites, clay minerals, palms, mangroves and crocodilians, based on a comprehensive literature review. It covers geological times from the Cambrian period to the Miocene epoch. Each data point includes a reference source and geographic location. In order to analyse the effect of global climate change on the latitudinal distribution patterns of climate-sensitive lithologies, we use recorded occurrences of coals, (mostly marine) evaporites, and glacial deposits (a combination of tillites, dropstones and glendonites) in this study, as distributions of other lithologies included in the database are less reliable latitude indicators. For instance, the record of palms, mangroves and crocodilians suffers from sampling bias as they are mostly collected from middle–high latitudes, while sample sizes are small for laterites and oolitic ironstones.

The dataset used in this study covers Devonian to Miocene times and is divided into 23 time intervals at the scale of geological stages (Table 1). The time range that we assign to each data point is entirely derived from the time ranges that Boucot, Chen & Scotese (2013) used to draw the maps, and we use the middle ages of these time intervals to determine the reconstruction times (Table 1). We use modern peats (as they may eventually become coals), evaporites and glacial sediments (tillites and 'glacio-marine' beds) from Ziegler *et al*. (2003) for reference. Coals and peats are generally considered as indicators of terrestrial humidity, reflecting climatic regimes in which precipitation exceeds or is equal to evaporation (Parrish, Ziegler & Scotese, 1982; Hallam, 1985; McCabe & Parrish, 1992; Price, Sellwood & Valdes, 1995). Evaporites are formed in climatic conditions where evaporation exceeds the combined effects of precipitation, marine or river influx, and runoff (Craggs, Valdes & Widdowson, 2011), yet, they may occur in temperate regions (Boucot, Chen & Scotese, 2013). Tillites, dropstones and glendonites in the dataset are glacial or glacial-origin deposits indicating cold climate, generally due to high

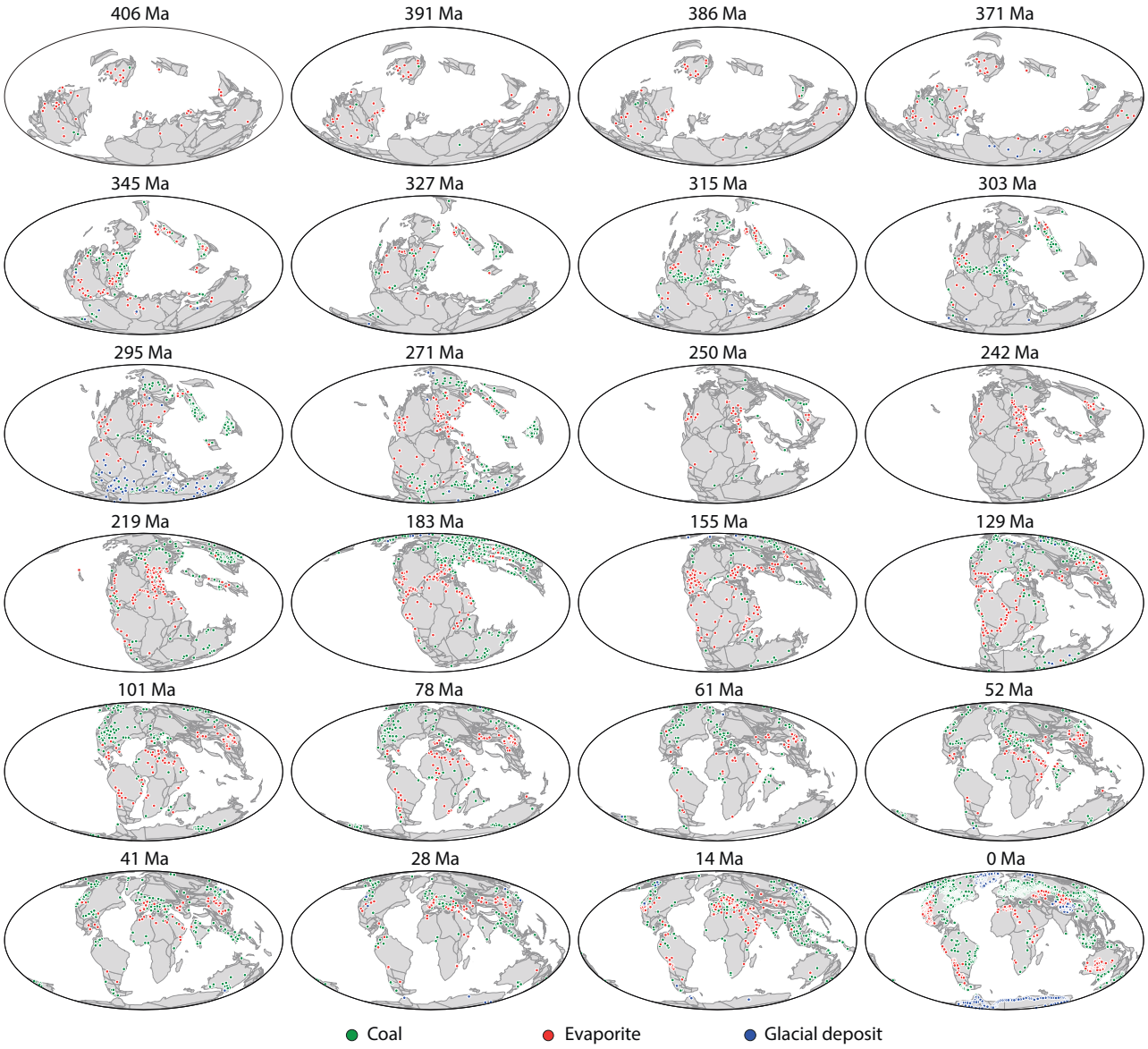

Figure 1. (Colour online) Locations of climate-sensitive lithologic data reconstructed using the plate motion model of Matthews *et al.* (2016): coals (green), evaporites (red) and glacial deposits (blue) since the Early Devonian (Ziegler *et al.* 2003; Boucot, Chen & Scotese, 2013). Ages at the top of each panel are reconstruction ages according to the timescale described in Table 1.

latitudes, but some could be related to high elevations (Boucot, Chen & Scotese, 2013).

The climatically sensitive lithologic deposits are distributed unevenly over different time intervals (Figs 1, 2). There are very few records of coals in the Devonian period (Figs 1, 2), with coals largely occurring in the Late Devonian stratigraphies (Boucot, Chen & Scotese, 2013). Yet a large number of coal records appear in Carboniferous, Permian, Late Triassic, Early Jurassic and Neogene times (Figs 1, 2a). Evaporites have relatively uniform richness over most of the time intervals, except in Devonian, Late Carboniferous, Early Permian and Palaeogene times (Figs 1, 2b), whereas, glacial deposit records are relatively rare and sparse over time (Figs 1, 2c) due to the dominance of greenhouse conditions in the Phanerozoic (Hay, 2016).

In this study, we primarily use the global plate tectonic model of Matthews *et al.* (2016) to reconstruct the lithologic data points back in time from present-day geographic locations. This tectonic model represents a combination of a tectonic model for Mesozoic and Cenozoic times (230–0 Ma) (Müller *et al.* 2016) and a tectonic model for Palaeozoic times (410–250 Ma) (Domeier & Torsvik, 2014), with a number of changes required to enable a smooth merging of the models as described by Matthews *et al.* (2016). It is a relative plate motion model that is ultimately tied to Earth's spin axis through an absolute reference frame (Matthews *et al.* 2016). We removed the true polar wander correction from the original absolute plate motion model (Domeier & Torsvik, 2014) to tie the relative rotations to a palaeomagnetic reference frame. Therefore, the tectonic reconstruction better reflects

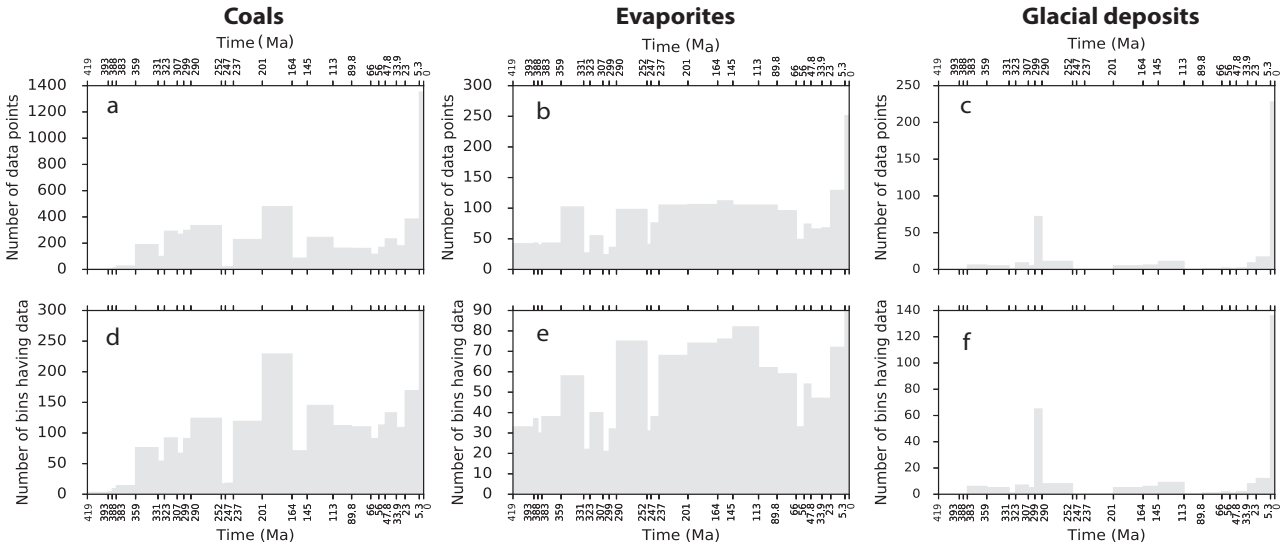

Figure 2. (a, b, c) Sum of data points of coals, evaporites and glacial deposits at each time interval since the Devonian period. (d, e, f) Sum of resampled data points for coals, evaporites and glacial deposits at each time interval since the Devonian period.

the true palaeolatitudinal distribution of palaeoclimate indicators (van Hinsbergen *et al*. 2015).

In order to test the sensitivity of the palaeolatitudinal distribution of climate-sensitive deposits to the choice of reconstruction model, except for the plate motion model of Matthews *et al*. (2016), we use two alternative reconstruction models of Scotese (2008) and Golonka (2007) which are both based on the reconstruction of Scotese (2004). The reconstruction model of Golonka (2007) uses palaeomagnetic data to constrain the palaeolatitudinal positions of continents and rotation of plates, and hot spots, where applicable, are used as reference points to calculate palaeolongitudes. A version of this model that includes an updated absolute reference frame is described in Wright *et al*. (2013), and the model is available in the supplementary materials of Wright *et al*. (2013). The reconstruction model of Scotese (2008) uses palaeomagnetic reference frames for 410–250 Ma (Ziegler *et al*. 1979) and 250–100 Ma (Ziegler, Scotese & Barrett, 1983), and a hotspot reference frame for 100–0 Ma (Müller, Royer & Lawver, 1993).

3. Methods

We first reconstructed the lithologic data for coals, evaporites and glacial deposits from their modern locations to ancient locations in geological time (Fig. 1) using the global plate motion model of Matthews *et al*. (2016). Due to the inconsistency of age assignments between some lithologic data and "underlying" terrane polygons, leading to unexpected reconstructed locations of these lithologic data, we only considered the data points whose time ranges of existence were within the time span and present-day spatial extent of the underlying terrane. We next binned the data points using a 5° × 5° mesh of the global surface, following Ziegler *et al*. (2003) (Fig. 3b). Each bin contained a

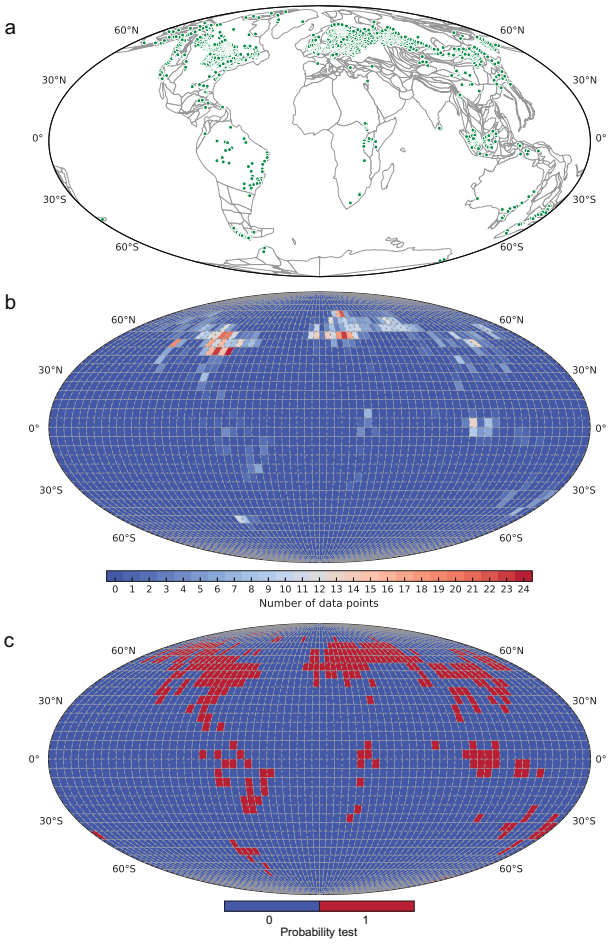

Figure 3. (Colour online) (a) Present-day locations of modern global peats (green points) from Ziegler *et al*. (2003). Grey polygons are modern terrane geometries. (b) Distribution of modern peat points binned using a 5°×5° mesh of the global surface. (c) Distribution of resampled modern peat points (red: bins containing at least one data point; blue: bins containing no data points).

variable number of data points or none; for example, a bin could contain 0–24 data point(s) for modern peats at present-day coordinates (Fig. 3b). The recorded data points were unevenly distributed spatially (Fig. 3a, b), largely due to sampling bias. To remove the bias, we resampled the data by collapsing all the samples into a single value for each bin: 1 where data existed (Fig. 3c, red bins), and 0 where there were no data points (Fig. 3c, blue bins). We subsequently summed up the numbers of resampled data in each 5° latitudinal strip (Fig. 4b). These steps significantly reduced the numbers of data points considered per latitudinal strip (compare the *y*-axis of Fig. 4a, b).

Plate tectonic motion (Golonka, 2007; Scotese, 2008; Matthews *et al*. 2016) leads to a biased distribution of lithologic deposits on Earth. Latitude bands containing more continental area are more likely to have more lithologic deposits preserved. In an attempt to remove this bias, we first calculated the continental area covered by each 5° latitudinal strip at each time interval since the Devonian period (Fig. 4c), using the HEALPix pixelization method that results in equal sampling of data on a sphere (Gorski *et al*. 2005) and therefore equal sampling of surface areas. We next corrected the number of resampled lithologic data in a 5° latitudinal strip using the continental area in the same strip to remove the bias due to the uneven distribution of continental areas through time. Subsequently, the results were scaled to represent probabilities of data appearing in a 5° latitudinal strip (Fig. 4d). In order to investigate the palaeolatitudinal zonal patterns of these climate indicators, we combined the data corrected for continental area bias from both hemispheres to form symmetric and composite zonal patterns, and normalized the results in a strip into probabilities with respect to the sum of all the values in the same strip (Fig. 4e). The symmetric zonal patterns erased the differences between the two hemispheres and can be used to indicate the influence of climate change on the distribution of climate-sensitive lithologic deposits (Scotese & Barrett, 1990; Ziegler *et al*. 2003).

We used SiZer (SIgnificant ZERo crossing of the derivatives; by Chaudhuri & Marron, 1999), a data analysis method to identify significant peaks from kernel density estimation to obtain probability density functions of zonal patterns (Fig. 4f, black lines). Instead of trying to find the one bandwidth that provides the closest match to the unknown true density, SiZer looks at the whole range of bandwidths. Peaks and troughs are identified by finding the regions of significant gradient (zero crossings of the derivative; Chaudhuri & Marron, 1999). In order to identify high-density intervals of distribution of these palaeoclimate indicators, we used the HDR method of Hyndman (1996) to compute the high-density latitude ranges with 50 % (Fig. 4f, grey area) and 95 % (Fig. 4f, light grey area) confidence intervals. HDR is a statistical method for calculating confidence intervals when the sampling distribution has multiple peaks. For discrete-valued distribution, HDR simply consists of those elements of

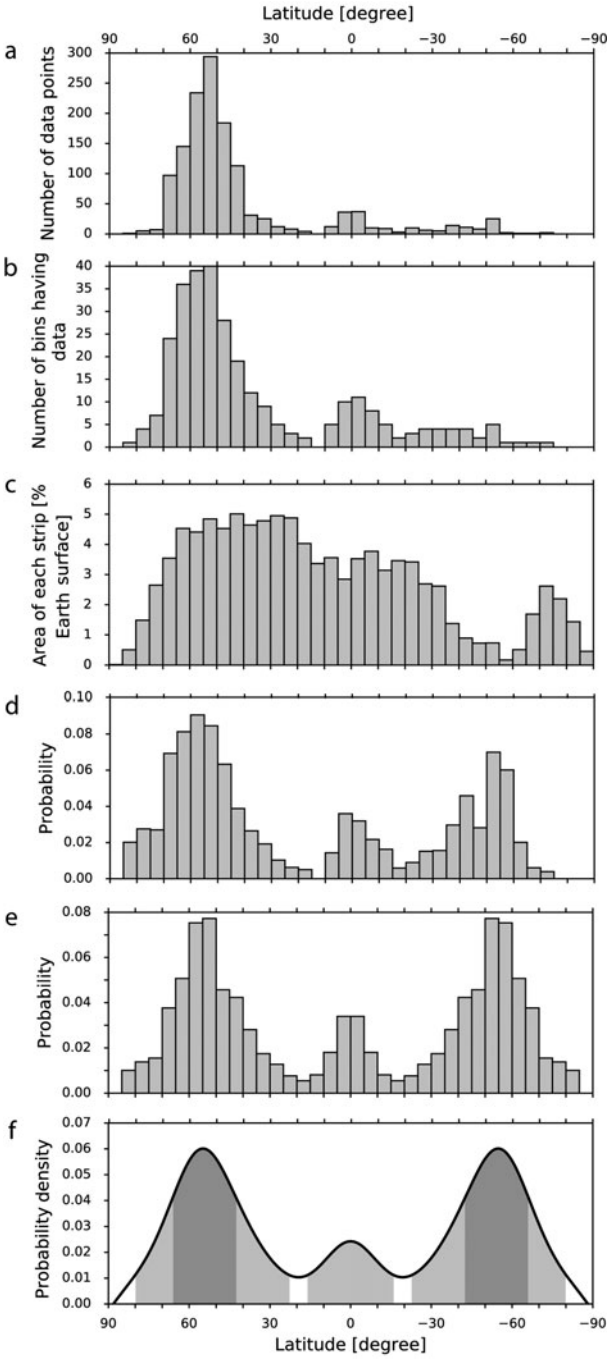

Figure 4. (a) Number of original modern peat points from Ziegler *et al*. (2003) in each 5° latitudinal strip. (b) Number of resampled modern peat points in each 5° latitudinal strip. (c) Modern continental area in each 5° latitudinal strip as a percentage of total modern continental area. (d) Distribution of resampled modern peat points with continental area bias corrected. (e) Distribution of modern peat points with sampling- and area-biases corrected. The two hemispheres are combined to form a symmetric distribution pattern (also known as zonal pattern; Scotese & Barrett, 1990; Ziegler *et al*. 2003). (f) Fitted probability density function (black line) using the method of SiZer from Chaudhuri & Marron (1999). High-density latitude ranges at confidence intervals of 50 % (grey area) and 95 % (light grey area) using the HDR method of Hyndman (1996).

the sample space with highest probability (Hyndman, 1996).

4. Results

4.a. Palaeolatitudinal distribution of coals, evaporites and glacial deposits

We counted the original data points for coals (Fig. 5a), evaporites (Fig. 6a) and glacial deposits (Fig. 7a) reconstructed using the plate tectonic model of Matthews *et al*. (2016) in each 5° latitudinal strip at each time interval since the Devonian period. Coals are distributed in a wide latitude range from the equator to the poles (Fig. 5a), while evaporites are concentrated between 60° N and 60° S (Fig. 6a). Glacial deposits generally occur in middle–high latitudes except for a record of glendonites appearing near the equator in the Early Carboniferous (Tournaisian–Visean) from an outer shelf environment with near-0°C seawater (Brandley & Krause, 1993*a*, *b*, 1994), a record of tillites in the Late Carboniferous (Kasimovian–Gzhelian) and a record of tillites in the Early Permian, both from a high-elevation periglacial environment (Becq-Giraudon, Montenat & Van den Driessche, 1996) (Fig. 7a). Therefore, these three records (highlighted with question marks in Fig 7) may not be reliable enough to indicate cold climate relevant to latitudinal change.

Generally, more data points of coals (Fig. 5a), evaporites (Fig. 6a) and glacial deposits (Fig. 7a) are sampled from the northern than the southern hemisphere since Pangaea break-up in the Early Jurassic (Ronov, Khain & Seslavinsky, 1984; Ronov, Khain & Balukhovsky, 1989; Scotese, 2001, 2004; Golonka *et al*. 2006; Blakey, 2008). During Early Devonian – Late Triassic time, the numbers of data points of these lithologies in the southern hemisphere exceed those in the northern hemisphere in general, with glacial deposits only occurring in the southern hemisphere in Early Devonian and Carboniferous times (Fig. 7a). This mainly reflects the fact that plate tectonic motions modify the continental configuration through time, which has led to more continental areas in the northern hemisphere since the Early Jurassic (Figs 5c, 8). Continental areas in the northern hemisphere have consistently increased since the Devonian period, while the areas in the southern hemisphere have decreased accordingly (Figs 5c, 8).

After removing the sampling- (Figs 5b, 6b, 7b) and continental area-biases (Figs 5d, 6d, 7d) over the data in each 5° strip at each time interval, the differences among strips at a time interval are evened out to some degree (for example, compare the *y*-axis of Fig. 5a, b, d). The zonal patterns for coals (Fig. 5e), evaporites (Fig. 6e) and glacial deposits (Fig. 7e) vary considerably over time.

We compute the high-density latitudinal ranges with 50 % and 95 % confidence intervals for coals (Fig. 5f), evaporites (Fig. 6f) and glacial deposits (Fig. 7f), respectively, at each time interval. Considering the extent of these 95 % confidence ranges, coals are relatively widely distributed on Earth's surface over the time period of interest, extending from the equator to the poles for many time periods (Fig. 5f, light grey area). Evaporites (95 % confidence) are generally concentrated within low–middle latitudes (0–60°) in two hemispheres, with a mean palaeolatitude of $26 \pm 3°$ in each hemisphere since the Devonian (Fig. 6f, light grey area). This result is consistent with the mean palaeolatitudes of $23 \pm 4°$ during Cenozoic–Mesozoic time and $21 \pm 4°$ during Permian–Carboniferous time (both with 95 % confidence), recalculated from palaeolatitudes of a global compilation of large evaporite basins extending back through Proterozoic time (Evans, 2006). Glacial deposits (95 % confidence) occur in Late Devonian, Carboniferous, Permian, Jurassic, Early Cretaceous and Late Palaeogene–modern times (Fig. 7f, light grey area). This is generally consistent with three main Phanerozoic ice ages during Carboniferous–Permian, Late Jurassic – early Cretaceous and Early Eocene–modern times (Frakes, Francis & Syktus, 1992).

Focusing on 50 % confidence intervals, coal latitudinal belts show strong fluctuation over time (Fig. 5f, dark grey area). They move from the middle latitudes towards the equator during the Devonian, but the original coal deposits in the Devonian are too few to provide much climatological insight (Boucot, Chen & Scotese, 2013). During the Carboniferous, they are strictly limited within 0–25° N and S; however, they separate into two latitudinal belts of 0–10° and 40–60° during the earliest Permian (Asselian–Sakmarian) (Fig. 5f). Subsequently, they undergo a poleward shift until reaching higher latitudes (60–90°) during the Late Jurassic, with a sharp equatorward movement in the Early Triassic and a rapid poleward shift in the Middle Triassic but these may be not reliable as they are based on very few data points (Figs 1, 2a). Starting from the Early Cretaceous, the distributions of coals contract towards the equator until the Miocene when there are two latitudinal belts at ∼30–50° and ∼0–15° on two hemispheres, with a rapid shift towards the equator during the Early Eocene. Modern peats are mainly distributed within ∼40–65° latitudes. Overall, the latitudinal belts determined for coals from probability density curves with 50 % confidence generally occur at low latitudes during Palaeozoic time, middle latitudes during Permian, Triassic and Cenozoic times, and high latitudes during Jurassic and Cretaceous times.

Evaporite latitudinal belts with 50 % confidence (Fig. 6f, grey area) mostly occur at low latitudes (∼0–30° N and S). They move poleward from the Early Devonian until the Early Carboniferous and then towards the equator until the Late Triassic. Starting from the Middle Triassic, they start to shift poleward until modern times at a mean latitude of ∼35° N and S, with a short and rapid poleward movement during the early Eocene (Lutetian).

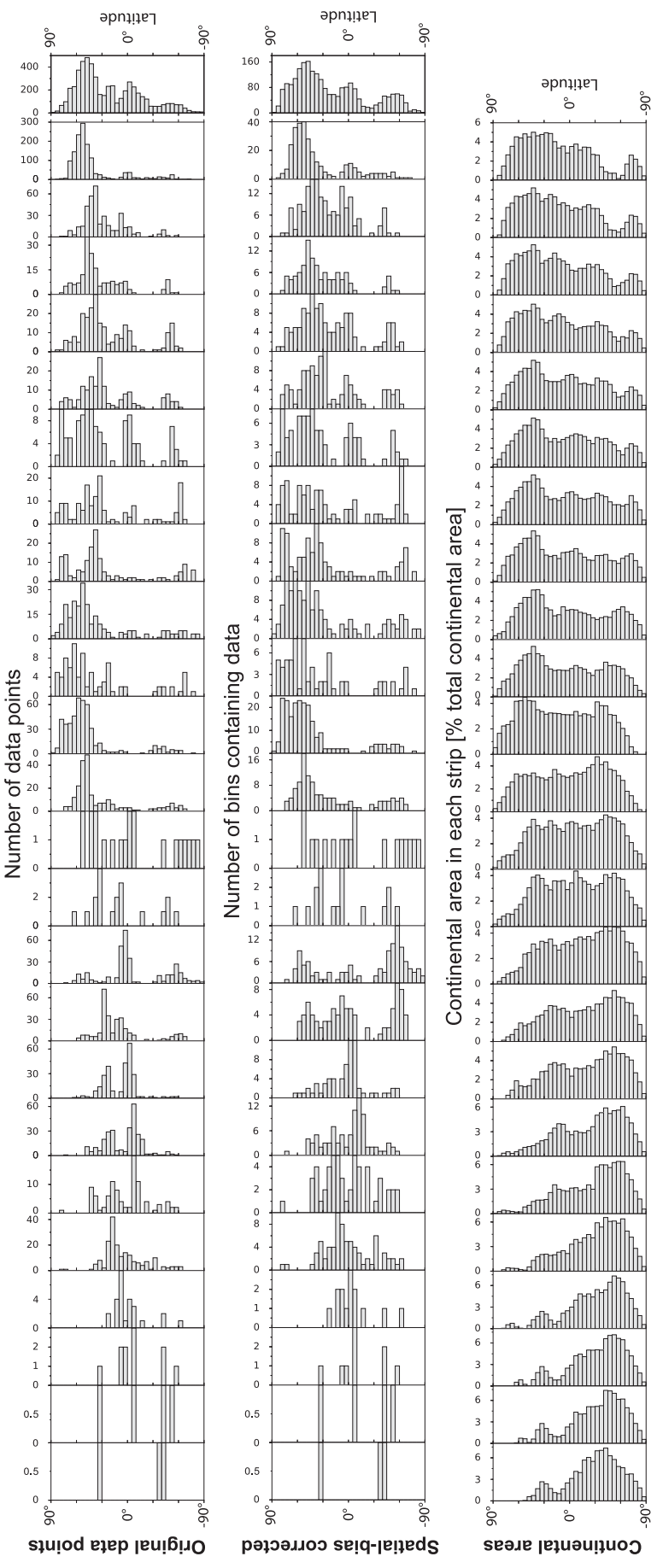

Figure 5. (a) Numbers of original coal points of Boucot, Chen & Scotese (2013) and Ziegler *et al.* (2003) reconstructed using the tectonic model of Matthews *et al.* (2016) in each 5° latitudinal strip for each time interval since the Devonian period. (b) Number of resampled coal points in each 5° latitudinal strip for each time interval. (c) Continental area in each 5° latitudinal strip as a percentage of Earth's surface for each time interval. (d) Distribution of coals with continental area corrected in each 5° latitudinal strip for each time interval. (e) Symmetric zonal pattern of coals with sampling- and continental area-biases removed. (f) Probability density function of symmetric zonal pattern of coals for each time interval. The cumulative results for all times are presented on the rightmost side with bold borders.

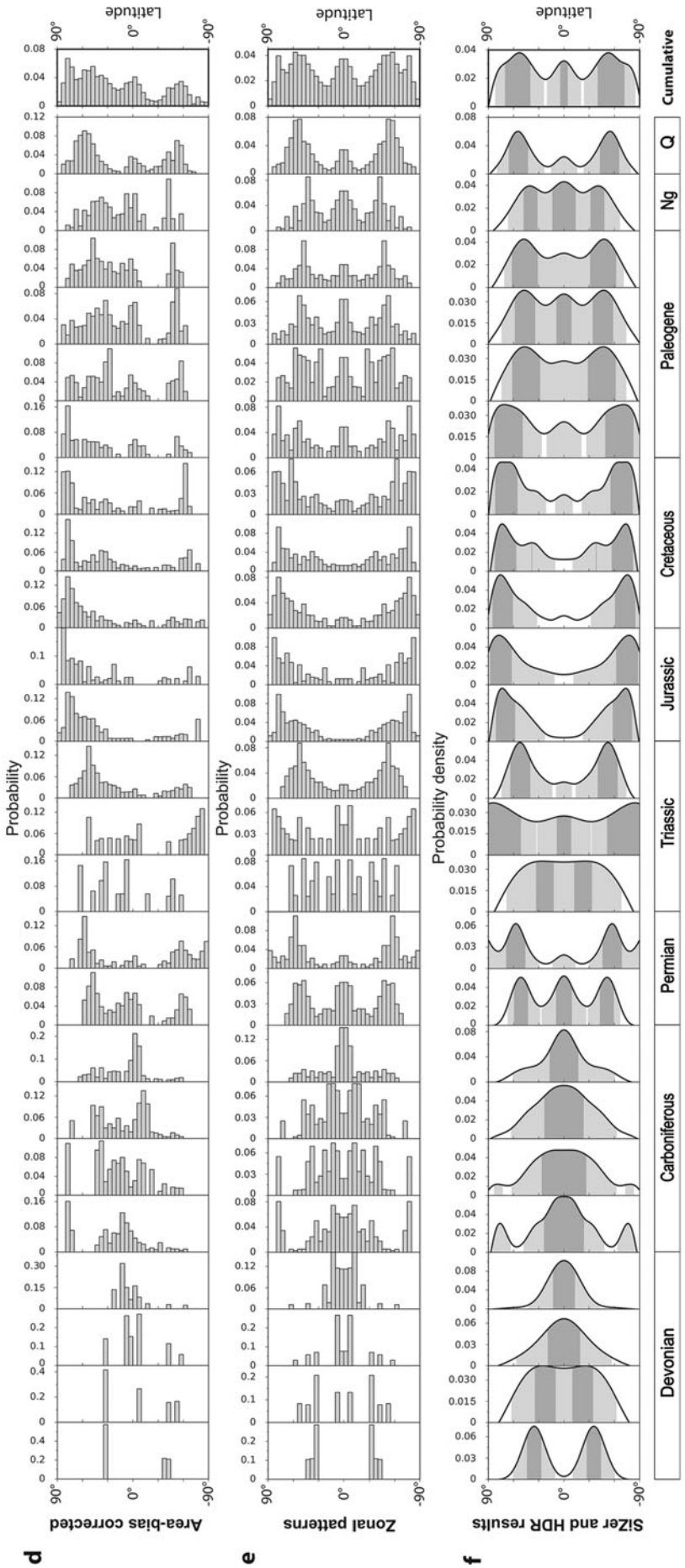

Figure 5. Continued.

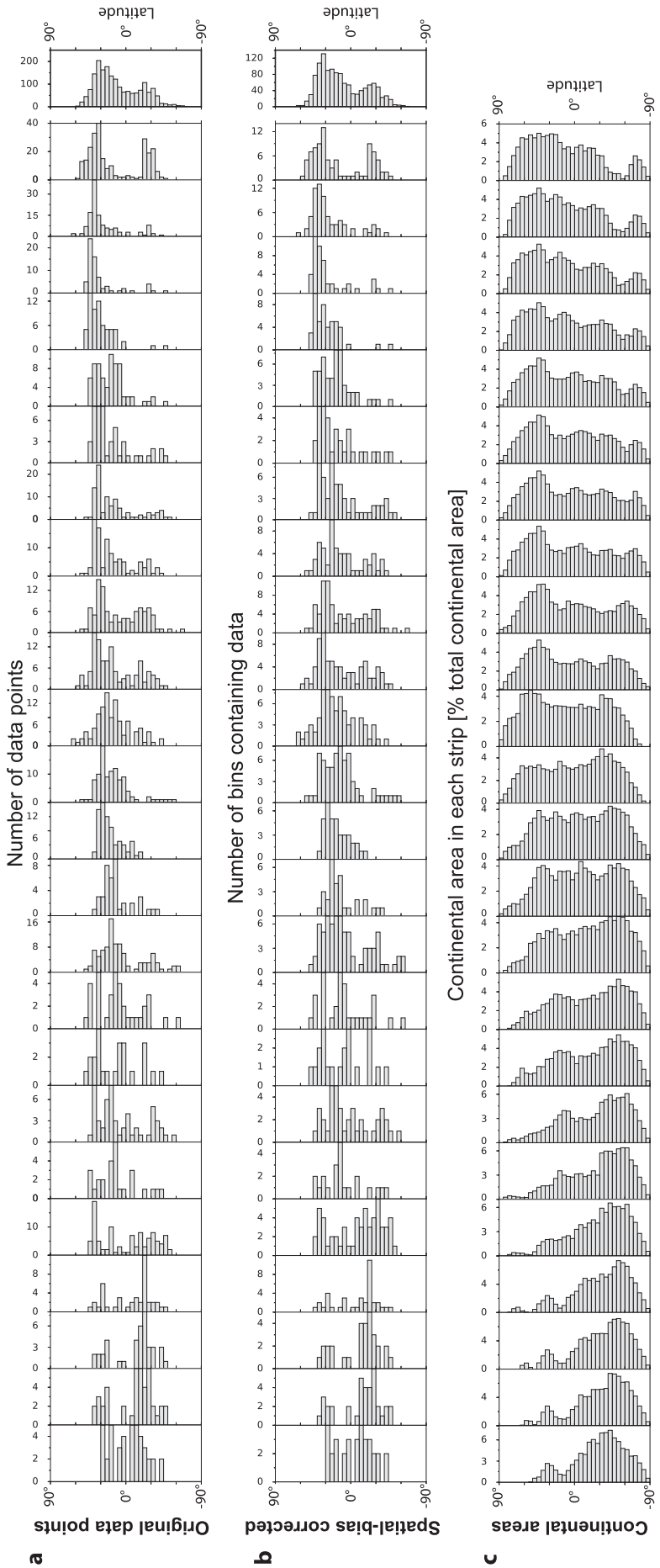

Figure 6. (a) Number of original evaporate points of Boucot, Chen & Scotese (2013) and Ziegler *et al.* (2003), reconstructed using the tectonic model of Matthews *et al.* (2016), in each 5° latitudinal strip for each time interval since the Devonian period. (b) Number of resampled evaporate points in each 5° latitudinal strip for each time interval. (c) Continental area in each 5° latitudinal strip as a percentage of total continental area for each time interval. (d) Distribution of evaporites with continental area corrected in each 5° latitudinal strip for each time interval. (e) Zonal pattern of evaporites with sampling- and continental area-biases corrected. (f) Probability density function of zonal pattern of evaporites for each time interval. The cumulative results for all times are presented on the rightmost side with bold borders.

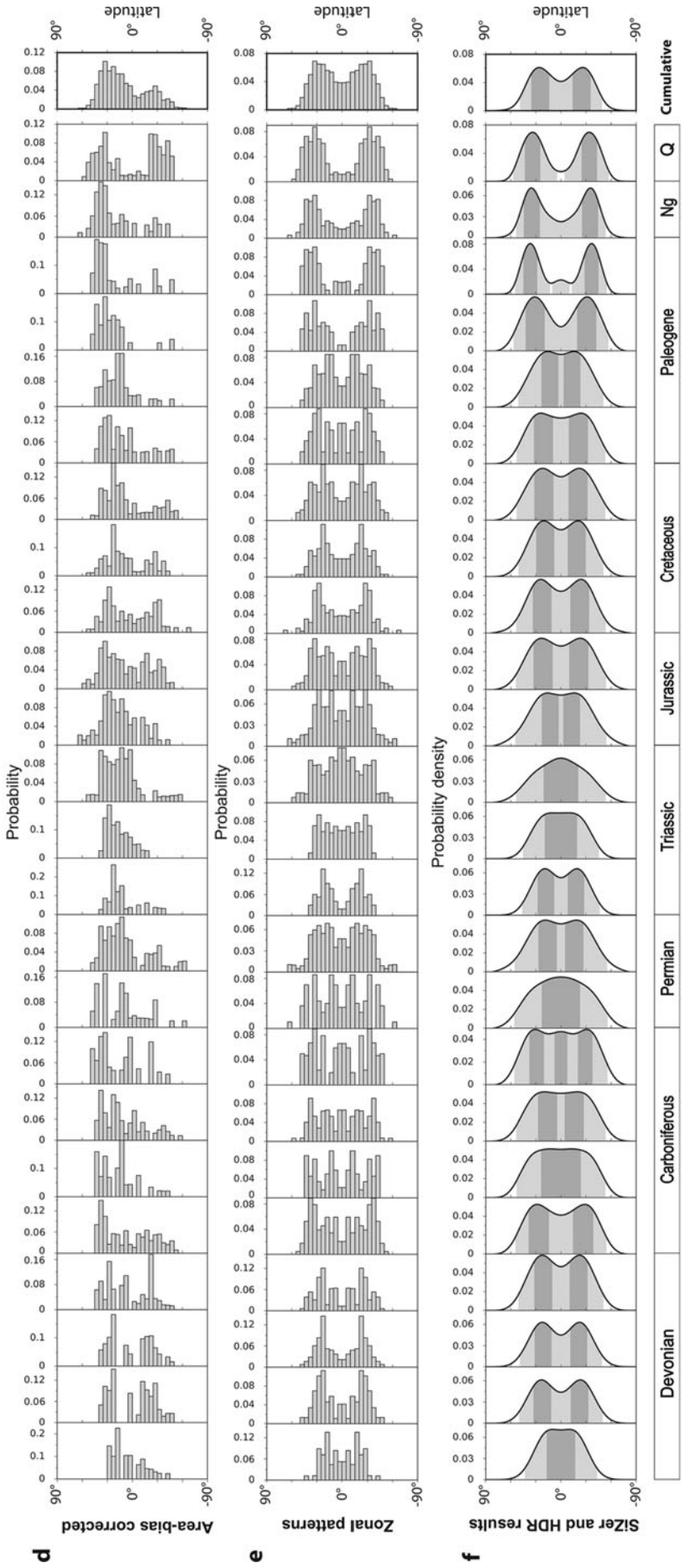

Figure 6. Continued.

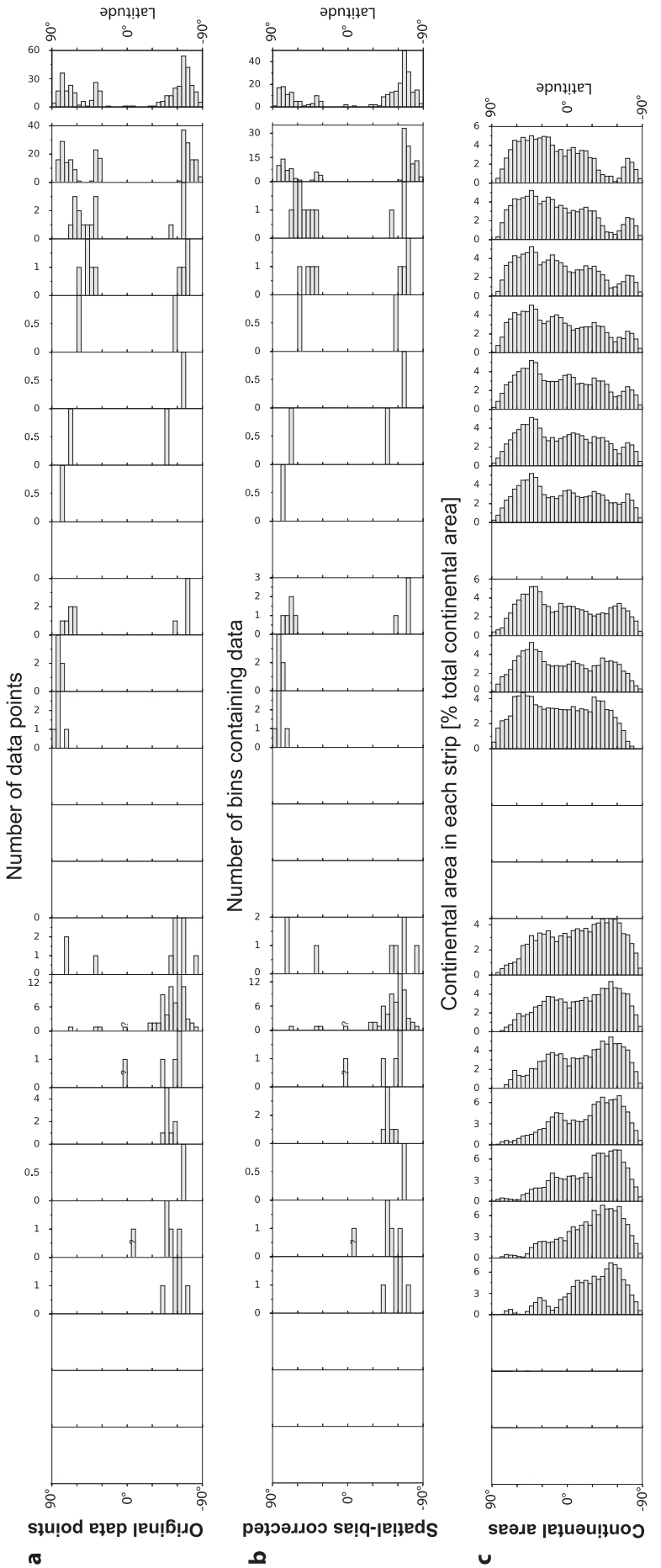

Figure 7. (a) Numbers of original glacial deposit points of Boucot, Chen & Scotese (2013) and Ziegler *et al.* (2003) reconstructed using the tectonic model of Matthews *et al.* (2016) in each 5° latitudinal strip for each time interval since the Devonian period. (b) Number of resampled glacial deposit points in each 5° latitudinal strip for each time interval. (c) Continental area in each 5° latitudinal strip as a percentage of total continental area for each time interval. (d) Distribution of glacial deposit with continental area corrected in each 5° latitudinal strip for each time interval. (e) Zonal pattern of glacial deposit with sampling- and continental area-biases corrected. (f) Probability density function of zonal pattern of glacial deposits for each time interval. The troughs with a question mark indicate records unlikely to represent latitudinal changes in climate. The cumulative results for all times are presented on the far right with bold borders.

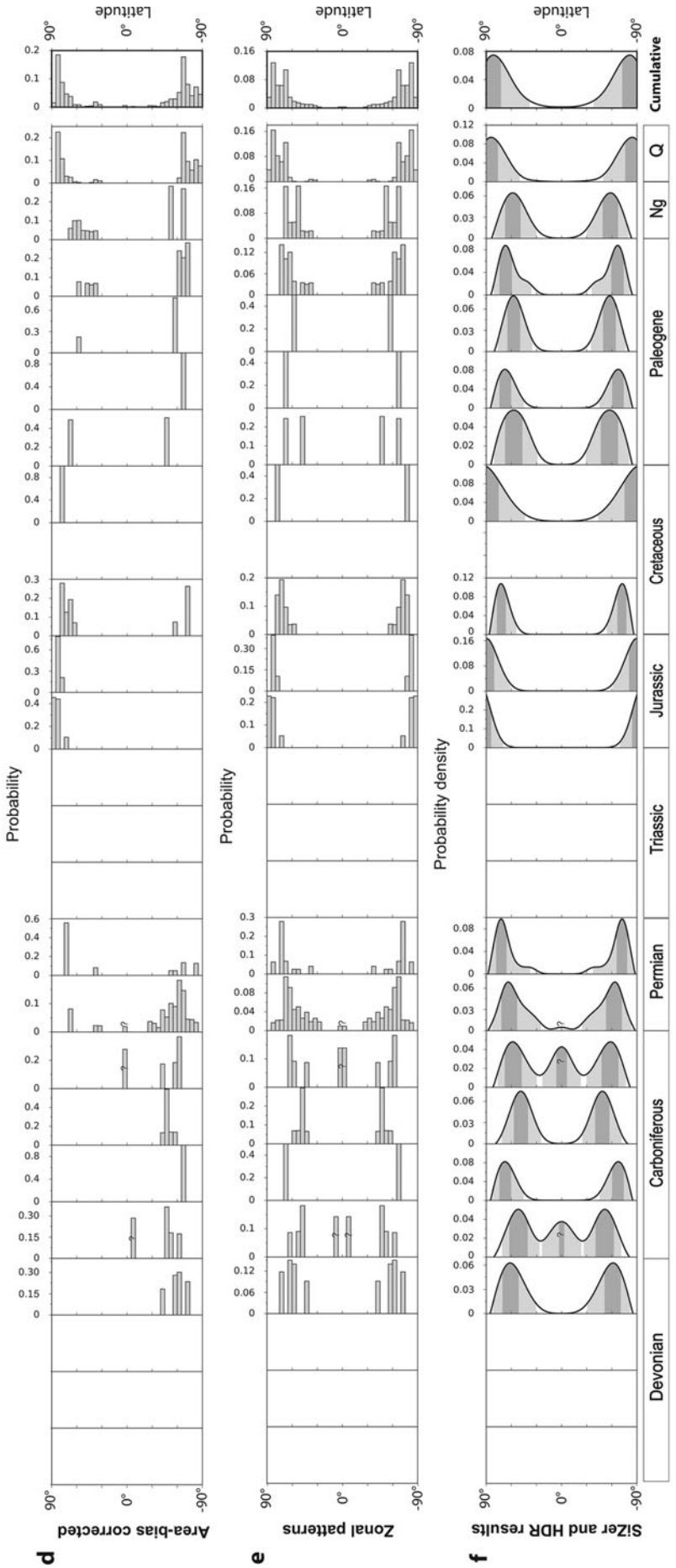

Figure 7. Continued.

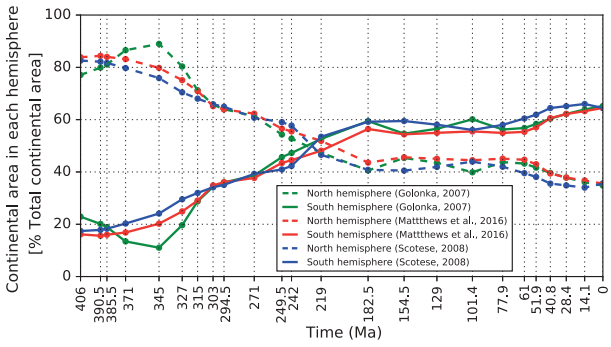

Figure 8. (Colour online) Continental area in the northern and southern hemispheres respectively as a percentage of total continental area at each time interval since the Devonian period.

The trends in how the highest-density latitudes of glacial deposits with 50 % confidence (Fig. 7f, grey area) shift northwards or southwards are similar to coals, but at higher latitude. They generally concentrate within middle–high latitudes through time (Fig. 7, grey area). They occur at ∼50–70° N and S latitudes during the Late Devonian and then move equatorward to middle latitudes (∼40–60°) during most of the Carboniferous, with a rapid poleward movement in the Late Mississippian. The Late Pennsylvanian – Early Permian transition is marked by a rapid shift of glacial deposits towards high latitudes. They remain at high latitudes during Jurassic and Cretaceous times, and then move to middle–high latitudes (∼50–75°) during Palaeogene and Miocene times. Modern glacial deposits mainly lie near the poles.

4.b. Sensitivity tests

4.b.1. Assumption of climate symmetry (zonal patterns)

In order to test the assumption that past climates were zonal and hemispherically symmetric, we investigated the latitudinal distributions of lithologies for each hemisphere independently through time, and estimated their high-density latitudinal belts using the same statistical methods (Supplementary Figs S1 and S2, available at https://doi.org/10.1017/S0016756818000110). At the first order, more lithologic data are distributed on the northern hemisphere over the timeframe, except for late Palaeozoic and Cenozoic times when more glacial deposits formed in the southern hemisphere. The distributions of coals and evaporites in the northern hemisphere (Supplementary Figs S1 and S2, available at https://doi.org/10.1017/S0016756818000110) are similar to the results with data combined over two hemispheres (Fig. 12a, c, further below). This is largely because of the uneven distribution of continental areas through time, leading to a biased distribution of lithologic deposits in the northern hemisphere. Overall, the data distribution warrants combining the two hemispheres in zonal patterns.

4.b.2. Continental area bias

In order to examine sensitivity of the zonal patterns of these lithologic deposits to continental area bias, we compute the zonal patterns for coals (Fig. 9a), evaporites (Fig. 9b) and glacial deposits (Fig. 9c) for each time interval since the Devonian using the plate motion model of Matthews *et al*. (2016) with (Fig. 9, blue area) and without (Fig. 9, red) continental area correction, respectively. The distribution patterns of coals using the two approaches are significantly different in Middle Devonian, most of Carboniferous, Early and Middle Triassic, Jurassic, Cretaceous and Early Palaeogene times. During these time periods except the Middle Devonian, the zonal patterns of coals without continental area correction are closer to the equator (Fig. 9, red). This mainly results from the uneven latitudinal distribution of continental areas, with very little to no continental coverage near the poles during these periods (Fig. 5c). Due to relatively small continental coverage near the equator (Fig. 5c), the zonal patterns of coals without area correction are closer to the poles during the Middle Devonian (Fig. 9, red).

The uneven distribution of continental areas through time has relatively less impact on the zonal patterns of evaporites (Fig. 9b) and glacial deposits (Fig. 9c). Evaporite zonal patterns are generally identical over time, except during Late Mississippian, Late Pennsylvanian, the earliest Permian, Middle Triassic and late Cretaceous times (Fig. 9b). Due to different continental coverage at different latitudes (Fig. 5c), the area correction leads to more poleward distributions of evaporites during Late Mississippian, Late Pennsylvanian and earliest Permian times but more equatorward during Middle Triassic and late Cretaceous times. With and without area correction, glacial deposit zonal patterns are mostly identical over time, except for most of Permian, Late Palaeogene and modern times, when the area correction results in more poleward distributions, and for Early and Late Mississippian and Late Pennsylvanian times, with more equatorward distributions (Fig. 9c). Overall, latitudinal distributions of coals show stronger sensitivity to uneven distributions of continents than evaporites and glacial deposits, which could be mainly due to coals having a wider latitudinal distribution than evaporites and glacial deposits over time.

4.b.3. Reconstruction model bias

We use alternative reconstruction models of Scotese (2008) and Golonka (2007) with modifications as described in Wright *et al*. (2013), in addition to the model of Matthews *et al*. (2016), to analyse the sensitivity of latitudinal distributions of coals, evaporites and glacial deposits to the reconstruction model. We use the same method described in the Methods section to obtain the probability density functions of the latitudinal distributions for these lithologies over time. The results indicate that the three reconstructions result in

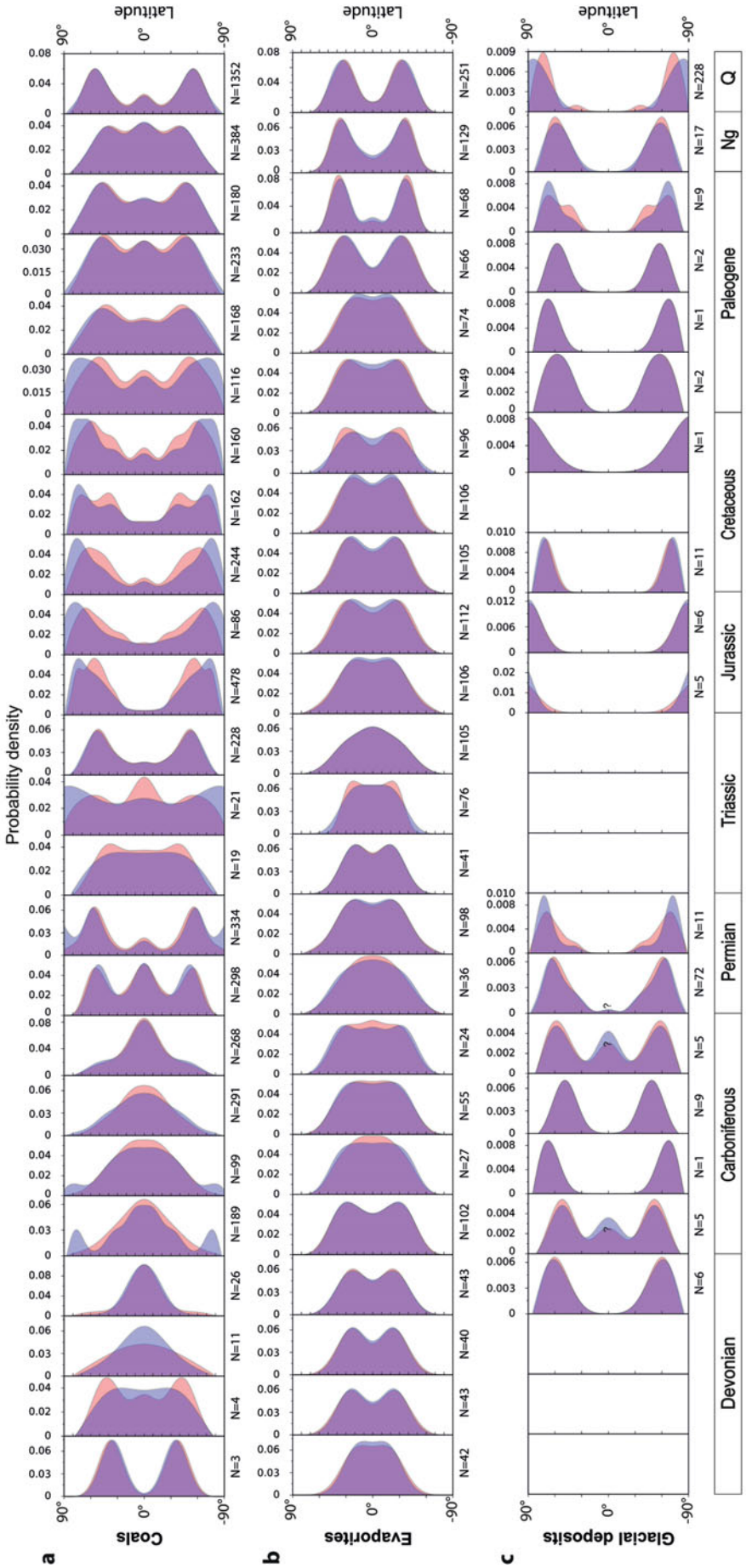

Figure 9. (Colour online) Zonal patterns of lithologic deposits of coals (a), evaporites (b) and glacial deposits (c), with continental area bias correction (blue) and without continental area bias correction (red), for each time interval since the Devonian period using the plate motion model of Matthews *et al.* (2016). The number of original data points at each time interval is reported at the bottom of each subplot.

only second-order differences through time (Fig. 10). Differences in the distributions are most pronounced where reconstructed palaeolatitudes differ for blocks that host a large proportion of data points for a given time interval.

The latitudinal distributions of coals reconstructed using the three tectonic models are generally similar over time, except during Early Devonian, Early Carboniferous, the earliest Permian, Middle and Late Palaeogene and Neogene times. In the Early Devonian, the latitudinal distributions of coals using the reconstruction of Golonka (2007) are more northward than those using the other two reconstructions, largely because North America and Eurasia in the model of Golonka (2007) are located further northward than in the other two models during this period (see Supplementary Material available at https://doi.org/10.1017/S0016756818000110). The more poleward location of Africa during the Early Carboniferous in the reconstruction of Matthews *et al*. (2016) leads to a more poleward distribution of coals. During the earliest Permian, numerous coal deposits occur in North and South China blocks. Their more northward locations in the model of Matthews *et al*. (2016), taken from the work of Domeier & Torsvik (2014), result in more occurrences at middle latitudes (see Supplementary Material available at https://doi.org/10.1017/S0016756818000110). The terranes in the reconstruction of Scotese (2008) are generally further north relative to the other two models during Middle and Late Palaeogene and Neogene times (see Supplementary Material available at https://doi.org/10.1017/S0016756818000110). This results in more poleward distributions of overall palaeoclimate lithologies (Fig. 10a).

The latitudinal distributions of evaporites among the three reconstructions are very similar since the Devonian (Fig. 10b), except for Early Devonian and Carboniferous times. In the Early Devonian, evaporites are spread further from the equator using the reconstruction of Golonka (2007) than the other two reconstructions, which is mainly due to more northward locations of North America and Eurasia in the model of Golonka (2007). More southward locations of numerous plates in the reconstruction of Golonka (2007) (see Supplementary Material available at https://doi.org/10.1017/S0016756818000110) result in more equatorial distributions of evaporites during the Carboniferous (Fig. 10b).

The latitudinal distributions of glacial deposits are also similar through time among the three considered reconstructions (Fig. 9c), except for the Late Devonian, Early and Middle Mississippian and most of the Permian. During the Late Devonian, more glacial deposits are distributed at high latitudes using the reconstruction of Scotese (2008), mainly due to the more southerly location of South America in this reconstruction than that in the other two reconstructions (see Supplementary Material available at https://doi.org/10.1017/S0016756818000110). The more equatorial locations of South America and NW Africa in the model of Scotese (2008) lead to more equatorial distributions of glacial deposits during Early and Middle Mississippian times. During most of the Permian period, Antarctica and Australia are closer to the South Pole in the reconstruction of Golonka (2007) (see Supplementary Material available at https://doi.org/10.1017/S0016756818000110), resulting in more poleward distribution of glacial deposits (Fig. 10c).

4.b.4. Spatial sampling resolution bias

We compare the use of three different spatial resolutions to bin the original data points to remove the effect of sampling bias on the distribution patterns of these climatically lithologic deposits, using the plate motion model of Matthews *et al*. (2016), for each time interval since the Devonian period: 10° (Fig. 11a), 5° (Fig. 11b) and 2° (Fig. 11c). The results indicate that there are too few strips containing data points, especially during the Devonian, to be able to obtain much statistical significance using 10° as the binning size (Fig. 11a). Using 2° as the binning size results in noisier distributions (Fig. 11c) and a more difficult analysis of distribution patterns. A spatial resolution of 5° is a good compromise that captures the data distribution yet results in less noise, and follows previous work that aids comparison with our work (Fig. 11b).

5. Discussion

5.a. Palaeolatitudinal distribution patterns of lithologic climate indicators over time

We present the high-density latitudinal ranges in one hemisphere, due to the assumed symmetry of two hemispheres, with 50 % and 95 % confidence intervals for coals (Fig. 12a), evaporites (Fig. 12b) and glacial deposits (Fig. 12c), respectively, at each time interval. We also present the cumulative high-density latitudinal ranges over the entire time period for these lithologies (rightmost panels in Fig. 12a, b, c). Overall, the latitudinal belts determined from probability density curves with 50 % confidence for coals have changed since the Devonian. Some previous studies concluded that the palaeolatitudinal distribution of coals has remained broadly similar since the Permian (Ziegler *et al*. 2003), whereas we have shown that results for earlier in the Palaeozoic are significantly different from results from the Permian to present (Fig. 12a, b, c). In addition, the temporal division at the scale of geological periods in previous studies did not attempt to resolve variations over shorter time periods, whereas the dataset used in this study is based on a time division at the scale of geological stages. The temporal resolution based on the scale of geological periods does not allow us to capture variations of latitudinal distribution patterns of climate-sensitive lithologic deposits within geological periods, such as the significant movement towards the equator from probability density curves with

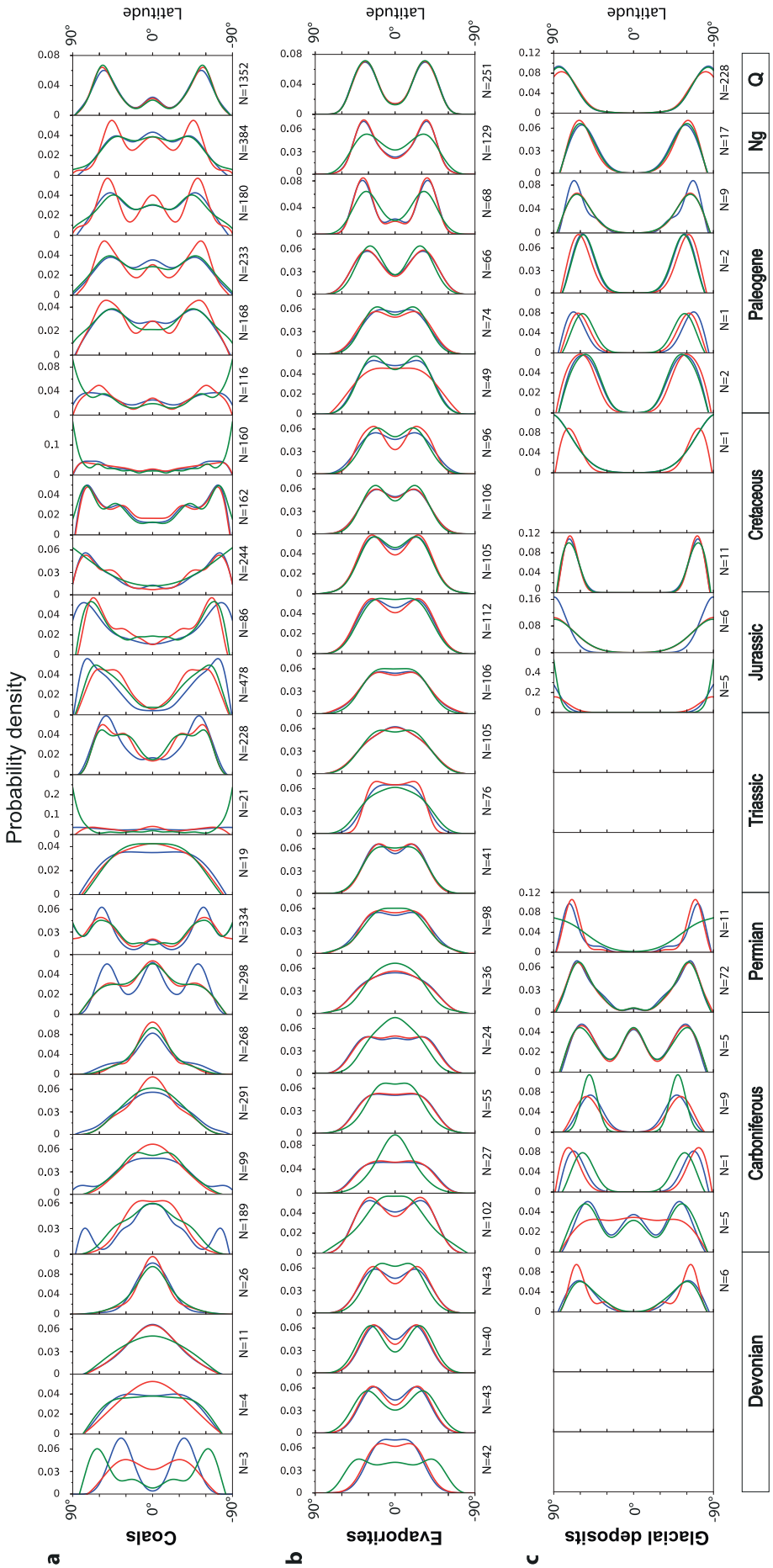

Figure 10. (Colour online) Latitudinal distribution of coals (a), evaporites (b) and glacial deposits (c), for each time interval since the Devonian period, using three reconstruction models (blue: Matthews *et al.* 2016; red: Scotese, 2008; green: Golonka, 2007). The number of original data points at each time interval is reported at the bottom of each subplot.

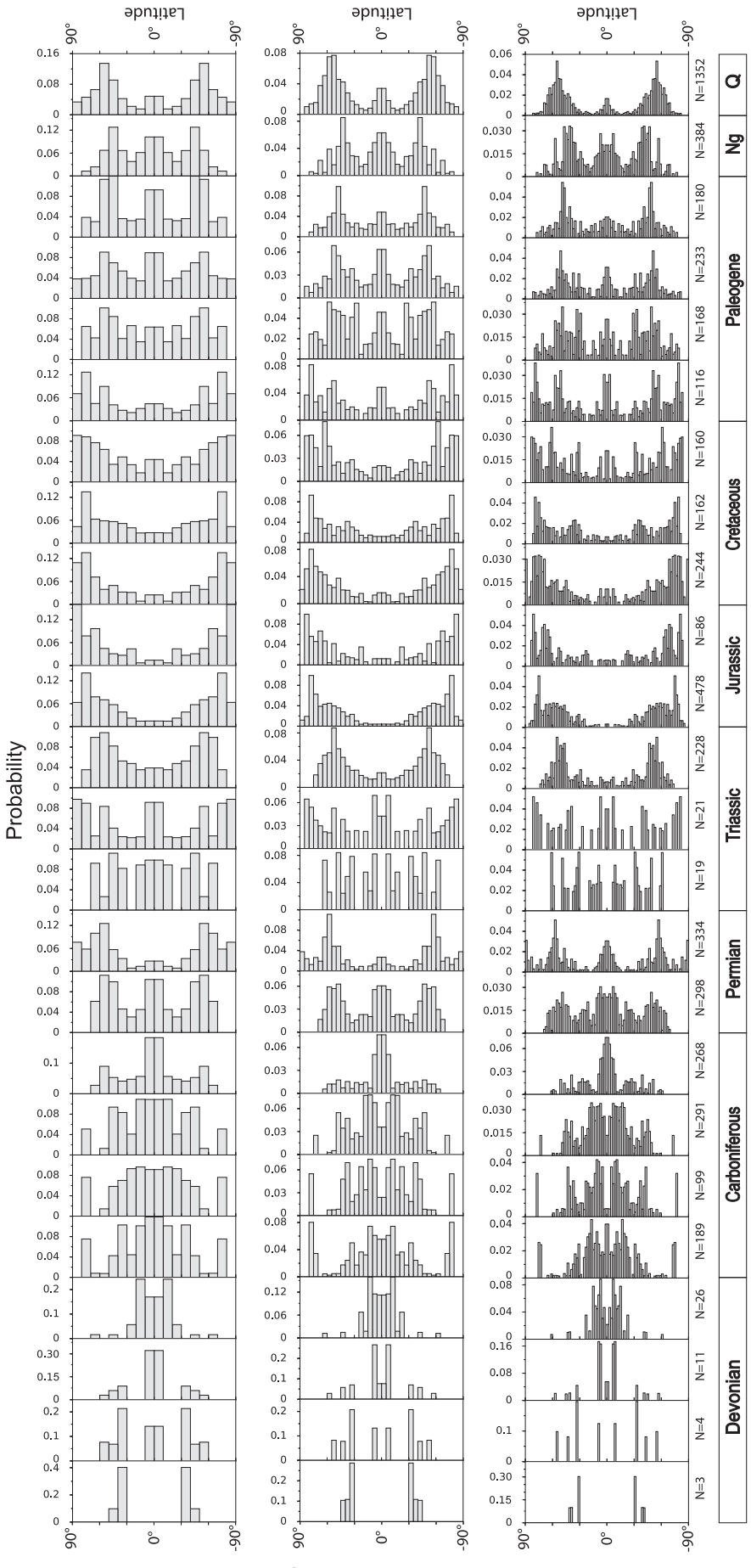

Figure 11. Distribution patterns of coals, reconstructed using the plate motion model of Matthews *et al.* (2016), for each time interval since the Devonian period using three different bin sizes (red: 10° (a); blue: 5° (b); green: 2° (c)) to bin data points to in order to remove the sampling bias. The number of original data points at each time interval is reported at the bottom of each subplot.

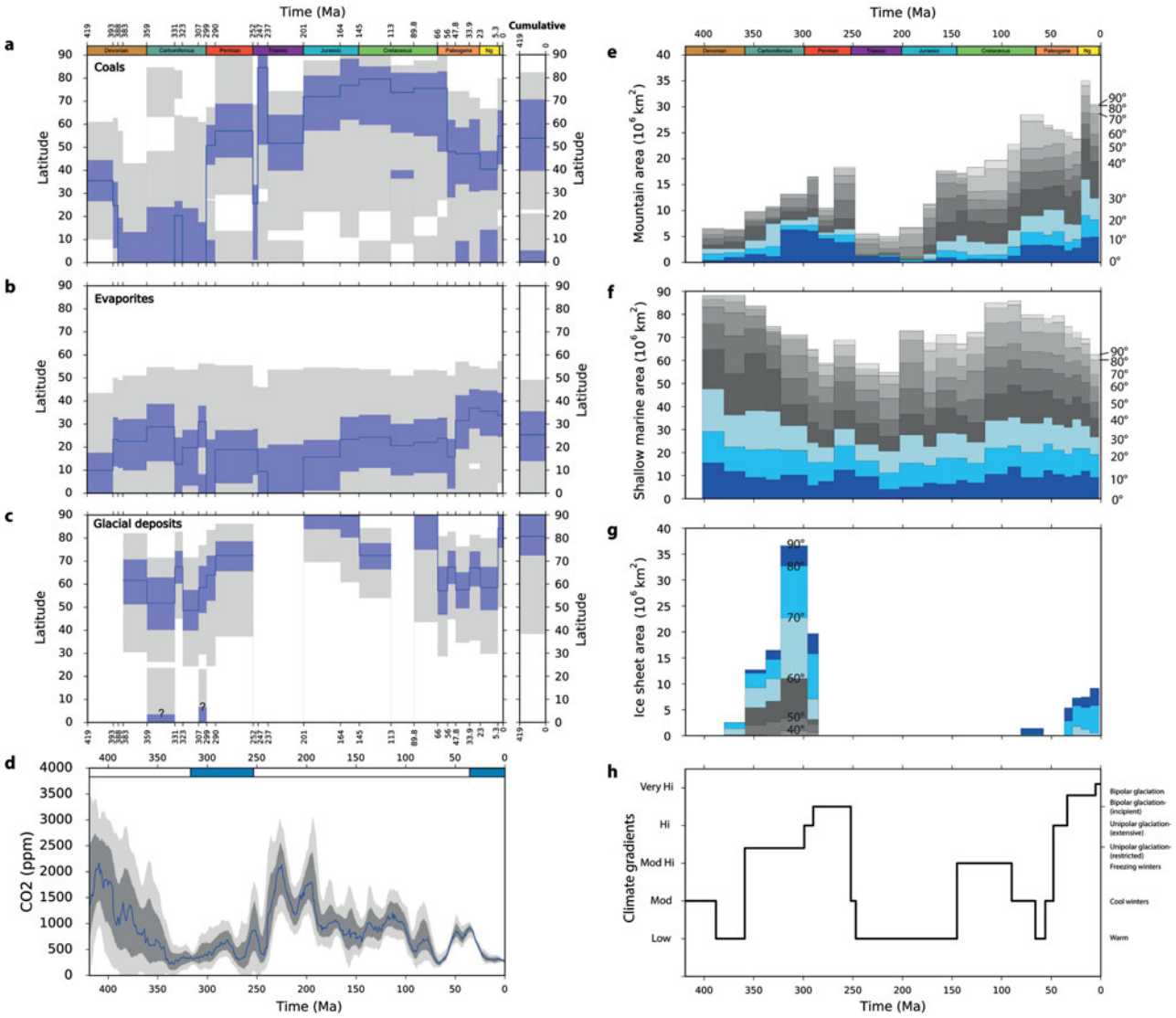

Figure 12. (Colour online) (a, b, c) High-density latitudinal belts of coals, evaporites and glacial deposits, with 50 % (blue area) and 95 % (light grey area) confidence intervals for each time interval since the Devonian period. The blue lines are the most significant peaks of latitudinal distribution. The areas with a question mark indicate records of limited use for climate interpretation. Cumulative high-density probabilities are presented on the rightmost side with bold borders. (d) Atmospheric CO_2 concentration curve since the Devonian period, derived from Foster, Royer & Lunt (2017). 68 % and 95 % confidence intervals are shown as dark and light grey bands. The blue line represents a locally weighted scatterplot smoothing (LOESS) fit, a nonparametric regression fit from Cleveland & Devlin (1988), through the data. Icehouse intervals and greenhouse intervals (Hay, 2016) are indicated by a blue band and a white band, respectively, at the top of the panel. (e) Global palaeolatitudinal distribution of mountain ranges since the Devonian period calculated from the set of palaeogeographic maps (Golonka *et al*. 2006; Cao *et al*. 2017). (f) Global palaeolatitudinal distribution of shallow marine environments (Golonka *et al*. 2006; Cao *et al*. 2017). (g) Global palaeolatitudinal distribution of ice sheets from the palaeogeographic maps (Golonka *et al*. 2006; Cao *et al*. 2017). (h) Climate temperature gradients since the Early Devonian derived from Boucot, Chen & Scotese (2013).

50 % confidence for coals between Early Palaeogene and Middle Palaeogene times in Figure 12a.

Highest-density latitudinal belts of evaporites with 50 % confidence exhibit relatively subtle shifts within a narrow range of latitudes over time (Fig. 12b), although they are very similar to the cumulative result covering the entire temporal range (right panel in Fig. 12b). Evans (2006) suggested that evaporite palaeolatitudes remain stable during Cenozoic–Mesozoic times (a mean palaeolatitude of $23 \pm 4°$) and during Devonian–Ediacaran times (a mean palaeolatitude of $14 \pm 2°$). This might be because the time division, weighting method or source dataset of Evans (2006) does not capture variations of mean latitudes of evaporites at finer-resolution time divisions. In addition, Evans (2006) argued that the distribution of evaporites over the past 2 billion years has remained bimodal about the equator rather than being centred on the equator as expected from general-circulation climate simulations (Hunt, 1982; Jenkins, 2000, 2001). These considerations are important to test predictions from climate models with differing obliquities. Our

results generally indicate a bimodal distribution of evaporites over the past ~400 Ma, except for Early Devonian, Early Carboniferous (Serpukhovian), earliest Permian (Asselian–Sakmarian) and Middle and Late Jurassic times during which the distribution is unimodal (Fig. 6f). These unimodal distributions should be treated with caution, since comparison with the unsmoothed distributions (Fig. 6e) suggests that the smoothing of the SiZer algorithm contributes to the existence of unimodal distributions in the final results. However, it is also apparent in both the smoothed and unsmoothed results that the clear bimodal pattern observed for the most recent time intervals is not clearly resolved within many older temporal intervals.

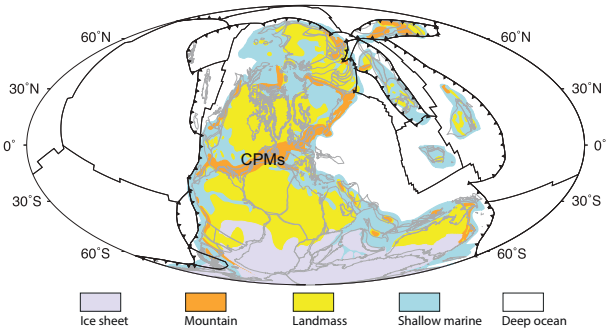

Figure 13. (Colour online) Global palaeogeography in the Late Carboniferous from Cao *et al.* (2017) showing the location of the Central Pangaean Mountains (CPMs). Black toothed lines indicate subduction zones, and other black lines denote middle-ocean ridges and transforms. Grey outlines delineate reconstructed present-day coastlines and terranes. Mollweide projection with 0° E central meridian.

5.b. Contributors to the palaeolatitudinal distribution of climate-sensitive lithologies

The evolution of latitudinal belts of coal samples with 50 % confidence interval (Fig. 12a) may reflect the complex Phanerozoic fluctuations in the latitudinal extent of continental humid zones. The latitudinal distribution of coals with 50 % confidence changes over long timescales (Figs 5, 12a), being concentrated at low latitudes during the Carboniferous period, middle latitudes during Permian and Triassic times, high latitudes during Jurassic – Early Palaeogene times, before returning to middle latitudes during Middle Palaeogene–modern times. The distribution during the Devonian period is unlikely to be reliable due to a lack of data samples (Figs 1, 2). The Carboniferous period is significantly different from post-Palaeozoic times (Fig. 12a). Abundant coal samples were accumulated in tropical regions (~0–25° N and S) during the Carboniferous period, while they were mostly deposited at middle or high latitudes during Mesozoic and Cenozoic times (Fig. 12a). This shift could indicate a climatic transition from humid to arid conditions from the Late Pennsylvanian through the Early Permian on equatorial Pangaea (Rowley *et al.* 1985; Ziegler, 1990; Parrish, 1993; Ziegler, Hulver & Rowley, 1997; Tabor & Montañez, 2004; Montañez *et al.* 2007; Tabor *et al.* 2008; Tabor & Poulsen, 2008). Tabor & Poulsen (2008) evaluated the climate factors possibly explaining this climate change, including changing continental configurations from tectonics, time-varying land–sea distribution, supercontinentality, monsoon, uplift/collapse of the Central Pangaean Mountains (CPMs) (Fig. 13), waxing and waning of ice sheets in Gondwanaland and atmospheric CO_2. They suggested that the northward drift of most of Pangaea across climate zones, increasing atmospheric CO_2 level and Gondwanaland deglaciation could have been the main factors controlling the low-latitude climate of Pangaea during Late Pennsylvanian – Early Permian times. The deglaciation of Gondwanaland is considered to be a possible cause of climate change over low-latitude Pangaea through its influence on large-scale atmospheric circulation (Ziegler *et al.* 1987; Perlmutter & Matthews, 1989; Cecil, 1990; Miller & West, 1993; Miller, McCahon & West, 1996; Soreghan, 1997; Cecil *et al.* 2003; Perlmutter & Plotnick, 2003; Poulsen *et al.* 2007). Late Palaeozoic climate simulations suggest that the deglaciation of Gondwana and atmospheric CO_2 rise could explain much of the Late Palaeozoic climate change over low-latitude Pangaea, and regional uplift/erosion of the CPMs has a secondary effect on tropical precipitation (Peyser & Poulsen, 2008). However, the change from dominantly humid palaeoclimate indicators in Pennsylvanian strata to arid and seasonal indicators in Permian strata is considered possibly related to the evolution of the CPMs (Goddéris *et al.* 2017).

We compared our results to a recent estimate of atmospheric CO_2 since the Devonian period (Foster, Royer & Lunt, 2017; Fig. 12d), and to additional aspects of Earth's palaeogeographic history extracted from digital palaeogeographic reconstructions (Golonka *et al.* 2006; Cao *et al.* 2017; Fig. 12e–g). Atmospheric CO_2 levels do not indicate significant changes at the beginning of the Permian period that would directly coincide with the poleward shift in coal distributions. The areas of tropical mountain ranges close to the equator (Fig. 12e), thought to be regions of significantly enhanced weathering rates, similarly do not record a significant change from the Late Pennsylvanian through the Early Permian (Fig. 12e). In addition, we computed Phanerozoic ice-sheet areas from palaeogeographic maps (Golonka *et al.* 2006; Cao *et al.* 2017), and the results indicate that ice sheets indeed considerably reduced during the Late Pennsylvanian – Early Permian transition (Fig. 12g). Plate tectonic configurations (Golonka, 2007; Scotese, 2008; Matthews *et al.* 2016) indicate that most of Pangaea moved rapidly northward during the Late Pennsylvanian – Early Permian transition. Walker, Wilkinson & Ivany (2002) argued that these motions influenced patterns of shallow-marine carbonates during Phanerozoic times through a long-term decrease in areas of tropical shelf

based on the palaeogeographic atlas of Scotese & Golonka (1992), although, a persistent decrease in the area of tropical shallow marine environments over the past ~400 Ma is less apparent in palaeogeographic maps of Golonka *et al*. (2006) and Cao *et al*. (2017) (Fig. 12f). The resulting migration of tropical basins from humid climate zones associated with the Intertropical Convergence Zone into the adjacent northern subtropical zone could be attributed to long-term tropical aridification (Ziegler *et al*. 1977; Witzke, 1990; Gibbs *et al*. 2002; Rees *et al*. 2002; Tabor *et al*. 2008).

It is important to consider some non-climatic factors that may influence the latitudinal distributions of these lithologies. Carboniferous coal-forming flora were dominated by pteridophytes with a low tolerance to groundwater fluctuations due to their shallow root system, making them less likely to form thick preserved coal seams even where favourable peat-forming conditions existed (Diessel, 1992). In contrast, post-Carboniferous coal measures were dominated by Gymnosperms from the Permian to the Cretaceous and angiosperms since the Triassic. They can occupy a wider range of latitudes due to their greater tolerance to groundwater fluctuations and adaptability in more fully marginal peat-forming conditions (Diessel, 1992). The evolution of plant groups through space and time could contribute to the changing distributions of coal deposits through time, especially its significant poleward shift in the Early Permian. Additionally, a further contributor to the Carboniferous low-latitude peak in coal distribution could be the relatively rare occurrence of extensive foreland-basin systems within the tropics during Pangaea assembly, ideal for the formation and preservation of coal (Nelsen *et al*. 2016). In summary, the major poleward shift in coal distributions beginning in the Early Permian is likely to be driven by a combination of processes, resulting from the interplay of tectonics, deglaciation, evolution of plants and palaeoclimate.

The changing latitudinal belts of evaporites with 50 % confidence (Fig. 12b) indicate the evolution of low-latitudinal arid zones over time, but the fluctuations are subtle relative to other indicators. During the Early Palaeogene, they underwent a relatively rapid shift away from the equator, contemporaneous with climate-driven shifts in coals and glacial deposits. In older times, the origins of changes are less clear (Fig. 12b). Ancient marine evaporite formation is not only related to dry climate but also tectonic setting (Warren, 2010). For instance, during the Early Devonian, many evaporites occurred in the northern margins of tropical Laurentia and low-latitude Siberia (Fig. 1), which could explain the equatorial distribution of evaporites during the time (Fig. 12b). The latitudinal belt of evaporites shifts poleward to mean latitudes of ~25° N and S during Middle Devonian – Early Carboniferous time (Fig. 12b). This could be mostly due to evaporites accumulating in the southern, western or eastern margins of Laurentia during the Middle Devonian – Early Carboniferous time (Fig. 1). From the assembly of Pangaea in the Late Carboniferous until the Middle Triassic (Ziegler *et al*. 1979), abundant evaporites occur in the western and eastern margins of low-latitude Pangaea (Fig. 1). Starting from the Late Triassic (~240 Ma) the pattern of rift basins formed during Pangaea break-up (notably the Atlantic margins and the Gulf of Mexico) will have exerted an additional control on evaporite distributions (Fig. 1).

Atmospheric CO_2 is thought to be a primary driver of both ice-sheet and climate variability (Montañez & Poulsen, 2013; Lowry *et al*. 2014; Foster, Royer & Lunt, 2017), and solar luminosity secondarily influences Palaeozoic glaciation (Lowry *et al*. 2014). Mountain uplift enhances silicate rock weathering, resulting in a decrease in atmospheric CO_2 concentrations (Kump & Arthur, 1997; Berner, 2004; Montañez & Poulsen, 2013; Foster, Royer & Lunt, 2017). The latitudinal distribution patterns of glacial deposits reported in this study (Fig. 12c) record three major Phanerozoic glacial periods, during Carboniferous–Permian, Late Jurassic – early Cretaceous and Cenozoic times (Frakes, Francis & Syktus, 1992). The late Palaeozoic icehouse is the longest-lived ice age of the Phanerozoic (Montañez & Poulsen, 2013). Ice sheets were abundant over the South Pole during this period. This ice age corresponds to intense mountain uplift around tropical Pangaea (Fig. 12e) which could have contributed to late Palaeozoic cooling through enhanced silicate weathering (Kump *et al*. 1999; Goddéris *et al*. 2017). The high temperature gradients during the time, derived from the comprehensive global-scale compilation of lithologies (Boucot & Gray, 2001; Boucot, Chen & Scotese, 2013), also indicate a cooling (Fig. 12h). The Cenozoic glaciation corresponds to remarkable topographic uplift (Fig. 12e) of the Himalaya – Tibetan Plateau (Molnar & England, 1990) contributing to atmospheric CO_2 decrease through enhanced silicate weathering and resulting high temperature gradients (Fig. 12h). Therefore, our results suggest that mountain uplift could have been an important factor in the two major ice ages in late Palaeozoic and Cenozoic times through decreased atmospheric CO_2 and enhanced temperature gradients. Yet, other factors including organic carbon burial and outgassing through volcanism and metamorphism (e.g. Pearson & Palmer, 2000) might also contribute to the drawdown of atmospheric CO_2.

5.c. Workflow limitations

The presented workflow uses a 5°×5° grid of Earth's surface to bin lithology data points. By resampling the data points, we removed the spatial sampling bias. However, latitude strips at or near the equator have larger areas than the polar ones (see fig. 1 in Vilhena & Smith, 2013), which leads to over-binning in high-latitude strips. Ideally, an equal-area gridding scheme would be created to correct spatial sampling bias in the dataset (Vilhena & Smith, 2013), and this

could be considered in future work. However, we used the simpler 5° × 5° binning so that our results are comparable to the previous study of Ziegler *et al*. (2003).

There is also a temporal sampling bias in the workflow. The reconstruction ages used to construct the climatically sensitive lithologic data to ancient geographic locations represent discrete time periods of several millions of years. Because the reconstructed palaeogeographic locations of the lithologic data points change within the time range for which their age is assigned in the source data, sample locations are not truly defined by one point palaeolocation, and could be represented by an average location over a given time period in future work. Providing a continuous representation of palaeolatitudinal distribution patterns indicated from palaeoclimate lithologic data remains an important challenge. The temporal resolution in this study does not allow us to capture some short-term fluctuations which may be interpreted from more detailed records (e.g. Horton, Poulsen & Pollard, 2010; Montañez *et al*. 2016). For instance, our workflow considers the time interval 290–252 Ma during the Permian period as a single stage, and cannot reflect the fluctuations indicated from atmospheric CO_2 level during that time (Fig. 12a, d). Higher temporal resolution would make it possible to refine climate reconstructions.

A further improvement to our analysis could be to use palaeogeographic maps rather than continental polygons to correct for the bias due to the uneven distribution of areas through time over the lithologic data. Such maps have the potential to provide a clearer definition of which areas within the continental polygons used here are likely to host certain types of lithologies associated specifically with shallow marine or terrestrial environments. However, such palaeogeographic maps (e.g. Ronov, Khain & Seslavinsky, 1984); Ronov, Khain & Balukhovsky, 1989); Scotese, 2001, 2004; Golonka *et al*. 2006; Blakey, 2008; Cao *et al*. 2017) are more interpretive than continental polygons and typically do not use divisions of the geological timescale that are exactly consistent either with each other or with the time range definitions of the lithologic data considered here, and remains an outstanding problem in terms of how to obtain palaeogeographic maps and lithologies at the same temporal resolution.

6. Conclusions

This study provides a framework to investigate the shifting climatic zones through deep geological time by using plate reconstructions, a comprehensive database and new data analysis approaches. We quantified the palaeolatitudinal zonal patterns of climate-lithologic deposits of coals, evaporites and glacial deposits since the Devonian, with corrections for sampling- and area-biases, and used statistical methods (SiZer and HDR) to obtain probability density functions and estimate high-probability latitudinal belts. The sensitivity test of the latitudinal distributions of climate-sensitive lithologic deposits on uneven distribution of continental areas through time indicates that these climate indicators are sensitive to the correction of continental areas, and that the distribution of coals is more sensitive than evaporites and glacial deposits to this correction, particularly in Middle Devonian, Carboniferous, Early and Middle Triassic, Jurassic, Cretaceous and Early Palaeogene times. The latitudinal distributions of these lithologic indicators do not show strong sensitivity to the reconstruction model.

The distribution of coal palaeolatitudes herein, with higher temporal resolution than previous studies, shifted to significantly higher latitudes at the beginning of the Permian, contrasting with the previous suggestion that the shift started in the Carboniferous (Diessel, 1992). The changing distribution of coals over the period from the Permian to the present also cannot be considered to have been constant as proposed by Ziegler *et al*. (2003). Our results indicate a clearly bimodal distribution of evaporites over the past ∼400 Ma, except for the Early Devonian, Early Carboniferous, the earliest Permian and Middle and Late Jurassic (Fig. 6f). This suggests that the previously proposed bimodal or unimodal evaporite patterns could have alternated over geological times. The distribution of glacial deposits is consistent with previous interpretations of the main icehouse and greenhouse periods during the last ∼400 Ma.

We considered some of the main factors controlling the latitudinal distributions of the lithologic deposits over time. There is no single factor that dominates the changing distributions from the Early Devonian to the present. As many previous studies have noted, tectonic factors associated with Pangaea assembly and breakup and the waxing and waning of ice sheets in Gondwanaland could have been significant factors influencing the distributions of the lithologies, including the extent of tropical continental humid zones from the Late Pennsylvanian through the Early Permian. The evolution of plant groups through space and time has influenced coal distributions, especially in a significant poleward shift during the Early Permian due to the rise of Gymnosperms. Due to these many factors, care should be taken when using the latitudinal distribution of these lithologies to constrain both past global climate and the past positions of continents.

Acknowledgements. This work is supported by Australian Research Council (ARC) grants IH130200012 (R.D.M., S.Z., S.W.) and ARC DE160101020 (N.F.). W. Cao was also supported by a University of Sydney International Scholarship (USydIS). This work also benefited from support of the Alfred P. Sloan Foundation (G-2017-9997) and the Deep Carbon Observatory (DCO). We thank John Cannon and Michael Chin for help with GPlates and pyGPlates, and Sally Cripps, Rohitash Chandra, Rob Hyndman, Stephen Marron and Maelis Arnould for assistance with programming.

Supplementary material

To view supplementary material for this article, please visit https://doi.org/10.1017/S0016756818000110

References

Becq-Giraudon, J. F., Montenat, V. & Van Den Driessche, J. 1996. Hercynian high-altitude phenomena in the French Massif Central: tectonic implications. *Palaeogeography, Palaeoclimatology, Palaeoecology* **122**, 227–40.

Berner, R. A. 2004. *The Phanerozoic Carbon Cycle: CO2 and O2*. New York: Oxford University Press, 150 pp.

Blakey, R. C. 2008. Gondwana paleogeography from assembly to breakup – A 500 m.y. odyssey. In *Resolving the Late Paleozoic Ice Age in Time and Space* (eds C.R. Fielding, T.D. Frank & J.L. Isbell), pp. 1–28. Geological Society of America Special Paper no. 441.

Boucot, A. J., Chen, X. & Scotese, C. R. 2013. *Phanerozoic Paleoclimate: An Atlas of Lithologic Indicators of Climate*. SEPM, Concepts in Sedimentology and Paleontology vol. 11, 478 pp.

Boucot, A. J. & Gray, J. 2001. A critique of Phanerozoic climatic models involving changes in the CO_2 content of the atmosphere. *Earth-Science Reviews* **56**(1–4), 1–159.

Brandley, R. T. & Krause, F. F. 1993a. Carbonate and siliciclastic deposition on a wave swept, cold-water, low-latitude ramp: Lower Carboniferous Mount Head Formation, southwestern Alberta, Canada. *Canadian Society of Petroleum Geologists, Annual Convention, Program and Abstracts, Carboniferous to Jurassic Pangea*, 35 pp.

Brandley, R. T. & Krause, F. F. 1993b. Thinolite-type pseudomorphs of ikaite: cold water indicators in the Mt. Head (Early Carboniferous–Visean), Rocky Mountains, Canada. *Canadian Society of Petroleum Geologists, Annual Convention, Program and Abstracts, Carboniferous to Jurassic Pangea*, 34 pp.

Brandley, R. T. & Krause, F. F. 1994. Thinolite-type pseudomorphs after ikaite: indicators of cold water on the subequatorial western margin of Lower Carboniferous North America. In *Pangea: Global Environments and Resources* (eds V. Embry, B. Beauchamp & D.J. Glass), pp. 333–44. Canadian Society of Petroleum Geologists Memoir no. 17.

Cao, W., Zahirovic, S., Flament, N., Williams, S., Golonka, J. & Müller, R. D. 2017. Improving global paleogeography since the late Paleozoic using paleobiology. *Biogeosciences* **14**, 5425–39.

Cecil, C. B. 1990. Palaeoclimate controls on stratigraphic repetition of chemical and siliciclastic rocks. *Geology* **18**, 533–6.

Cecil, C. B., Dulong, F. T., West, R. R., Stamm, R., Wardlaw, B. & Edgar, N. T. 2003. Climate controls on the stratigraphy of a middle Pennsylvanian cyclothem in North America. In *Climate Controls on Stratigraphy* (eds C. B. Cecil & T. N. Edgar), pp. 151–80. Society of Economic Paleontologists and Mineralogists Special Publication no. 77.

Chaudhuri, P. & Marron, J. S. 1999. SiZer for exploration of structure in curves. *Journal of the American Statistical Association* **94**(447), 807–23.

Cleveland, W. S. & Devlin, S. J. 1988. Locally weighted regression: an approach to regression analysis by local fitting. *Journal of the American Statistical Association* **83**, 596–610.

Craggs, H. J., Valdes, P. J. & Widdowson, M. 2011. Climate model predictions for the latest Cretaceous: an evaluation using climatically sensitive sediments as proxy indicators. *Palaeogeography, Palaeoclimatology, Palaeoecology* **315–316**, 12–23.

Diessel, C. F. K. 1992. *Coal-Bearing Depositional Systems*. Berlin: Springer-Verlag, 72 pp.

Domeier, M. & Torsvik, T. H. 2014. Plate tectonics in the late Paleozoic. *Geoscience Frontiers* **5**(3), 303–50.

Evans, D. A. D. 2006. Proterozoic low orbital obliquity and axial-dipolar geomagnetic field from evaporite palaeolatitudes. *Nature* **444**(7115), 51–5.

Foster, G. L., Royer, D. L. & Lunt, D. J. 2017. Future climate forcing potentially without precedent in the last 420 million years. *Nature Communications* **8**, 14845. doi: 10.1038/ncomms14845.

Frakes, L. A., Francis, J. E. & Syktus, J. I. 1992. *Climate Modes of the Phanerozoic*. Cambridge: Cambridge University Press.

Gibbs, M. T., Rees, P. M., Kutzbach, J. E., Ziegler, A. M., Behling, P. J. & Rowley, D. B. 2002. Simulations of Permian climate and comparisons with climate-sensitive sediments. *The Journal of Geology* **110**, 33–55.

Godderis, Y., Donnadieu, Y., Carretier, S., Aretz, M., Dera, G., Macouin, M. & Regard, V. 2017. Onset and ending of the late Palaeozoic ice age triggered by tectonically paced rock weathering. *Nature Geoscience* **10**, 382–6.

Golonka, J. 2007. Late Triassic and Early Jurassic palaeogeography of the world. *Palaeogeography, Palaeoclimatology, Palaeoecology* **244**(1–4), 297–307.

Golonka, J., Krobicki, M., Pajak, J., Giang, N. V. & Zuchiewicz, W. 2006. *Global Plate Tectonics and Paleogeography of Southeast Asia*. Kraków: Faculty of Geology, Geophysics and Environmental Protection, AGH University of Science and Technology, 128 pp.

Gordon, W. A. 1975. Distribution by latitude of Phanerozoic evaporite deposits. *The Journal of Geology* **83**(6), 671–84.

Hallam, A. 1985. A review of Mesozoic climates. *Journal of the Geological Society* **142**(8), 433–45.

Hay, W. W. 2016. *Experimenting on a Small Planet: A History of Scientific Discoveries, a Future of Climate Change and Global Warming*, 2nd edn. New York: Springer, 819 pp..

Horton, D. E., Poulsen, C. J. & Pollard, D. 2010. Influence of high-latitude vegetation feedbacks on late Paleozoic glacial cycles. *Nature Geoscience* **3**, 572–7.

Hunt, B. G. 1982. The impact of large variations of the Earth's obliquity on the climate. *Journal of the Meteorological Society of Japan* **60**, 309–18.

Hyndman, R. J. 1996. Computing and graphing highest density. *The American Statistician* **50**(2), 120–6.

Jenkins, G. S. 2000. Global climate model high-obliquity solutions to the ancient climate puzzles of the Faint Young Sun Paradox and low-altitude Proterozoic Glaciation. *Journal of Geophysical Research* **105**, 7357–70.

Jenkins, G. S. 2001. High-obliquity simulations for the Archean Earth: implications for climatic conditions on early Mars. *Journal of Geophysical Research* **106**, 32903–13.

Kump, L. R. & Arthur, M. A. 1997. Global chemical erosion during the Cenozoic: weatherability balances the budgets. In *Tectonic Uplift and Climate Change* (ed. W. F. Ruddiman), pp. 399–426. New York: Plenum Press.

Kump, L. R., Arthur, M. A., Patzkowsky, M. E., Gibbs, M. T., Pinkus, D. S. & Sheehan, P. M. 1999. A weathering hypothesis for glaciation at high atmospheric pCO_2 during the Late Ordovician. *Palaeogeography, Palaeoclimatology, Palaeoecology* **152**, 173–87.

Lowry, D. P., Poulsen, C. J., Horton, D. E., Torsvik, T. H. & Pollard, D. 2014. Thresholds for Paleozoic ice sheet initiation. *Geology* **42**, 627–30.

Matthews, K. J., Maloney, K. T., Zahirovic, S., Williams, S. E., Seton, M. & Müller, R. D. 2016. Global plate boundary evolution and kinematics since the late Paleozoic. *Global and Planetary Change* **146**, 226–50.

McCabe, P. J. & Parrish, J. T. 1992. Tectonic and climatic controls on the distribution and quality of Cretaceous coals. In *Controls on the Distribution and Quality of Cretaceous Coals*. (eds P. J. McCabe & J. T. Parrish), pp. 1–15. Geological Society of America Special Paper no. 267.

Miller, K. B., McCahon, T. J. & West, R. R. 1996. Lower Permian (Wolfcampian) palaeosol-bearing cycles of the U.S. Midcontinent: evidence of climatic cyclicity. *Journal of Sedimentary Research* **66**, 71–84.

Miller, K. B. & West, R. R. 1993. A reevaluaation of Wolfcampian cyclothems in northeastern Kansas: significance of subaerial exposure and flooding surfaces. *Kansas Geological Survey Bulletin* **235**, 1–26.

Molnar, P. & England, P. 1990. Late Cenozoic uplift of mountain ranges and global climatic change: chicken or egg? *Nature* **346**, 29–34.

Montañez, I. P., McElwain, J. C., Poulsen, C. J., White, J. D., DiMichele, W. A., Wilson, J. P., Griggs, G. & Hren, M. T. 2016. Climate, pCO_2 and terrestrial carbon cycle linkages during late Palaeozoic glacial–interglacial cycles. *Nature Geoscience* **9**, 824–8.

Montañez, I. P. & Poulsen, C. J. 2013. The Late Paleozoic Ice Age: an evolving paradigm. *Annual Review of Earth and Planetary Sciences* **41**(1), 629–56.

Montañez, I. P., Tabor, N. J., Niemeier, D., DiMichele, W. A., Frank, T. D., Fielding, C. R. & Isbell, J. L. 2007. CO_2-forced climate and vegetation instability during Late Palaeozoic deglaciation. *Science* **315**, 87–91.

Müller, R. D., Royer, J. Y. & Lawver, L. A. 1993. Revised plate motions relative to the hotspots from combined Atlantic and Indian Ocean hotspot tracks. *Geology* **21**(3), 275–8.

Müller, R. D., Seton, M., Zahirovic, S., Williams, S. E., Matthews, K. J., Wright, N. M., Shephard, G. E., Maloney, K. T., Barnett-moore, N., Bower, D. J. & Cannon, J. S. 2016. Ocean basin evolution and global-scale reorganization events since Pangea breakup. *Annual Review of Earth and Planetary Science Letters* **44**, 107–38.

Nelsen, M. P., DiMichele, W. A., Peters, S. E. & Boyce, C. K. 2016. Delayed fungal evolution did not cause the Paleozoic peak in coal production. *Proceedings of the National Academy of Sciences* **113**(9), 2442–7.

Parrish, J. T. 1993. Climate of the supercontinent Pangaea. *The Journal of Geology* **101**, 215–33.

Parrish, J. T., Ziegler, A. M. & Scotese, C. R. 1982. Rainfall patterns and the distribution of coals and evaporites in the Mesozoic and Cenozoic. *Palaeogeography, Palaeoclimatology, Palaeoecology* **40**(1–3), 31–66.

Pearson, P. N. & Palmer, M.R. 2000. Atmospheric carbon dioxide concentrations over the past 60 million years. *Nature* **406**, 695–9.

Perlmutter, M. A. & Matthews, M. D. 1989. Global cyclostratigraphy – a model. In *Quantitative Dynamic Stratigraphy* (ed. T. A. Cross), pp. 223–60. Englewood Cliffs, New Jersey: Prentice Hall.

Perlmutter, M. A. & Plotnick, R. E. 2003. Hemispheric asymmetry of the marine stratigraphic record: conceptual proof of a unipolar ice cap. In *Climate Controls on Stratigraphy* (eds C. B. Cecil & T. N. Edgar),. Society of Economic Paleontologists and Mineralogists Special Publication, vol. 77, pp. 51–66.

Peyser, C. E. & Poulsen, C. J. 2008. Controls on Permo-Carboniferous precipitation over tropical Pangaea: a GCM sensitivity study. *Palaeogeography, Palaeoclimatology, Palaeoecology* **268**(3–4), 181–92.

Poulsen, C. J., Pollard, D., Montañez, I. P. & Rowley, D. 2007. Late Palaeozoic tropical climate response to Gondwana deglaciation. *Geology* **35**, 771–4.

Price, G. D., Sellwood, B. W. & Valdes, P. J. 1995. Sedimentological evalaution of general circulation model calculations for the 'greenhouse' Earth: Cretaceous and Jurrassic case studies. *Sedimentary Geology* **100**, 159–80.

Rees, P. M., Ziegler, A. M., Gibbs, M. T., Kutzbach, J. E., Behling, P. J. & Rowley, D. B. 2002. Permian phytogeographic patterns and climate data/model comparisons. *The Journal of Geology* **110**, 1–31.

Ronov, A., Khain, V. & Balukhovsky, A. 1989. *Atlas of Lithological–Paleogeographical Maps of the World, Mesozoic and Cenozoic of Continents and Oceans*. Leningrad: USSR Academy of Sciences, 77 pp.

Ronov, A., Khain, V. & Seslavinsky, K. 1984. *Atlas of Lithological–Paleogeographical Maps of the World, Late Precambrian and Paleozoic of Continents*. Leningrad: USSR Academy of Sciences, 70 pp.

Rowley, D. B., Raymond, A., Parrish, J. T., Lottes, A. L., Scotese, C. R. & Ziegler, A. M. 1985. Carboniferous palaeogeographic, phytogeographic, and palaeoclimatic reconstructions. *International Journal of Coal Geology* **5**, 7–42.

Scotese, C. R. 2001. *Atlas of Earth History, Volume 1: Paleogeography*. Arlington, Texas: PALEOMAP Project, 52 pp.

Scotese, C. R. 2004. A Continental Drift flipbook. *The Journal of Geology* **112**(6), 729–41.

Scotese, C. R. 2008. *The PALEOMAP Project PaleoAtlas for ArcGIS, Volume 2: Cretaceous Paleogeographic and Plate Tectonic Reconstructions*. Arlington, Texas: PALEOMAP Project.

Scotese, C. R. & Barrett, S. F. 1990. Gondwana's movement over the South Pole during the Palaeozoic: evidence from lithological indicators of climate. In *Palaeozoic Palaeogeography and Biogeography* (eds W. S. McKerrow & C. R. Scotese). Geological Society of London, Memoir no. 12, 75–85.

Scotese, C. R. & Golonka, J. 1992. *Paleogeographic Atlas. PALEOMAP Progress Report 20-0692*. Arlington: Department of Geology, University of Texas, 34 pp.

Soreghan, G. S. 1997. Walther's Law, climate change, and Upper Paleozoic cyclostratigraphy in the Ancestral Rocky Mountains. *Geology* **67**, 1001–4.

Swanson-Hysell, N. L. & Mac Donald, F. A. 2017. Tropical weathering of the Taconic orogeny as a driver for Ordovician cooling. *Geology* **45**(8), 719–22.

Tabor, N. J. & Montañez, I. P. 2004. Permo-Pennsylvanian alluvial palaeosols (north-central Texas): high-resolution indicator records of the evolution of early Pangaean palaeoclimate. *Sedimentology* **51**, 851–84.

Tabor, N. J., Montañez, I. P., Scotese, C. R., Poulsen, C. J. & Mack, G. H. 2008. Paleosol archives of environmental and climatic history in paleotropical western Pangea during the latest Pennsylvanian through Early Permian. In *Resolving the Late Paleozoic Ice Age in Time and Space* (eds C. R. Fielding, T. D. Frank & J. L. Isbell), pp. 291–303. Geological Society of America Special Paper no. 441.

Tabor, N. J. & Poulsen, C. J. 2008. Palaeoclimate across the Late Pennsylvanian-Early Permian tropical palaeolatitudes: a review of climate indicators, their distribution, and relation to palaeophysiographic climate factors. *Palaeogeography, Palaeoclimatology, Palaeoecology* **268**(3–4), 293–310.

van Hinsbergen, D. J. J., de Groot, L. V., van Schaik, S. J., Spakman, W., Bijl, P. K., Sluijs, A., Langereis, C. G. & Brinkhuis, H. 2015. A paleolatitude calculator for paleoclimate studies. *PLoS ONE* **10**(6), 1–21.

Vilhena, D. A. & Smith, A. B. 2013. Spatial bias in the marine fossil record. *PLoS ONE* **8**(10), e74470. doi: 10.137.1/journal.pone.0074470.

Walker, L. J., Wilkinson, B. H. & Ivany, L. C. 2002. Continental drift and Phanerozoic carbonate accumulation in shallow shelf and deep marine settings. *The Journal of Geology* **110**, 75–88.

Warren, J. K. 2010. Evaporites through time: tectonic, climatic and eustatic controls in marine and nonmarine deposits. *Earth-Science Reviews* **98**, 217–68.

Witzke, B. J. 1990. Palaeoclimatic constraints for palaeozoic Palaeolatitudes of Laurentia and Euramerica. In *Palaeozoic Palaeogeography and Biogeography* (eds W. S. McKerrow & C. R. Scotese), pp. 57–73. Geological Society of London Memoir no. 12.

Wright, N., Zahirovic, S., Müller, R. D. & Seton, M. 2013. Towards community-driven paleogeographic reconstructions: integrating open-access paleogeographic and paleobiology data with plate tectonics. *Biogeosciences* **10**(3), 1529–41.

Ziegler, A. M. 1990. Phytogeographic patterns and continental configurations during the Permian Period. In *Palaeozoic Palaeogeography and Biogeography* (eds W. S. McKerrow & C. R. Scotese),. Geological Society of London Memoir no. 12, pp. 363–79.

Ziegler, A. M., Eshel, G., McAllister Rees, P., Rothfus, T. A., Rowley, D. B. & Sunderlin, D. 2003. Tracing the tropics across land and sea: Permian to present. *Lethaia* **36**, 227–54.

Ziegler, A. M., Hansen, K. S., Johnson, M. E., Kelly, M. A., Scotese, C. R. & Van der Voo, R. 1977. Silurian continental distribution, palaeogeography, climatology, and biogeography. *Tectonophysics* **40**, 13–51.

Ziegler, A. M., Hulver, M. L. & Rowley, D. B. 1997. Permian world topography and climate. In *Late Glacial and Post-Glacial Environmental Changes – Quaternary, Carboniferous–Permian and Proterozoic* (ed. I. P. Martini), pp. 111–46. Oxford: Oxford University Press.

Ziegler, A. M., Raymond, A., Geirlowski, T. C., Horrell, M. A., Rowley, D. B. & Lottes, A. L. 1987. Coal, climate and terrestrial productivity: the present and early Cretaceous compared. In, *Coal and Coal-bearing Strata: Recent Advances* (ed. A. C. Scott). Geological Society of London Special Paper no. 32, pp. 25–49.

Ziegler, A. M., Scotese, C. R. & Barrett, S. F. 1983. Mesozoic and Cenozoic paleogeographic maps. In *Tidal Friction and the Earth's Rotation II: Proceedings of a Workshop Held at the Centre for Interdisciplinary Research (ZiF) of the University of Bielefeld, 28 September–3 October 1981* (eds P. Brosche & J. Sündermann), pp. 240–52. Berlin: Springer Verlag.

Ziegler, A. M., Scotese, C. R., McKerrow, W. S., Johnson, M. E. & Bambach, R.K. 1979. Paleozoic paleogeography. *Annual Review of Earth and Planetary Sciences* **7**, 473–502.

Appendix: Software availability

SiZer analysis is performed in MatLab using the 'Smoothing' package (Chaudhuri & Marron, 1999) available at http://www.stat.unc.edu/faculty/marron/marron_software.html. SiZer can also be found in the package 'feature' (version 1.2.13) in 'R' statistical software (version 3.3.2). HDR from Hyndman (1996) is performed using the 'hdrcde' package (version 3.1) in 'R' statistical software (version 3.3.2). The HEALPix method is conducted using the library 'healpy' (version 1.10.3) in Python 2.0 and its documentation is available at http://healpy.readthedocs.io/en/latest/index.html.

Article 3

The interplay of dynamic topography and eustasy on continental flooding in the late Paleozoic

The interplay of dynamic topography and eustasy on continental flooding in the late Paleozoic

Wenchao Cao[1,*], Nicolas Flament[2], Sabin Zahirovic[1], Simon Williams[1] and R. Dietmar Müller[1]
[1]EarthByte Group, School of Geosciences, The University of Sydney, NSW 2006, Australia
[2]GeoQuEST Research Centre, School of Earth and Environmental Sciences, University of Wollongong, NSW 2522, Australia

**Corresponding author*: Wenchao Cao (wcao3204@uni.sydney.edu.au)

Abstract. Global sea level changes can be inferred from sequence stratigraphic and continental flooding data. These methods reconstruct sea level from peri-cratonic and cratonic basins that are assumed to be tectonically stable are sometimes called reference districts, from which spatio-temporal correlations across basins are used to estimate global sea level change over time. However, it has been understood that long-wavelength (typically hundreds of km) and low-amplitude (<2 km) vertical displacements of the Earth's surface due to mantle flow, namely dynamic topography, can occur in the absence of crustal deformation from horizontal plate motions. Dynamic topography can drive marine inundation or regional emergence of continents and must be taken into consideration with eustasy estimates. Global plate tectonic reconstructions for the late Paleozoic indicate that some regions (i.e. South China basin) used as reference districts to establish the chronology of Paleozoic eustatic sea level changes were close to subduction zones and therefore likely affected by dynamic topography during the Paleozoic.

We compared the continental flooding history with modeled dynamic topography and published global long-term sea level curves. We analysed the dynamic topography of the reference districts that were used to reconstruct eustatic curves. Our results indicate that the trend in global-scale flooding over the late Paleozoic generally correlates with global sea level curves. The first-order flooding history of North America correlates with some estimates of global long-term sea-level change, and dynamic topography could explain second-order flooding low during the Pennsylvanian. The Paleozoic inundation of South America does not follow long-term variations in eustatic sea level. The flooding lows during the Early Carboniferous and high during the Late Carboniferous are at odds with estimates of eustasy and can be explained by dynamic uplift and subsidence, respectively. Our dynamic topography models indicate that the Yangtze Platform of South China experienced significant dynamic subsidence during the transition from Permian to Triassic largely due to proto-Pacific subduction and its northward motion to collide with North China. The reference districts – Western New York, Oklahoma and Kansas, and West Texas in North America – were to some degree affected by dynamic uplift and subsidence associated with the long-living Panthalassa subduction zones, closure of the Rheic Ocean and African upwellings during late Paleozoic times. These indicate that some published global sea level curves may include non-eustatic signals that include uplift or subsidence from dynamic topography. Therefore, the interpretation of stratigraphic data gathered from these regions should be treated with caution when used to estimate global sea level variations.

Key words: dynamic topography, eustatic sea level, continental inundation, mantle flow, plate tectonic model, mantle structure

1. Introduction

Eustatic sea level changes during the Paleozoic have been reconstructed by interpreting sequence stratigraphy (e.g. Vail et a., 1977; Hallam, 1992; Haq and Schutter, 2008; Snedden and Liu, 2010). Sequence stratigraphy is a semi-quantitative method that makes it possible to reconstruct relative variations in sea level from stratigraphic sections in pericratonic and cratonic basins. Correlations between sea level events recorded in sedimentary strata across several basins are used to build short-term eustatic sea level curves (Haq et al., 1987; Haq and Schutter, 2008). For the Cretaceous, long-term fluctuations in eustatic sea level are established considering the mean age of the oceanic crust, the production rate of oceanic lithosphere at mid-ocean ridges, episodes and duration of emplacement of seamounts and large igneous provinces on the seafloor, sediment input into the ocean, and continental flooding data (Haq, 2014). Of these indicators, only continental flooding data are available for the Paleozoic. A key assumption in the sequence stratigraphic approach to reconstruct past sea levels is that these chosen regions used as reference districts (Fig. 1) to establish the chronology of Paleozoic sea level changes are assumed to be tectonically stable. However, it has long been known that long-wavelength vertical deflections of the solid Earth's surface as a result of mantle flow, called dynamic topography, may occur without any crustal thickening or thinning (Gurnis et al., 1990; Gurnis, 1993; Liu et al., 2008; Moucha et al., 2008; Spasojević et al., 2012; Flament et al., 2013). This issue has been recognised by stratigraphers who are aware of the effect of dynamic topography on long-term sea level change (Haq, 2014; Kominz et al., 2008). Recent developments in global tectonic reconstructions of the late Paleozoic (Matthews et al., 2016; Young et al., 2008) indicate that some of the regions (e.g. the Yangtze platform of South China during the Permian) used to reconstructed

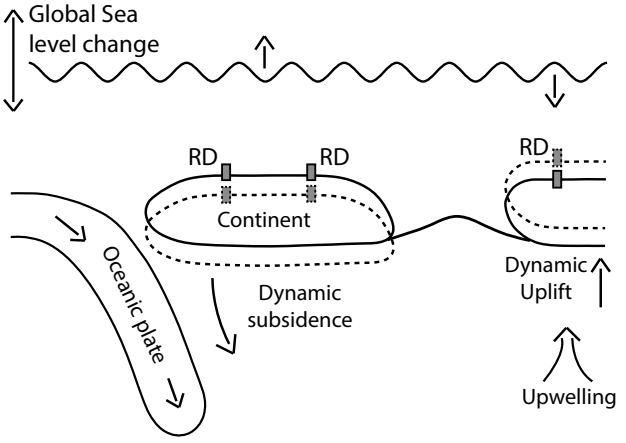

Figure 1. A cartoon illustrating the mechanisms of dynamic change – uplift and subsidence – under different scenarios. RD: reference districts that are used to reconstruct global sea level change.

global sea level change could be affected by tectonic activity and mantle flow. Therefore, whether the estimated sea level change using this method can truly represent global sea level change is debated (Hallam et al., 1992; Cloetingh and Haq, 2015). Additionally, estimates from continental flooding derived from paleogeographic maps and used in reconstructions of past eustatic sea levels require parameterizing the evolution of the poorly constrained shapes of continents, which leads to large uncertainties (Bond, 1979; Harrison et al., 1981; Algeo and Seslavinsky, 1995; Flament et al., 2013); in addition, continental flooding is also affected by dynamic topography (e.g. Mitrovica et al., 1989; Gurnis 1990; Spasojevic et al., 2012; Müller et al., 2018a).

Published eustatic sea level curves commonly suggest a long-term decrease in global sea level over the late Paleozoic (e.g. Vail et al., 1977; Hallam, 1992; Haq and Schutter, 2008). This is thought to be associated with the late Paleozoic aggregation of the Pangea supercontinent leading to an increase in the volume of ocean basins (Worsley et al., 1984; Vail et al., 1977; Hallam, 1992; Haq and Schutter, 2008; Conrad, 2013; Guillaume et al., 2016). The sea level curve of Haq and Schutter (2008) (hereafter

HS08) has become the most widely-used model of the Paleozoic sea level history and provides important constraints for studies in oceanic geochemistry composition (Munnecke et al., 2010; Flament et al., 2013) and past climates (DiMichele et al., 2009; Munnecke et al., 2010) in Paleozoic times. It was assembled from the interpretation of the sedimentary record in tectonically stable basins largely from North America, Europe and China for the late Paleozoic (~400–250 Ma). In this study, we use HS08 as reference sea level curve in the main body text and discuss two other global sea level curves – Hallam (1992), which we refer to as H92, and Algeo and Seslavinsky (1995), which we refer to as AS95 – in the discussion section.

We estimated the flooding ratios (defined as area of continental shallow seas as a percentage of total area of the continent at a certain time interval) of the North and South American continents individually, as well as the flooding ratio for all continents combined, from a set of time-dependent paleogeographic maps (Cao et al., 2017) in which the paleo-coastlines represent the maximum transgression surfaces. We computed dynamic topography for the continents using two forward mantle flow models based on time-dependent boundary conditions from two distinct tectonic reconstructions by Matthews et al. (2016) and Young et al. (2018). We then compared the resulting continental flooding ratios with modelled dynamic topography and published global long-term sea level curves (H08, H92 and AS95). We mapped the mantle temperature along cross sections to identify the origin of changes in dynamic topography. We predicted the evolution of dynamic topography at the reference districts used to reconstruct the late Paleozoic eustatic curves (Fig. 1). Our study highlights that combining digital paleogeographic reconstructions, geological observations, plate reconstruction models and models of past mantle flow provides insights into understanding mechanisms of continental inundation and distinguish global or regional sea level change over deep time (e.g. Hallam, 1984; Gurnis, 1993; Spasojevic and Gurnis, 2012).

2. Methods

2.1 Paleogeography and tectonic reconstructions

We use a set of digital time-dependent global paleogeographic maps extending back to the late Paleozoic (Cao et al., 2017), which document the ancient distribution of ice sheets, mountains, land mass, shallow seas and deep ocean basins for the last 402 million years (Myr). These maps were built on a set of published global paleogeographic maps compiled by Golonka et al. (2006) using paleoenvironmental and paleolithofacies data sets and not related to global sea level curves. They were tested and refined by the incorporation of paleoenvironmental data from the Paleobiology Database by Cao et al. (2017). In these maps, paleo-coastlines indicate the maximum transgression surfaces, so that the resulting continental flooding ratios represent maximum marine inundation. All the digital paleogeographic maps at present-day coordinates are available in the Supplementary materials of Cao et al. (2017). This facilitates the calculation of continental flooding ratios and also makes it possible to efficiently link the digital paleogeographic maps to alternative plate tectonic models.

We consider the global plate tectonic reconstructions of Matthews et al. (2016) (KM16) and Young et al. (2018) (AY18), both with continuously closing plate boundaries extending into the late Paleozoic (410–0 Ma). The reconstructions describe some possible past locations and motion velocities of plates and subduction zones through time. The reconstruction of KM16 is based on the reconstructions of Domeier and Torsvik (2014) for the period 410–250 Ma and of Müller et al. (2016) for the period 230–0 Ma, except that absolute plate motions are based on a different

true polar wander-corrected reference frame (Torsvik et al., 2012). The reconstruction of AY18 is built on the reconstruction of KM16 but adopting different scenarios for the closure of the Rheic Ocean and motion of circum- Paleo-Tethys blocks and the paleomagnetic reference frame of Torsvik and Voo (2002) for the period 410-250 Ma. Plate speeds and trench migration rates during the Paleozoic are significantly lower in AY18 than in KM16 (Young et al., 2018). In addition, the AY18 reconstruction better reproduces the present-day structure of the lowermost mantle when used as a surface boundary constraint in numerical mantle flow models (Young et al., 2018).

We quantitatively estimated late Paleozoic flooding ratios for the North and South American continents individually, and for all continents combined, from the digital paleogeographic maps (Cao et al., 2017) reconstructed back in time using the tectonic models of KM16 and AY18, respectively. Ronov (1994) and Algeo and Seslavinsky (1995) used a similar metric to estimate the flooding history of the main continents over time. The calculated continental flooding ratios are the same using the two reconstructions of KM16 and AY18 as expected, although the reconstructed locations of the continents are different (Fig. 2). In this study, we primarily focused on the North America and South America continents for the following reasons: (1) The sedimentary, paleoenvironmental and paleo-lithofacies records in these two continents in late Paleozoic times have been extensively studied and their paleogeographies are relatively well-constrained (e.g. Golonka et al., 2006; Limarino and Spalletti, 2006; Scotese, 2008, 2016; Cao et al., 2017). (2) The paleo-latitudinal constraints from paleomagnetic data for the two regions in the late Paleozoic are relatively reliable compared to

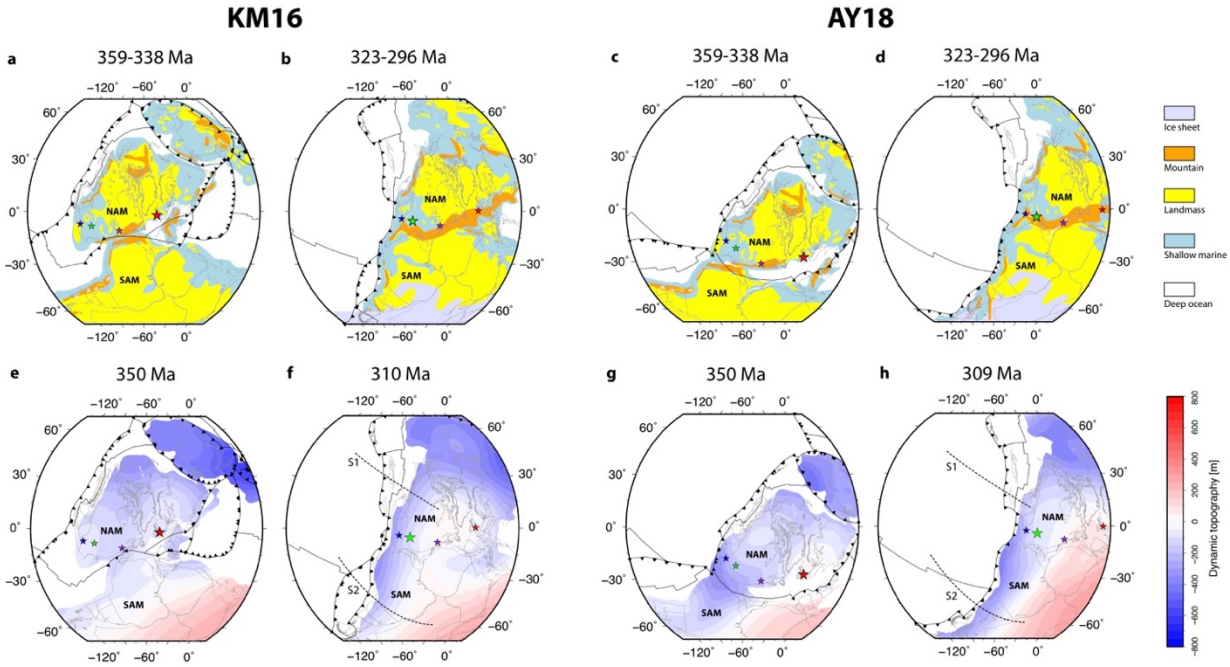

Figure 2. (a-d) Paleogeography of North America (NAM) and South America (SAM) between 359-338 Ma (reconstructing age: 348 Ma) and 323-296 Ma (reconstructing age: 302 Ma) derived from Cao et al. (2017), reconstructed using two plate tectonic models of Matthews et al. (2016) (KM16) and Young et al. (2018) (AY18), respectively. (e-h) Dynamic topography of North America and South America predicted by mantle flow models using the tectonic reconstructions of KM16 and AY18 as time-dependent boundary conditions, respectively. Cross section 1 (S1) on panels f and h is anchored to North America and cross section 2 (S2) is anchored to South America. The four coloured stars on panels a-h indicate the reconstructed locations of the reference districts used to reconstruct the global sea level curve of Haq and Schutter (2008) (purple star: Western New York, red star: Britain, green star: Oklahoma & Kansas, blue star: West Texas). Black dotted lines on all panels indicate subduction zones and other black lines denote mid-ocean ridges and transform faults. Grey outlines delineate reconstructed present-day coastlines and terranes. Mollweide projection with 60°E central meridian.

smaller blocks such as North China, South China and Tarim. (3) The paleo-longitudinal location of North America is poorly constrained and very different between the two reconstructions considered here. Here, we investigate which paleo-longitude of North America is more consistent with geological observations, based on the dynamic topography predicted by numerical models of mantle flow. (3) North America and South America were continuously affected by plate tectonic activity during the late Paleozoic, including circum Panthalassa subduction zones and the closure of Rheic Ocean and Paleo-Tethys Ocean. These two continents are a natural laboratory to study the interaction between plate tectonic motions and deep Earth mantle processes.

2.2 Mantle flow model setup and dynamic topography computation

Convection models. We modeled thermochemical convection within Earth's mantle in a 3D spherical shell with depth- and temperature-dependent viscosity and thermal expansivity, as in Hassan et al. (2016) and Flament (2018). We used the finite element code *CitcomS* (Zhong et al., 2000, 2008) to solve equations for the conservation of mass, momentum and energy under the extended Boussinesq approximation (Christensen and Yuen, 1985). Bower et al. (2015) modified *CitcomS* to incorporate the thermal structure of the lithosphere and of shallow slabs into the convection models using a progressive data assimilation method. The method of Bower et al. (2015) makes it possible to reconstruct the time-dependent mantle flow consistent with global plate motion models (e.g. Matthews et al., 2016; Young et al., 2018), and in turn to compare the predictions of the flow models to independent constraints. For example, the present-day temperature field can be compared to tomography models (e.g. Flament et al., 2017). Global plate tectonic reconstructions with continuously closing plate boundaries (e.g. Gurnis et al., 2012; Domeier et al., 2014; Matthew et al., 2016; Young et al., 2018) are required to derive surface velocities that are imposed as time-dependent surface boundary condition in the mantle flow reconstructions (e.g. Hassan et al., 2015; Cao et al., 2018; Young et al., 2018). The resulting predictions of the location of past downwellings and upwellings and associated dynamic topography from the flow models (e.g. Zhang et al., 2012; Flament et al., 2013) can be compared to the geological record of Phanerozoic marine inundation of continents (e.g. Gurnis, 1993; Spasojevic and Gurnis, 2012) and of the past vertical motion of continents (e.g. Flament et al, 2013; Flament et al., 2014; Shephard et al., 2014). Here we considered two model cases: Case KM16 is based on the global tectonic reconstruction of Matthews et al. (2016) and Case AY18 is based on the global tectonic reconstruction of Young et al. (2018).

Governing parameters. As in Young et al. (2018), the Rayleigh number, which controls the vigour of convection, is

$$Ra = \frac{\alpha_0 \rho_0 g_0 \Delta T h_M^3}{\kappa_0 \eta_0},$$

and the dissipation number, which controls viscous dissipation, is

$$Di = \frac{a_0 g_0 R_0}{C_{P_0}},$$

where α_0, ρ_0, g_0, ΔT, h_M, κ_0, η_0, R_0 and C_{P_0} are the thermal expansivity, density, gravity acceleration, temperature change across the mantle, mantle thickness, thermal diffusivity, viscosity, Earth radius and heat capacity (see Table 1 for values). The viscosity of the mantle depends on temperature and depth following the law:

$$\eta = \eta(r)\eta_0 exp\left\{\frac{\left[E_\eta + Z_\eta(R_0 - r)\right]}{\left[R\left(T + T_{off}\right)\right]} - \frac{\left[E_\eta + Z_\eta(R_0 - R_c)\right]}{\left[R\left(T_{CMB} + T_{off}\right)\right]}\right\},$$

where $\eta(r)$ is a pre-factor varying with the depth in the lower mantle: 0.02 (<160 km), 0.002 (160-310 km), 0.02 (310-660 km) and 0.2 (>660 km). r, R_C, E_η, Z_η, R, T, T_{off} and T_{CMB} represent the radius, the radius of Earth's core, the activation energy, activation volume, universal gas constant, dimensional temperature, temperature offset and temperature at the CMB (see Table 1 for values).

Model setup and initial conditions. We briefly outline the setup and initial conditions of our models, which are similar to those in Hassan et al. (2015) and Young et al. (2018). Earth's mantle is represented by a spherical shell composed of approximately 13 million mesh nodes, so that the vertical resolution is ~15 km near the surface and ~27 km near the CMB. The horizontal resolution is ~ 50 km near the surface and ~ 28 km near the CMB. Our calculations are started from 410 Ma. The initial condition contains slabs that are inserted down to 425 km depth from the surface boundary at a dip of 45° and to 1,200 km depth at a dip of 90° (as in Flament et al., 2017). The initial model condition includes a basal thermal boundary layer (225 km thick), a surface thermal boundary layer of thickness derived from the age of the lithosphere via a thermal boundary layer cooling model as in Bower et al. (2015), and an adiabatic temperature profile (gradient: 0.3 K/km) between the two. The oceanic lithosphere is assumed to be 90 Myr (123 km thick) old for the period of interest (410-250 Ma), and the age of the continental lithosphere is defined as in Flament et al. (2014). A compositionally distinct layer (4.7 % denser than ambient mantle and 113 km thick, making its volume 2% of that of the mantle) is embedded within the basal thermal boundary layer. This layer is used to model the basal structure of the mantle (e.g. Flament et al., 2017). During the model run, slabs are assimilated down to a maximum of 350 km depth, below which the model is dynamic (e.g. Young et al., 2018).

Table 1. Model parameters. Reference values are indicated by the subscript "0" indicates reference values. CMB: core-mantle boundary.

Parameter	Symbol	Value	Units
Thermal expansivity	α_0	3×10^{-5}	K^{-1}
Density	ρ_0	4,000	kg/m^3
Gravity acceleration	g_0	9.81	m/s^2
Temperature difference	ΔT	3,100	K
Mantle thickness	h_M	2,867	km
Thermal diffusivity	κ_0	1×10^{-6}	m^2/s
Viscosity	η_0	1.1×10^{21}	Pa s
Rayleigh number	R_a	7.8×10^7	–
Earth radius	R_0	6,371	km
Heat capacity	Cp_0	1,200	$J\ kg^{-1}\ K^{-1}$
Dissipation number	D_i	1.56	–
Core radius	R_C	3,504	–
Activation energy	E_η	275	KJ/mol
Activation volume	Z_η	1.9×10^{-6}	m^3/mol
Universal gas constant	R	8.31	$J\ mol^{-1}\ K^{-1}$
Temperature offset	T_{off}	452	K
Temperature at CMB	T_{CMB}	3,380	K
Shallow mantle density	ρ_{sm}	3,340	kg/m^3

Dynamic topography computation. We computed the dynamic topography with a free-slip boundary conditions and ignoring the buoyancy and lateral viscosity variations above 250 km depth (see Flament, 2018 for more detail). We computed the time-dependent air-loaded dynamic topography in 10 Myr intervals following: $h = \frac{\sigma}{\rho_{sm} g_0}$, where σ is the total normal stress and ρ_{sm} is the density of the shallow mantle (e.g. Cao et al., 2018).

3. Results

3.1 Continental flooding history from paleogeographic reconstructions

The global-scale trends indicate a broad decrease in flooding of continents throughout the late Paleozoic (orange line in Fig. 3a). Flooding continuously decreases from ~45% in the Devonian (402-359 Ma) to ~31% in the Middle Permian (285-269 Ma) with only a slight increase to ~35% in the late Permian-early Triassic (269-248 Ma). However, we note that this increase in flooding during the late Permian-early Triassic is not observed in the paleogeographic maps of Ronov (1994), Blakey (2003, 2008) and Walker et al. (2002) (Fig. 9 in Cao et al., 2017).

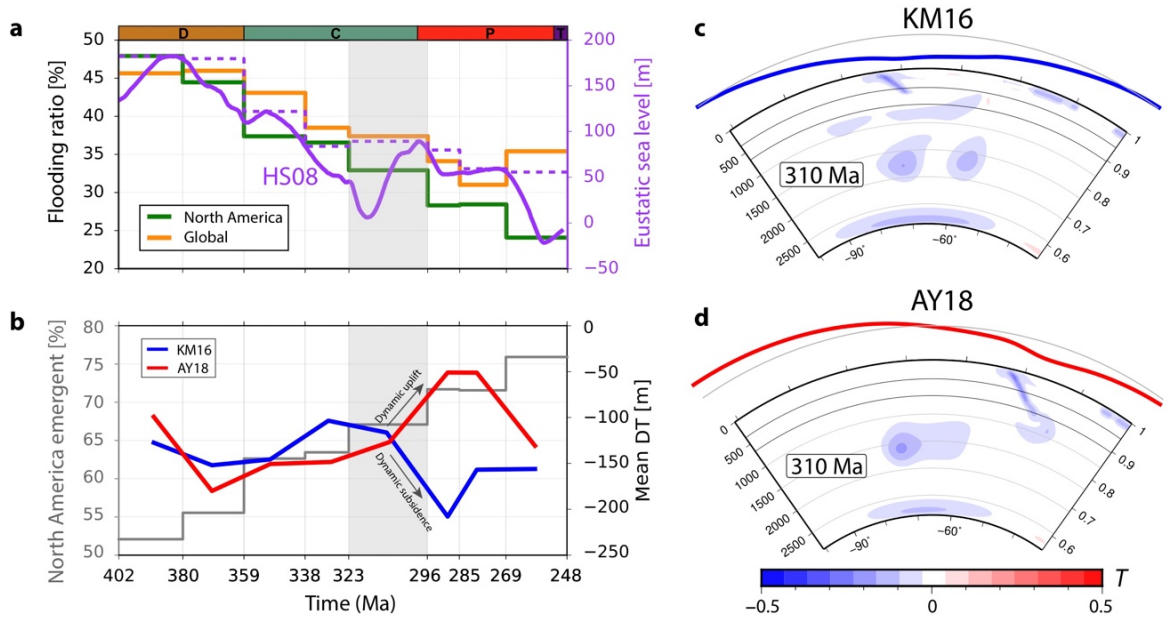

Figure 3. (a) Late Paleozoic continental flooding ratios of the North America continent and all continents combined derived from the paleogeography of Cao et al. (2017), and the global sea level curve of Haq and Schutter (2008). The dashed line represents the global sea level highstands for each time interval. (b) Continental emergent ratios of the North America continent derived from the paleogeography of Cao et al. (2017), and the average dynamic topography of the continent predicted by mantle flow simulations using two tectonic reconstructions of KM16 (blue line) and AY18 (red line) as time-dependent boundary conditions. (c-d) Mantle temperature and dynamic topography sections along section 1 (anchored to North America, location shown in Fig. 2) for cases KM16 and AY18. The blue and red lines above each section are air-loaded dynamic topography (the grey line shows mean dynamic topography, which is by definition equal to zero). The numbers above the color scale denote non-dimensional temperatures and the number below the color scale denote dimensional temperatures. The solid black lines at 660 and 350 km depth denote the upper-lower mantle boundary and the depth above which buoyancy is ignored in the computation of dynamic topography, respectively.

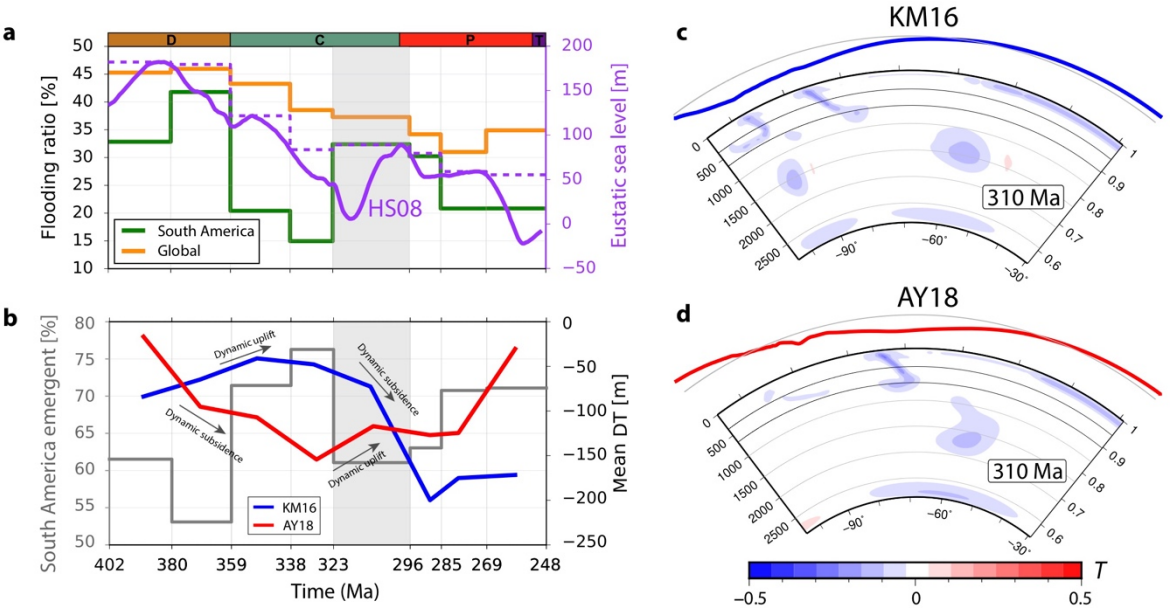

Figure 4. (a) Late Paleozoic continental flooding ratios of the South America continent and all continents combined derived from the paleogeography of Cao et al. (2017), and global sea level curve of Haq and Schutter (2008). The dashed line represents the global sea level highstands for each time interval. (b) Continental emergent ratios of the South America continent derived from the paleogeography of Cao et al. (2017), and the average dynamic topography of the continent predicted by mantle flow simulations using two tectonic reconstructions of KM16 (blue line) and AY18 (red line) as time-dependent boundary conditions. (c-d) Mantle temperature and dynamic topography sections along section 1 (anchored to North America, location shown in Fig. 2) in cases KM16 and AY18. The blue and red lines above each section are air-loaded dynamic topography (black lines show mean dynamic topography, which is by definition equal to zero). The numbers above the color scale denote non-dimensional temperatures and the number below the color scale denote dimensional temperatures. The solid black lines at 660 km and 350 km depth denote the upper-lower mantle boundary and the depth above which buoyancy is ignored in the computation of dynamic topography, respectively.

At the continental scale, the flooding ratios of North America consistently decrease from 45% in the Devonian (402-359 Ma) to ~23% in the late Permian-earliest Triassic (269-248 Ma) (green line in Fig. 3a). In contrast, South America experienced a more variable inundation history (green line in Fig. 4b) with an increase from 32% in the Middle Devonian (402-380 Ma) to 42% in the Late Devonian (380-359 Ma) and then a rapid decrease to 20% in the early Mississippian (359-338 Ma). In the late Mississippian (338-323 Ma), it continued to decrease down to ~15% to reach its lowest value during 338-323 Ma. This was followed by a rapid increase to 32% flooding in the Pennsylvanian (323-296 Ma). In the early Permian (296-285 Ma), it recorded 30% flooding before experiencing another low value of flooding (i.e. ~20%) during the rest of Permian and the earliest Triassic (285-248 Ma).

3.2 Dynamic topography for the continents

Late Paleozoic tectonics were characterized by the collision of Laurussia and Gondwana, by the closure of the Rheic Ocean and of the Paleo-Tethys Ocean, and by the formation of the central Pangean mountains (Matthews et al., 2016; Young et al., 2018). The active margins of western North America and South America were enduringly influenced by long-lived eastern circum Panthalassa subduction zones. The collision of Laurussia and Gondwana led to the closure of the Rheic Ocean and formation of central Pangean mountains (Fig. 2b, d). As a result, North America experienced extensive negative dynamic topography especially along its western margins over the late Paleozoic, indicated by both time-dependent mantle flow model cases KM16 and AY18 (Fig. 2e-f). Similarly, South America also experienced a pronounced negative dynamic topography history at its western margins (Fig. 2g-h). These two continents were also affected by the African large-scale upwelling that dynamically supported topography in the eastern regions of North and South America (Fig. 2e-h). The calculated average dynamic topography for North America (Fig. 3b) and South America (Fig. 4b) over time shows that the overall dynamic topography was always negative in the late Paleozoic for both cases KM16 and AY18.

Specifically, the mean dynamic topography for North America in Case KM16 (Fig. 3b) (blue line in Fig. 3b) remained stable for the periods between 402-323 Ma (−150 to −100 m) and between 285−248 Ma (−190 to −150 m), but it experienced a fast decrease from −100 m to −210 m between 323−285 Ma. In Case AY18, there was no significant change between 402−323 Ma, then a dramatic increase from approximately −140 m to −50 m between 323−285 Ma. This was followed by a rapid decrease to less than −200 m between 285−248 Ma. The mean dynamic topography for South America over time shows distinct trends between Case KM16 and Case 18 (Fig. 4b). In Case KM16, it increased from approximately −80 m between 402−380 Ma to −40 m between 359−338 Ma and then rapidly decreased to −200 m between 296−285 Ma. It subsequently remained stable at

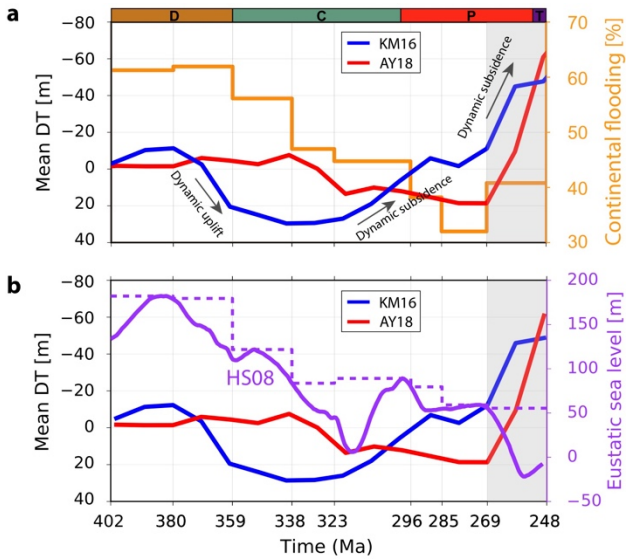

Figure 5. (a) Comparison between global-scale flooding ratios derived from the paleogeography of Cao et al. (2017) and average dynamic topography for all continents for cases KM16 (blue line) and AY18 (red line) through time. (b) Comparison between the global eustatic curve of Haq and Schutter (2008) (purple lines) and the average dynamic topography for all continents for cases of KM16 (blue line) and AY18 (red line).

about −170 m between 285−248 Ma. In contrast, Case AY18 indicates a rapid decrease in mean dynamic topography from approximately −20 m between 402−338 Ma to −150 m between 338−323 Ma, and then a persistent decrease to about −30 m in the late Permian-earliest Triassic (269−248 Ma).

The evolution of mean dynamic topography for all continents in cases KM16 and AY18 show different dynamic history during the Devonian − middle Permian (402−269 Ma) but similar during the late Permian and the earliest Triassic (269−248 Ma) (Fig. 4). Specifically, Case KM16 (blue line in Fig. 4a) showed short-lived and minor dynamic subsidence of ~10 m during the middle Devonian (402−380 Ma) and then a stronger dynamic uplift from approximately −10 m at 380 Ma to 30 m at 338 Ma. It subsequently indicated long-term and significant dynamic subsidence until −50 m at 248 Ma. In Case AY18 (red line in Fig. 5a), the mean dynamic topography for the global continents remained stable between approximately −10 m and 20 m during the whole time period except for late Permian-earliest Triassic period, marked by a modest increase of 20 m from 338 Ma to 319 Ma. However, in the late Permian-earliest Triassic, Case AY18 indicated that global continents experienced dramatic dynamic subsidence at a rate of 4 m/Myr.

4 Discussion

4.1 Mechanisms of continental flooding

4.1.1 North America

The first-order flooding history of North America correlates with long-term sea level changes in the late Paleozoic (Fig. 3a). The average dynamic topography of the continent remained relatively stable throughout most of the timeframe in both cases of KM16 and AY18 (Fig. 3b). This suggests that eustasy was the main driver of inundation of North America in the late Paleozoic (Fig. 3). A second-order flooding decrease during the Pennsylvanian (323−296 Ma) compared to global sea level change (Fig. 3a) can be explained by dynamic uplift in Case AY18 (red line in Fig. 3b). The rates of dynamic topography change for North America during this time period show that this dynamic uplift occurred nearly all over the North American continent, but with a larger amplitude in the eastern regions (Fig. 6c).

4.1.2 South America

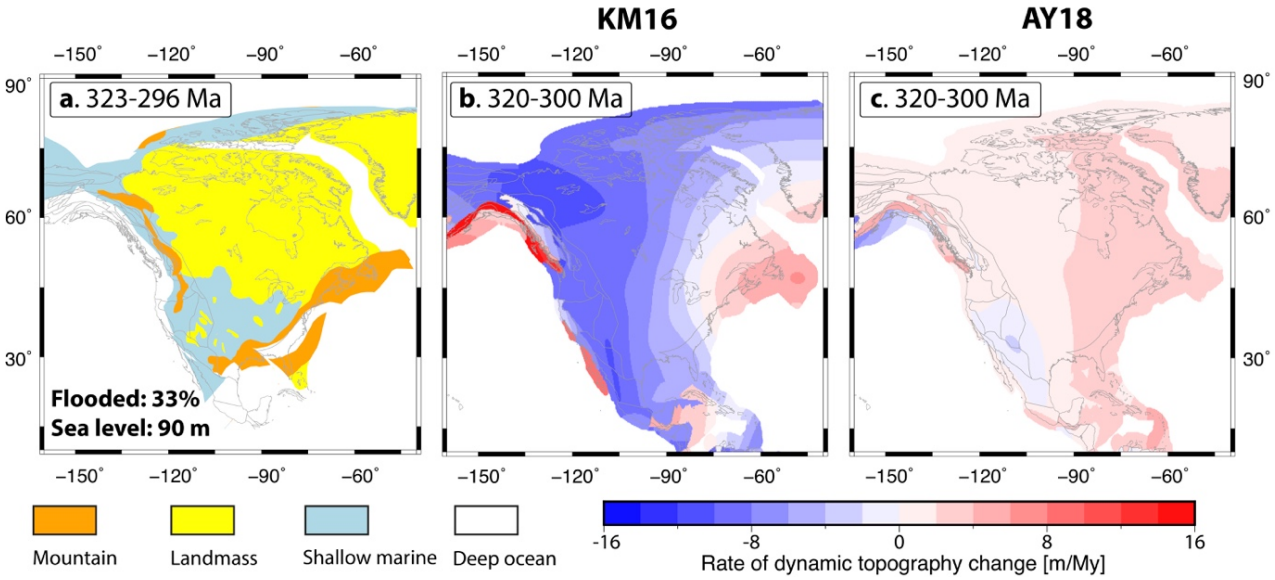

Figure 6. (a) North American paleogeography between 323-296 Ma derived from the paleogeographic maps of Cao et al. (2017). (b-c) Rates of dynamic topography change for North America between 320-300 Ma in cases KM16 (b) and AY18 (c). All maps are in the plate frame of reference. Grey outlines indicate present-day coastlines and terranes.

The inundation history of the South American continent does not follow long-term variations in global sea level in the late Paleozoic (Fig. 4a). Flooding was relatively low in the Mississippian but high in the Pennsylvanian compared to global sea level changes (Fig. 4a). The flooding low during the early Mississippian (359−338 Ma) may be attributed to dynamic uplift predicted by Case KM16 (blue line in Fig. 4b). The map of rate of dynamic topography change (Fig. 7b) shows that the dynamic uplift mostly occurred in southern South America and some regions in its center and north. However, the variations are small, mostly at a rate of less than 2 m/Myr, and hence the effects of the dynamic topography may not be enough to explain the

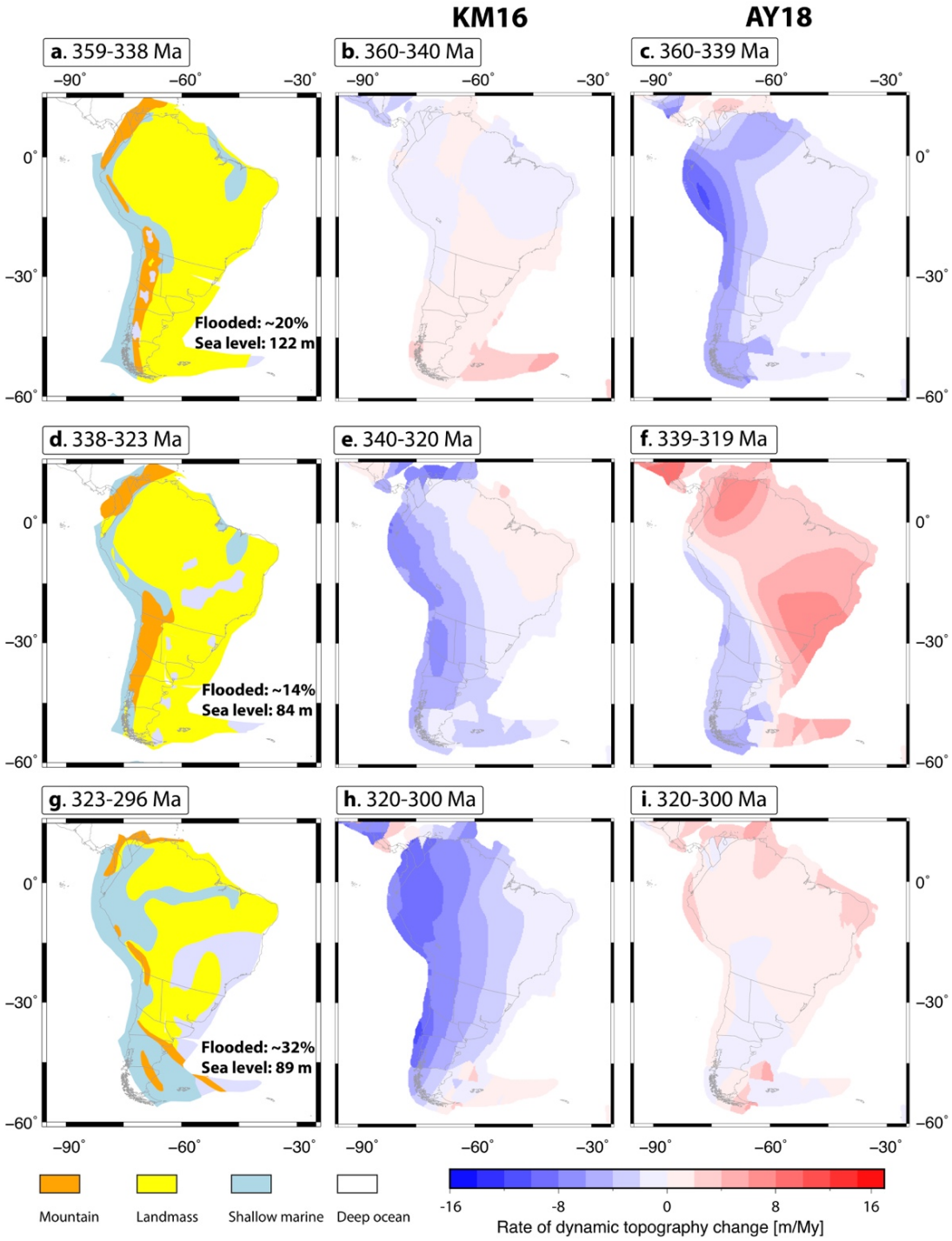

Figure 7. Paleogeography of South America between 359−338 Ma (a), 323−295 Ma (d) and 295−285 Ma (g) derived from the paleogeographic maps of Cao et al. (2017) and rates of dynamic topography change for South America in cases KM16 (b, e, h) and AY18 (c, f, i). All maps are in the plate frame of reference. Grey outlines indicate present-day coastlines and terranes.

flooding low during this period. The lowest flooding during the late Mississippian (338−323 Ma) could have been caused by dynamic uplift during the time indicated from Case AY18 models (Fig. 7f). The map of rate of change of dynamic topography shows that South America experienced broad dynamic uplift by up to 8 m/Myr during the late Mississippian, except for parts of its southwestern margin (Fig. 7f).

During the Early Pennsylvanian, South America was extensively flooded with a west-east inland seaway (Fig. 7g). The rise in global sea level during this time (purple line in Fig. 4a) contributed to this change in regional flooding. Case KM16 predicts extensive dynamic subsidence over the whole continent, with magnitude up to −10 m/Myr along its western margins (Fig. 7h). Tectonically, this dynamic subsidence is linked to the double Panthalassan subduction zones along western South America in the reconstruction of KM16. These two subduction zones define the boundaries of the Patagonia Plate and isolate it from the western Farallon and Phoenix plates and the eastern South America Plate (Fig. 2h). The Patagonia Plate consistently subducted beneath South America until it completely vanished in the early Permian (Matthews et al., 2016). The mantle temperature along a cross section through the western margin of South America during the Early Pennsylvanian (section S2 in Fig. 2f) shows the two slabs sinking beneath the western margins of South America, leading to significant dynamic subsidence along the margin (Fig. 4c). The dynamic subsidence contributed to the increase in flooding over time.

4.1.3 Global continental flooding

Conrad and Husson (2009) discussed the connection between continental dynamic topography and global sea level. They showed that a net deflection of continental areas by mantle flow will be balanced by an opposing net deflection of oceanic areas as the total of the dynamic support of the globe integrates to zero, which leads to a net offset of sea level. Our numerical models indicate that the dynamic history of global continents in Case KM16 appears to be comparable to global sea level changes for the late Paleozoic except for the late Permian-early Triassic (blue line in Fig. 5b). This scenario suggests that the global sea level curves may contain a dynamic topography signal that is not accounted for. In contrast, mantle flow in Case AY18 predicts stable dynamic history of continents except for the late Permian-early Triassic (red line in Fig. 5b), suggesting that there may not be much impact from deep Earth's processes on global sea level changes. The variations in modelled dynamic topography between Case KM16 and Case AY18 are associated with adopting different regional tectonic reconstructions for the closure of the Rheic Ocean and circum- Paleo-Tethys blocks, and difference of the global RMS speed which is faster in the KM16 model than that in AY18 model typically for the period before ~250 Ma (Young et al., 2018). Gurnis et al., (1993) suggested that plate speeds are an important factor controlling variations in rates of subduction and continental inundation during the Phanerozoic.

During the late Permian − early Triassic, the dynamic topography of all continents combined indicates notable dynamic subsidence for both cases KM16 and AY18 (Fig. 5). Our time-dependent global dynamic topography models show that Asia and western North and South America underwent the most dynamic subsidence during this time period (Fig. 8). A eustatic low has been widely recognized in this period (Vail et al., 1977; Hallam, 1992; Algeo and Seslavinsky, 1995; Haq and Schutter, 2008). Guillaume et al. (2016) reviewed global sea level changes during this time and argued that the eustatic low in the late Permian - early Triassic was difficult to explain by tectonics and climatic factors and might be due to global dynamic topography. Our models in both cases predict a

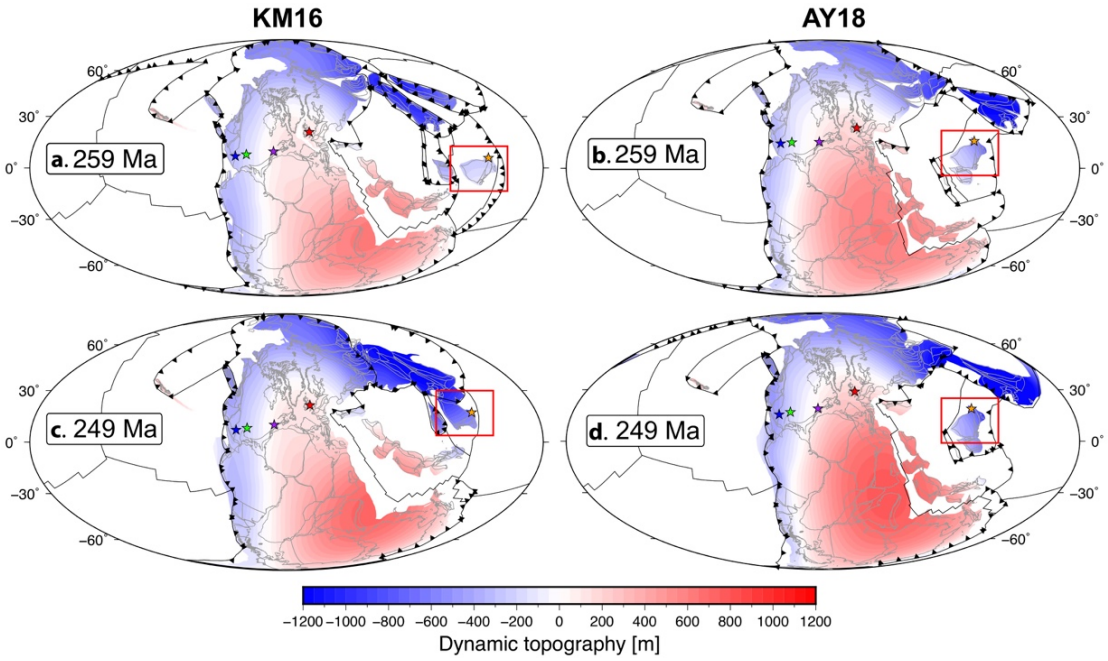

Figure 8. Global continental dynamic topography at 259 Ma and 249 Ma both in the mantle frame of reference for cases KM16 (a, c) and AY18 (b, d). The red boxes highlight the locations of South China. The five colored stars on panels e-h indicate the reconstructed locations of the reference districts used to estimate global sea level (Haq and Schutter, 2008; purple star: Western New York, red star: Britain, green star: Oklahoma and Kansas, blue star: West Texas; orange star: South China). Black dotted lines on all panels indicate subduction zones and other black lines denote mid-ocean ridges and transforms. Grey outlines delineate reconstructed present-day coastlines and terranes. Mollweide projection with 0°E central meridian.

considerable dynamic subsidence of the continents which would have elevated relative sea levels. Therefore, our results do not indicate that the fall in global sea level during the late Permian was related to global dynamic topography. We note that the eustatic low in the curve of HS08 is estimated dominantly based on stratigraphic data in South China, and that both cases KM16 and AY18 suggest that South China underwent significant dynamic subsidence during the late Permian (Fig. 8d, 9e). This dynamic subsidence was due to the subduction of the Izanagi Plate (Fig. 8) and the northward motion of South China to collide with North China. The predicted dynamic subsidence of South China highlights the importance to examine whether the regions that are used to reconstruct global sea level changes are affected by mantle flow. We note that cases KM16 and AY18 do not predict and mantle plume under South China at ~260 Ma (Emeishan LIP), but that a mantle upwelling could explain the apparent sea level low for South China during the late Permian.

4.2 Dynamic topography evolution of reference districts used to interpret eustatic sea level change

We investigate the history of dynamic topography for each of the reference districts used to establish the late Paleozoic chronology of global sea level change (Haq and Schutter, 2008; Fig. 9) for both cases KM16 and AY18. We quantified the absolute value of the maximum rate of dynamic topography change for each reference district for the duration when it is used as a reference district. For instance, for the Western New York reference district, the time interval with the maximum change in dynamic topography in its duration as a reference district is 370−360 Ma (Fig. 10), and the maximum rate of dynamic topography change for this reference district is 7.7 m/Myr (Fig. 10). The results show that rates of dynamic topography change for the reference district in Britain are ~3 m/Myr in the KM16 case and 0.5 m/Myr in the AY18 case during the Mississippian. In contrast, South China

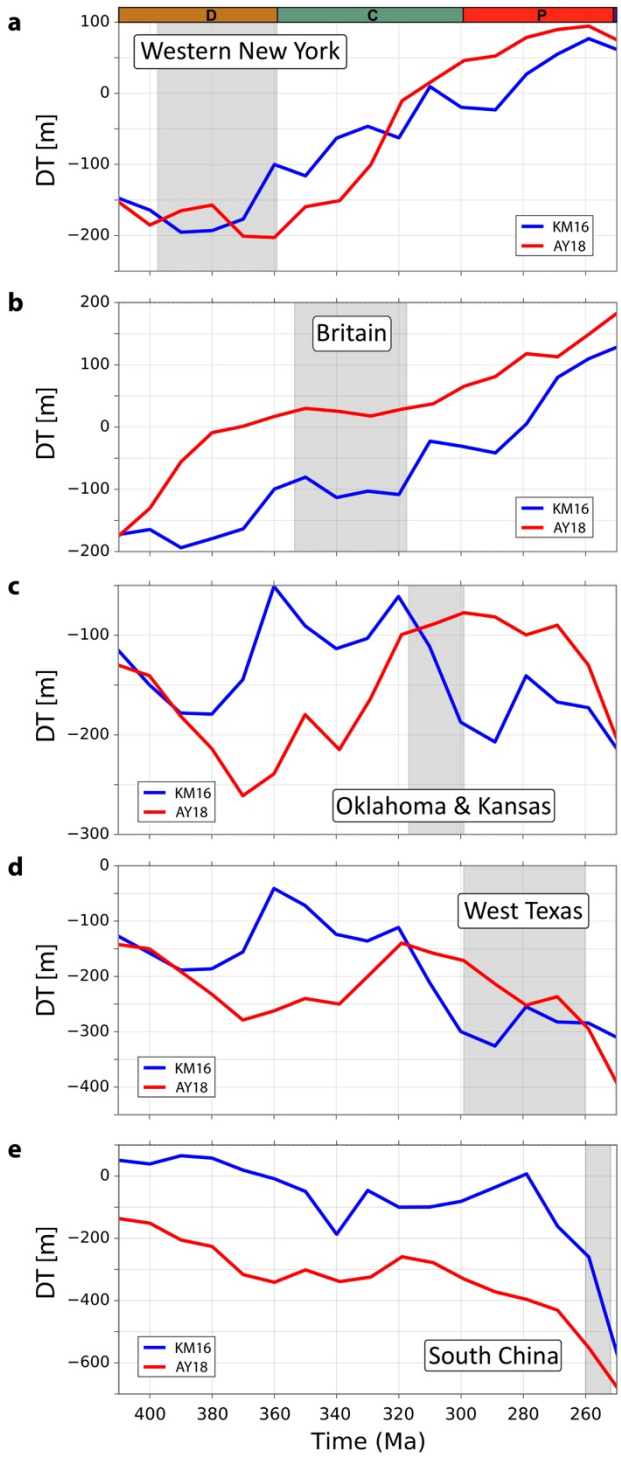

Figure 9. Late Paleozoic dynamic topography history of reference districts − New York (a), Britain (b), Oklahoma & Kansas (c), West Texas (d) and South China (e) −, used to build global sea level curve of Haq and Schutter, (2008), in the KM16 (blue lines) and AY18 (red lines) cases. The shaded boxes represent the periods during which the reference districts are used to generate the global sea level curve.

underwent pronounced dynamic subsidence at a maximum rate of dynamic topography change of more than 14 m/Myr in the both cases during the Late Permian and the earliest Triassic. Maximum rates of dynamic topography change for Western New York were 8 m/Myr in Case KM16 and 4 m/Myr in Case AY18, respectively, during the Late Early − Late Devonian. Oklahoma and Kansas are different for the two cases: change by 8 m/Myr in Case KM16 but by 1 m/Myr only in Case AY18 during the Pennsylvanian. West Texas shows similar results, with a rate of 7 m/Myr in Case KM16 and 6 m/Myr in Case AY18 during the Permian.

Overall, the reference district in Britain was the least affected by dynamic topography in cases KM16 and AY18, both with a maximum rate of dynamic topography change of less than 3 m/Myr during the Mississippian, indicating that it can be used as a reliable reference district for that period. Oklahoma and Kansas were also a dynamically stable reference district but only in Case AY18. South China, the reference district for the period between the Late Permian − earliest Triassic, was significantly affected by dynamic topography during that period, and as a consequence its stratigraphy for the period may reflect relative sea level change rather than global sea level change. Western New York and West Texas were also affected by dynamic topography, although to a lesser extent, for the time periods for which they are used as reference district. According to the mantle flow models, the reference districts used to reconstruct eustatic curves which are most affected by dynamic

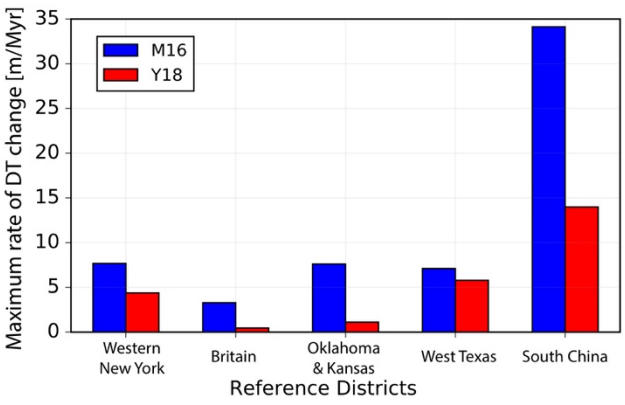

Figure 10. Maximum rates of dynamic topography change for the reference districts used to reconstruct the global sea level curve of Haq and Schutter, (2008) in cases KM16 (blue) and AY18 (red), respectively. The definition of the maximum rate of dynamic topography change is described in the text.

topography are those in North America and South China.

4.3 Influence of tectonic reconstruction choice on modelled dynamic topography

Our dynamic topography models strongly depend on the input tectonic reconstructions. KM16 and AY18 adopted different Paleozoic reference frames, and different scenarios for the evolution of the Panthalassa oceanic plates, the closure of the Rheic Ocean and the motion of circum- Paleo-Tethys tectonic blocks. This results in different mantle flow and dynamic topography for the late Paleozoic (Figs. 3-8). Because dynamic topography averages to zero globally by definition (e.g. Conrad and Husson, 2009; Flament, 2018), regional differences in subduction-driven dynamic topography must be compensated somewhere else, leading to global differences.

The dynamic topography predicted for Case KM16 better explains some of the discrepancies between flooding and global sea level changes for North America (Fig. 3). For instance, during the Pennsylvanian, Case KM16 indicates an extensive dynamic subsidence in North America (Figs. 3, 6). The mantle temperature structure along a cross section through the western margin of North America (cross section S1 in Fig. 2) shows the Farallon slab sinking beneath the Side Mountain Ocean which is close to the western margins of North America (Fig. 3c), and the cold and dense feature driving downwelling that pulls western North America down (Fig. 3c). However, in Case AY18, the Farallon slab does not considerably result in dynamic subsidence of North America due to rapid trench migration (Fig. 3d). Indeed, the predicted dynamic uplift for Case AY18 during this time period (Fig. 3f) is associated with the upwelling African plume (Fig. 2f).

The dynamic topography for Case AY18 better explains the continental flooding of South America than those in Case KM16 (Fig. 4). In the plate tectonic model of AY18, there is only one subduction zone along the western margin of South America (Fig. 2h). The associated subducted slab does not significantly change the dynamic topography at the margins (Figs. 2, 4, 7). Instead, South America is extensively uplifted by the African superswell (Figs. 2, 4, 7).

4.4 Comparison with other published Paleozoic eustatic curves

We compared our global flooding history and average dynamic topography of global continents with the alternative two global sea level curves, including H92 and AS95 (Fig. 11). The global sea level curve of H92 was reconstructed based on sequence stratigraphic data largely from North America and European regions. Although it suggests a first-order agreement on the late Paleozoic global sea level change with HS08, it indicates a rise in global sea level during the Mississippian and early Pennsylvanian and a fall during the rest of Pennsylvanian, contrary to what HS08 predict for the same intervals. The curve of AS95 was constructed using continental flooding and suggests less fluctuation in global sea levels – two sea level increases during the Devonian and Early and Middle Permian and two falls in Early Carboniferous and Late Permian (black line in Fig. 11). All variations are relatively small but have large uncertainty of ~100 m (grey-shaded area in Fig. 11). The comparisons between these two global sea level curves and global average dynamic topography of continents over the late Paleozoic indicate that H92 has similar trends with the evolution of global average dynamic topography of continents only in the Middle Devonian (402−380 Ma) for Case KM16, and in some times during the Late Carboniferous and Early Permian (323−269 Ma) for Case AY18. For AS95, only in the Late Carboniferous and Early and Middle Permian (323−268 Ma) for Case KM16, and only in a period during the Carboniferous (338−320 Ma) for Case AY18.

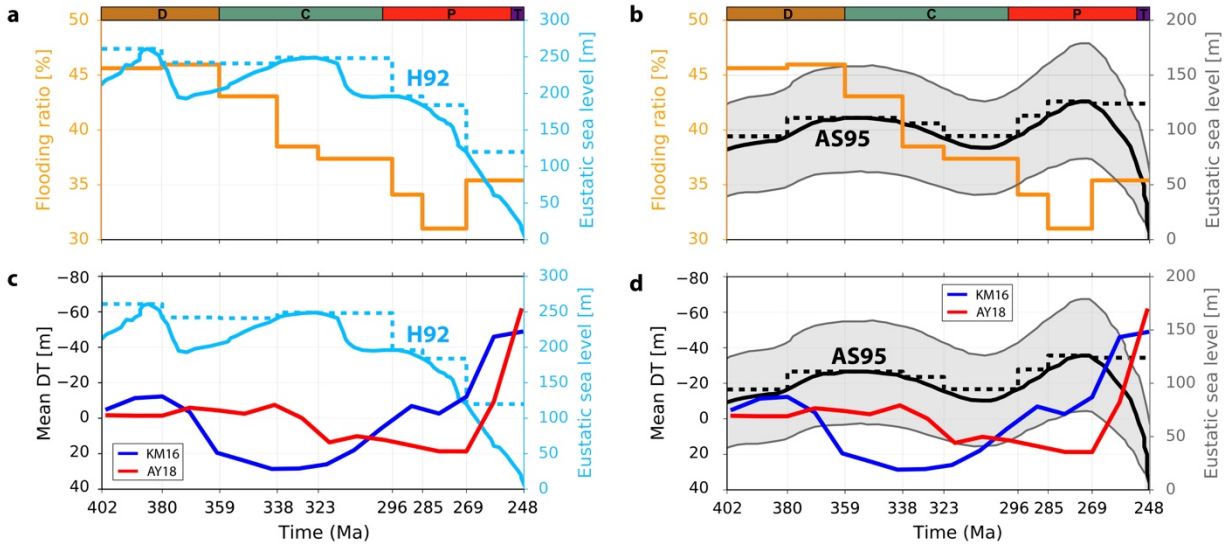

Figure 11. (a, b) Comparison between global flooding ratios derived from the paleogeography of Cao et al. (2017) and global sea level curves of Hallam (1992, light blue lines – H92), Algeo and Seslavinsky (1995, black lines and grey-shaded range representing uncertainty – AS95). (c, d) Comparison between the average dynamic topography for all continents for cases of KM16 (blue line) and AY18 (red line) and global eustatic curves of H92 (light blue lines) and AS95 (black line and uncertainty range).

Overall, compared with HS08, H92 and AS95 indicate less similarity to the evolution of global average dynamic topography of the continents over time.

However, these published Paleozoic eustatic curves (e.g. Vail et al., 1977; Hallam, 1992; Algeo and Seslavinsky, 1995; Haq and Schutter, 2008) all have uncertainties to some degree due to the lack of geological constraints in deep geological times. It is now widely understood that estimating past global sea level change cannot be achieved by using the rock record alone (Miller et al., 2005; Haq et al., 1987; Haq and Schutter, 2008; Haq and Al-Qahtani, 2005), and time-dependent models of flow of the Earth's mantle are crucial to establish the reference frame of past global sea level change (Flament et al., 2013; Moucha et al., 2008; Spasojević and Gurnis, 2012; Müller et al., 2008, Haq, 2014; Kominz et al., 2008). There is no systematic understanding of how mantle processes have influenced sea level globally over long geological timescales (beyond 100 million years ago) as yet. Therefore, understanding and quantifying the effect of the dynamics of the solid Earth on past sea level changes and continental flooding by combining global plate tectonic reconstructions, cutting-edge mantle flow models, and geological observations is important.

4.4 Comparison to previous geodynamic models

Gurnis (1993) and Spasojevic and Gurnis (2012) produced dynamic topography models to study the Phanerozoic marine inundation of continents and to study global sea level change and vertical motions of continents since the Late Cretaceous, respectively. These studies presented a series of instantaneous flow models, in contrast to the time-evolving mantle flow models presented here. Although Zhang et al. (2012) used time-dependent models to investigate changes in global dynamic topography since the late Paleozoic, they focused on the vertical motions of the Slave and Kaapvaal Cratons when comparing their results to geological data. The dynamic models of Gurnis (1993) were global-scale and extended further back in time than those in this study, yet the approach of geodynamic modelling in that study solved for buoyancy flux only, with no temperature variations and no lateral viscosity variations. The geodynamic models of Spasojevic and Gurnis (2012) were also global, but limited to the last 100 Myr because they combined forward models

with backward advection models based on mantle tomography; the latter of which have limited predictive power further back in geological time (Conrad and Gurnis, 2003). The dynamic models of Müller et al. (2018a) were global and time-dependent but limited to the last 140 Myr. Gurnis (1993) and Müller et al. (2018a) carried out a global and quantitative analysis considering continental flooding, eustatic sea level and dynamic topography. Spasojevic and Gurnis (2012) developed models to predict continental flooding globally, and identified which of dynamic topography or eustasy controlled the continental flooding of North America, Eurasia and Australia over the last 100 Myr. Here, we discuss the effects of eustasy and dynamic topography for North America and South America between 400-250 Ma.

4.5 Limitations, uncertainties and mismatches between geologic observations and dynamic topography models, and future work

4.5.1 Estimates of continental flooding

The estimates of flooded continental areas may vary when using different paleogeographic maps. To check whether other published paleogeographic maps produce different flooding histories, we calculated the flooding ratios of South America continent from the static paleogeographic maps of Scotese (2008, 2016) for the late Paleozoic using the same method as we did for the maps of Cao et al. (2017). The resulting flooding ratios indicated a persistent decrease of flooding from ~60% during the Early Devonian to ~13% during the late Permian, suggesting a first-order agreement with global sea level changes. The flooding ratios were always higher than our results except for the late Permian. However, it is unclear whether the paleogeographic maps of Scotese (2008, 2016) are independent from global sea level curves. The detailed regional paleo-environmental maps of South America built based on independent sedimentary records in the late Paleozoic (Limarino and Spalletti, 2006) indicate more similar flooding history to that recorded in the paleogeographic maps adopted here (Cao et al., 2017; Golonka et al., 2006). We used the maps of Golonka et al. (2006) as in Cao et al. (2017) because: (1) they are independent from eustatic sea level curves, (2) they are the only set of available digital global time-dependent paleogeographic maps covering the Paleozoic, (3) they have been tested and updated with the incorporation of new paleoenvironmental data sets (Cao et al., 2017) and hence may represent the most reliable late Paleozoic global paleogeography reconstructions. Incorporating with other geological data, such as stratigraphic data, paleoenvironment and paleo-lithofacies data to further constrain the paleogeographic reconstructions is needed (e.g. Wright et al., 2013; Cao et al., 2017). However, applying this approach to global-scale for deep geological times, it is time-consuming.

4.5.2 Uncertainty in mantle flow models

Uncertainties in our numerical mantle flow models primarily stem from the following sources: the initial conditions of the model, the assimilated tectonic reconstructions and the rheology of the mantle. Given that Flament (2018) has tested and discussed the sensitivities of the mantle flow models to the initial conditions, including boundary conditions and governing parameters, we herein briefly discuss this part. The amplitude of dynamic topography predicated by our global mantle flow models strongly depends on model setup and governing parameters (Flament et al., 2013; Flament, 2018), although it is demonstrated that paleogeographically-constrained mantle flow models compare well to time-dependent surface geological constraints (e.g. Flament et al., 2014, 2015). The predicted present-day mantle temperature can be compared to tomography models in order to test the predictive power of the forward mantle flow models (Zhong and Rudolph, 2015; Flament et al., 2017; Flament, 2018). However, the present-day structure of the

mantle is not very sensitive to plate motions before ~250−275 Myr ago because most subducted slabs likely sink down to core-mantle boundary in less than ~250−275 Myr (van der Meer et al., 2010; Butterworth et al., 2014). The adopted plate tectonic reconstructions as boundary conditions for mantle flow models are another source of uncertainty because the global plate tectonic reconstructions determine the location of past subduction systems and plate motion history, however, their paleogeographic coordinates especially paleo-longitudes are poorly constrained. While lateral viscosity variations are considered in the models, they are limited to three orders of magnitude, which is less than suggested by laboratory experiments (e.g. Karato and Wu, 1993). Achieving large viscosity contrasts in global time-dependent models of mantle flow remains a numerical challenge (e.g. Stadler et al., 2010).

5 Conclusions

The study combines geological observations, plate tectonic models and reconstructions of past mantle flow to provide insights into understanding the mechanisms of continental flooding and interactions between surface and deep Earth processes over geological time. We estimated the late Paleozoic marine inundation history of North America and South America individually, and all continents combined, from flexible time-varying paleogeographic reconstructions that are independent of eustatic sea level curves. We extracted dynamic topography for the continents from forward mantle flow models assimilating two distinct tectonic reconstructions as time-dependent boundary conditions. We compared the resulting continental flooding ratios with modelled dynamic topography and several published global long-term sea level curves. Our results indicate that the trend in global-scale flooding over the late Paleozoic generally correlates with global sea level curves. The first-order flooding history of North America correlates with global long-term sea level changes and dynamic topography can explain the second-order flooding low during the Pennsylvanian. The inundation history of South America does not follow long-term variations in global sea level. The flooding low in the Carboniferous and high in the Early Permian compared to global sea level changes can be accounted for by the dynamic uplift and subsidence predicted by mantle flow models during these times. Our global mantle flow models suggest that some estimates of global sea level changes might be affected by dynamic topography, while the eustatic low in the late Permian can be explained by dynamic topography. The reference district used to reconstruct late Paleozoic eustatic sea level changes which are most affected by dynamic topography is the Yangtze platform of South China for late Permian−earliest Triassic times. Some reference districts in North America are to some degree affected by mantle flow associated with the long-lived Panthalassa subduction zones, closure of Rheic Ocean and African upwellings. The interpretation of stratigraphic data gathered from these regions should be treated with caution when used to estimate global sea level variations.

Acknowledgments

W. Cao was supported by a University of Sydney International Scholarship (USydIS). N.F was supported by ARC grant DE160101020. R.D.M, S.Z. and S.W. were supported by ARC grant IH130200012. Figures were constructed using *Generic Mapping Tools* (Wessel and Smith, 1998; Wessel et al., 2013), *GPlates* (www.gplates.org) (Müller et al., 2018b) and *Python 2.0*. The *HEALPix* method (Górski et al. 2005) was used for calculation of areas of paleogeography. Mantle flow models and dynamic topography computations were carried out using resources from the National Computational Infrastructure (NCI), which is supported by the Australian Government.

Information about the supplement

We provide a figure showing global continental dynamic topography for late Paleozoic times in the mantle frame of reference for cases KM16 and AY18.

The Supplement related to this article can be found at http://portal.gplates.org/portal/dt/.

References

Algeo, T.J., Seslavinsky, K.B., 1995. Reconstructing eustatic and epeirogenic trends from Paleozoic continental flooding records. In: Haq, B.U. (Ed.), Sequence Stratigraphy and Depositional Response to Eustatic, Tectonic and Climatic Forcing. Kluwer, Dordrecht, pp. 209–246.

Blakey, R. C., 2003. Carboniferous Permian global paleogeography of the assembly of Pangaea, in: Fifteenth International Congress on Carboniferous and Permian Stratigraphy, edited by: Wong, T. E., Royal Netherlands Academy of Arts and Sciences, Utrecht, the Netherlands, 443–465.

Blakey, R. C., 2008. Gondwana paleogeography from assembly to breakup–A 500 m.y. odyssey, in: Resolving the Late Paleozoic Ice Age in Time and Space, edited by: Christopher R. Fielding, C. R., Frank, T. D., and Isbell, J. L., Geol. S. Am. S. 441, 1–28, https://doi.org/10.1130/2008.2441(01).

Bond, G.C., 1979. Evidence for some uplifts of large magnitude in continental platforms. Tectonophysics 61, 285–305. https://doi.org/10.1016/0040-1951(79)90302-0.

Bower, D.J., Gurnis, M., Flament, N., 2015. Assimilating lithosphere and slab history in 4-D Earth models. Phys. Earth Planet. Inter. 238, 8–22. https://doi.org/10.1016/j.pepi.2014.10.013

Butterworth, N.P., Talsma, A.S., Müller, R.D., Seton, M., Bunge, H.-P., Schuberth, B.S.A., Shephard, G.E., Heine, C., 2014. Geological, tomographic, kinematic and geodynamic constraints on the dynamics of sinking slabs. J. Geodyn. 73, 1–13. https://doi.org/10.1016/j.jog.2013.10.006.

Cao, X., Flament, N., Müller, D., Li, S., 2018. The dynamic topography of eastern China since the latest Jurassic Period. Tectonics 37, 1274–1291. https://doi.org/10.1029/2017TC004830.

Cao, W., Zahirovic, S., Flament, N., Williams, S.E., Golonka, J., Muller, R.D., 2017. Improving global paleogeography since the late Paleozoic using paleobiology. Biogeosciences 14, 5425–5439. https://doi.org/10.5194/bg-14-5425-2017.

Christensen, U.R., Yuen, D.A., 1985. Layered convection induced by phase transitions. J. Geophys. Res. Solid Earth 90, 10291–10300. https://doi.org/10.1029/JB090iB12p10291.

Cloetingh, S., Haq, B.U., 2015. Inherited landscapes and sea level change. Science 347 (6220). https://doi.org/10.1126/science.1258375.

Conrad, C.P., 2013. The solid Earth's influence on sea level. GSA Bulletin 125 (7-8), 1027–1052. https://doi.org/10.1130/B30764.1.

Conrad, C. P., Gurnis, M., 2003. Seismic tomography, surface uplift, and the breakup of Gondwanaland: Integrating mantle convection backwards in time, Geochem. Geophys. Geosyst. 4(3), 1031. doi:10.1029/2001GC000299.

Conrad, C.P., Husson, L., 2009. Influence of dynamic topography on sea level and its rate of change. Lithosphere 1, 110–120. https://doi.org/10.1130/L32.1.

DiMichele, W.A., Montañez, I.P., Poulsen, C.J., Tabor, N.J., 2009. Climate and vegetational regime shifts in the late Paleozoic ice age earth. Geobiology 7, 200–226. https://doi.org/10.1111/j.1472-4669.2009.00192.x.

Domeier, M., Torsvik, T.H., 2014. Plate tectonics in the late Paleozoic. Geosci. Front. 5 (3), 303–350. https://doi.org/10.1016/j.gsf.2014.01.002.

Flament. N., 2018. Present-day dynamic topography and lower mantle structure from paleogeographically-constrained mantle flow models. Geophysical Journal International ggy526, https://doi.org/10.1093/gji/ggy526.

Flament, N., Gurnis, M., Müller, R.D., 2013. A review of observations and models of

dynamic topography. Lithosphere 5 (2), 189–210. https://doi.org/10.1130/L245.1.

Flament, N., Gurnis, M., Müller, R.D., Bower, D.J., Husson, L., 2015. Influence of subduction history on South American topography. Earth Planet. Sci. Lett. 430, 9–18. http://dx.doi.org/10.1016/j.epsl.2015.08.006.

Flament, N., Gurnis, M., Williams, S., Seton, M., Skogseid, J., Heine, C., Müller, R.D., 2014. Topographic asymmetry of the South Atlantic from global models of mantle flow and lithospheric stretching. Earth Planet. Sci. Lett. 387, 107–119. https://doi.org/10.1016/j.epsl.2013.11.017.

Flament, N., Williams, S., Müller, R.D., Gurnis, M., Bower, D.J., 2017. Origin and evolution of the deep thermochemical structure beneath Eurasia. Nat. Commun. 8, 14164. https://doi.org/10.1038/ncomms14164.

Golonka, J., Krobicki, M., Pajak, J., Nguyen, V.G., Zuchiewicz, W., 2006. Global plate tectonics and paleogeography of Southeast Asia. Fac. Geol. Geophys. Environ. Prot. AGH Univ. Sci. Technol. Arkadia, Krakow, Pol.

Górski, K.M., Hivon, E., Banday, A.J., Wandelt, B.D., Hansen, F.K., Reinecke, M., Bartelmann, M., 2005. HEALPix: A framework for high-resolution discretization and fast analysis of data distributed on the sphere. Astrophys. J. 622, 759-771.

Guillaume, B., Pochat, S., Monteux, J., Husson, L., Choblet, G., 2016. Can eustatic charts go beyond first order? Insights from the Permian–Triassic. Lithosphere 8, 505–518. https://doi.org/10.1130/L523.1.

Gurnis, M., 1990. Ridge spreading, subduction, and sea level fluctuations. Science 250 (4983), 970–972. DOI: 10.1126/science.250.4983.970.

Gurnis, M., 1993. Phanerozoic narine inundation of continent driven by dynamic topography above subducting slabs. Nature 364, 590–593. https://doi.org/10.1038/364589a0.

Gurnis, M., Turner, M., Zahirovic, S., DiCaprio, L., Spasojevic, S., Müller, R.D., Boyden, J., Seton, M., Manea, V.C., Bower, D.J., 2012. Plate tectonic reconstructions with continuously closing plates. Comput. Geosci. 38, 35–42.

Hallam, A., 1984. Pre-Quaternary sea-level changes. Annu. Rev. Earth Planet. Sci. 12, 205–243.

Hallam, A., 1992. Phanerozoic sea-level changes. Columbia University Press.

Haq, B.U., 2014. Cretaceous eustasy revisited. Global and Planetary Change 113, 44–58. https://doi.org/10.1016/j.gloplacha.2013.12.007.

Haq, B.U., Al-Qatani, a. M., 2005. Phanerozoic cycles of sea-level change on the Arabian Platform. GeoArabia 10 (2), pp. 127-160. DOI: 10.1126/science.116164.

Haq, B.U., Hardenbol, J., Vail, P., 1987. Chronology opf fluctuating sea levels since the Triassic. Science, 235, 1156–1167. https://doi.org/10.1126/science.235.4793.1156.

Haq, B.U., Schutter, S.R., 2008. A chronology of Paleozoic sea-level changes. Science 322 (5898), 64–68. DOI: 10.1126/science.1161648.

Harrison, C.G.A., Brass, G.W., Saltzman, E., Sloan Ii, J., Southam, J., Whitman, J.M., 1981. Sea level variations, global sedimentation rates and the hypsographic curve. Earth Planet. Sci. Lett. 54 (1), 1–16. doi.org/10.1016/0012-821X(81)90064-9.

Hassan, R., Flament, N., Gurnis, M., Bower, D.J., Müller, D., 2015. Provenance of plumes in global convection models. Geochemistry, Geophys. Geosystems 16, 1465–1489. doi.org/10.1002/2015GC005751.

Hassan, R., Müller, R.D., Gurnis, M., Williams, S.E., Flament, N., 2016. A rapid burst in hotspot motion through the interaction of tectonics and deep mantle flow. Nature 533, 239. doi:10.1038/nature17422.

Karato, S., Wu, P., 1993. Rheology of the upper mantle: A synthesis. Science 260 (5109), 771–778. DOI: 10.1126/science.260.5109.771.

Kominz, M.A., Browning, J. V., Miller, K.G., Sugarman, P.J., Mizintseva, S., Scotese, C.R., 2008. Late Cretaceous to Miocene sea-level estimates from the New Jersey and Delaware coastal plain coreholes: An error analysis. Basin Res. 20, 211–226. https://doi.org/10.1111/j.1365-2117.2008.00354.x.

Limarino, C.O., Spalletti, L.A., 2006. Paleogeography of the upper Paleozoic basins of southern South America: An overview. J. South Am. Earth Sci. 22 (3-4), 134–155. https://doi.org/10.1016/j.jsames.2006.09.011.

Liu, L., Spasojević, S., Gurnis, M., 2008. Reconstructing Farallon plate subduction beneath North America back to the Late Cretaceous. Science 322 (5903), 934–938. DOI: 10.1126/science.1162921.

Matthews, K.J., Maloney, K.T., Zahirovic, S., Williams, S.E., Seton, M., Mueller, R.D., 2016. Global plate boundary evolution and kinematics since the late Paleozoic. Glob. Planet. Change 146, 226–250. https://doi.org/10.1016/j.gloplacha.2016.10.002.

Miller, K.G., Kominz, M.A., Browning, J. V., Wright, J.D., Mountain, G.S., Katz, M.E., Sugarman, P.J., Cramer, B.S., Christie-Blick, N., Pekar, S.F., 2005. The phanerozoic record of global sea-level change. Science 310, 1293–1298. https://doi.org/10.1126/science.1116412.

Mitrovica, J.X., Beaumont, C., Jarvis, G.T., 1989. Tilting of continental interiors by dynamical effects of subduction. Tectonics 8, 1079–1094. https://doi.org/10.1029/TC008i005p01079.

Moucha, R., Forte, A.M., Mitrovica, J.X., Rowley, D.B., Quéré, S., Simmons, N.A., Grand, S.P., 2008. Dynamic topography and long-term sea-level variations : There is no such thing as a stable continental platform. Earth and Planetary Science Letters 271 (1-4), 101–108. https://doi.org/10.1016/j.epsl.2008.03.056

Müller, R.D., Cannon, J., Qin, X., Watson, R.J., Gurnis, M., Williams, S., Pfaffelmoser, T., Seton, M., Russell, S.H.J., Zahirovic, S., 2018b. GPlates–Building a Virtual Earth Through Deep Time. Geochemistry, Geophys. Geosystems. 19, 2243-2261. https://doi.org/10.1029/2018GC007584.

Müller, R.D., Hassan, R., Gurnis, M., Flament, N., Williams, S.E., 2018a. Dynamic topography of passive continental margins and their hinterlands since the Cretaceous. Gondwana Res. 53, 225–251. https://doi.org/10.1016/j.gr.2017.04.028.

Müller, R.D., Sdrolias, M., Gaina, C., Steinberger, B., Heine, C., 2008. Long-term sea-level fluctuations driven by ocean basin dynamics. Science 319 (5868), 1357–1362. DOI: 10.1126/science.1151540.

Müller, R.D., Seton, M., Zahirovic, S., Williams, S.E., Matthews, K.J., Wright, N.M., Shephard, G.E., Maloney, K.T., Barnett-Moore, N., Hosseinpour, M., 2016. Ocean basin evolution and global-scale plate reorganization events since Pangea breakup. Annu. Rev. Earth Planet. Sci. 44, 107–138. 10.1146/annurev-earth-060115-012211.

Munnecke, A., Calner, M., Harper, D.A.T., Servais, T., 2010. Ordovician and Silurian sea–water chemistry, sea level, and climate: a synopsis. Palaeogeogr. Palaeoclimatol. Palaeoecol. 296 (3-4), 389–413. https://doi.org/10.1016/j.palaeo.2010.08.001.

Ronov, A.B., 1994. Phanerozoic transgressions and regressions on the continents: a quantitative approach based on areas flooded by the sea and areas of marine and continental deposition. Am. J. Sci. 294, 777-801. https://doi.org/10.2475/ajs.294.7.777.

Scotese, C.R., 2008. The PALEOMAP Project PaleoAtlas for ArcGIS, v.1, Volume 4, Late Paleozoic Paleogeographic, Paleoclimatic, and Plate Tectonic Reconstructions, PALEOMAP Project, Arlington, Texas.

Scotese, C.R., 2016. PALEOMAP PaleoAtlas for GPlates and the PaleoData Plotter Program, PALEOMAP Project. http://www.earthbyte.org/paleomapA paleoatlasAforAgplates/.

Shephard, G.E., Flament, N., Williams, S., Seton, M., Gurnis, M., Müller, R.D., 2014. Circum-Arctic mantle structure and long-wavelength topography since the Jurassic. J. Geophys. Res. Solid Earth 119, 7889–7908. https://doi.org/10.1002/2014JB011078.

Snedden, J.W., Liu, C., 2010. A compilation of Phanerozoic sea-level change, coastal onlaps and recommended sequence designations. Search and Discovery Article 40594.

Spasojevic, S., Gurnis, M., 2012. Sea level and vertical motion of continents from dynamic earth models since the Late Cretaceous. AAPG Bulletin 96, 2037–2064.

https://doi.org/10.1306/03261211121.
Stadler, G., Gurnis, M., Burstedde, C., Wilcox, L.C., Alisic, L., Ghattas, O., 2010. The dynamics of plate tectonics and mantle flow: from local to global scales. Science 329, 1033-1038. DOI: 10.1126/science.1191223.
Torsvik, T.H., Van der Voo, R., 2002. Refining Gondwana and Pangea palaeogeography: Estimates of Phanerozoic non-dipole (octupole) fields. Geophys. J. Int. 151, 771–794. https://doi.org/10.1046/j.1365-246X.2002.01799.x.
Torsvik, T.H., Van der Voo, R., Preeden, U., Mac Niocaill, C., Steinberger, B., Doubrovine, P. V, van Hinsbergen, D.J.J., Domeier, M., Gaina, C., Tohver, E., 2012. Phanerozoic polar wander, palaeogeography and dynamics. Earth-Science Rev. 114 (3-4), 325–368. https://doi.org/10.1016/j.earscirev.2012.06.007.
Vail, P.R., Mitchum, R.M., Thompson, S., 1977, Seismic stratigraphy and global changes of sea level: Part 4. Global cycles of relative changes of sea level, in Payton, C.E., ed., Seismic Stratigraphy: Applications to Hydrocarbon Exploration: American Association of Petroleum Geologists Memoir 26, p. 83–97.
van Der Meer, D.G., Spakman, W., Van Hinsbergen, D.J.J., Amaru, M.L., Torsvik, T.H., 2010. Towards absolute plate motions constrained by lower-mantle slab remnants. Nat. Geosci. 3, 36. https://doi.org/10.1038/ngeo708.
Walker, L.J., Wilkinson, B.H., Ivany, L.C., 2002. Continental Drift and Phanerozoic Carbonate Accumulation in Shallow-Shelf and Deep-Marine Settings. The Journal of Geology 110, 75–87. https://doi.org/10.1086/324318.
Wessel, P., W. H. Smith, 1998. New, improved version of Generic Mapping Tools released. Eos, Trans. Am. Geophys. Union n 79(47), 579–579. doi:10.1029/98EO00426.
Wessel, P., W. H. Smith, R. Scharroo, J. Luis, F. Wobbe, 2013. Generic Mapping Tools: Improved version released. Eos, Trans. Am. Geophys. Union 94(45), 409–410. doi:10.1002/2013EO450001.
Worsley, T.R., Nance, D., Moody, J.B., 1984. Global tectonics and eustasy for the past 2 billion years. Mar. Geol. 58 (3-4), 373–400. https://doi.org/10.1016/0025-3227(84)90209-3.
Wright, N., Zahirovic, S., Müller, R.D., Seton, M., 2013. Towards community-driven paleogeographic reconstructions: integrating open-access paleogeographic and paleobiology data with plate tectonics. Biogeosciences 10, 1529–1541. doi:10.5194/bg-10-1529-2013.
Young, A., Flament, N., Maloney, K., Williams, S., Matthews, K., Zahirovic, S., Müller, R.D., 2018. Global kinematics of tectonic plates and subduction zones since the late Paleozoic Era. Geosci. Front. In press. https://doi.org/10.1016/j.gsf.2018.05.011.
Zhang, N., Zhong, S., Flowers, R.M., 2012. Predicting and testing continental vertical motion histories since the Paleozoic. Earth Planet. Sci. Lett. 317–318, 426–435. https://doi.org/10.1016/j.epsl.2011.10.041.
Zhong, S., McNamara, A., Tan, E., Moresi, L., Gurnis, M., 2008. A benchmark study on mantle convection in a 3-D spherical shell using CitcomS. Geochemistry, Geophys. Geosystems 9, 1–32. https://doi.org/10.1029/2008GC002048.
Zhong, S., Rudolph, M.L., 2015. On the temporal evolution of long-wavelength mantle structure of the Earth since the early Paleozoic. Geochemistry, Geophys. Geosystems 16, 1599–1615. https://doi.org/10.1002/2015GC005782.
Zhong, S., Zuber, M.T., Moresi, L., Gurnis, M., 2000. Role of temperature-dependent viscosity and surface plates in spherical shell models of mantle convection. J. Geophys. Res. Solid Earth 105, 11063–11082. https://doi.org/10.1029/2000JB900003.

Discussion

1. Reconstructing digital global paleogeography

Global paleogeographic reconstructions have been built commonly using paleoenvironmental and paleo-lithofacies data (Ronov, et al., 1984, 1989; Smith et al., 1994; Scotese, 2001, 2004; Golonka et al., 2006; Blakey, 2008). My digital global paleogeographic reconstructions since the late Paleozoic were built on the set of published paleogeographic maps of Golonka et al. (2006). However, due to the lack of geological data especially in deeper geological time, the paleogeography in the areas with no/poor data coverage were interpolated using neighbouring environments (Golonka et al., 2007b, 2009, 2012). Incorporation of paleoenvironmental data indicated by the marine fossil collections from the PBDB in my study provided more constraints for the paleogeographic reconstructions. However, due to the potential uncertainties of the ages of the fossil data in the PBDB, a comprehensive evaluation of the PBDB records and the original paleogeographic compilations is recommended.

It remains challenging to determine the accurate locations of paleo-coastlines due to frequent transgressions and regressions resulting from sea level changes. However, the maximum transgression surface during a given time period can be relatively precisely determined, therefore, the paleo-coastlines in the original paleogeographic maps of Golonka et al. (2006) represent maximum transgression surfaces. As a consequence, I only considered marine fossil collections from the PBDB to improve the maximum transgression surfaces and paleogeography, because terrestrial fossils were not helpful in this case. Therefore, the calculated continental flooding ratios from these maps represent maximum flooding histories.

Although the consistencies between the paleogeography and the paleo-environments indicated by the marine fossil collections were significantly improved (average 75% to nearly 100%), the regions for which the paleogeographic reconstructions were modified were mainly in North America, South America, Europe and Africa for Late Carboniferous, Middle Permian, Triassic, Jurassic, Late Cretaceous and most of Cenozoic times. The spatial coverage of fossil data points was still very heterogeneous, with relatively few data points across large areas of the globe for some time periods. Therefore, it is important to combine other geological data, such as stratigraphic data from regional seismic interpretations constrained by well log data, the StratDB Database (http://sil.usask.ca), Macrostrat Database (https://macrostrat.org/) and other sources of paleoenvironmental and paleo-lithofacies data, to further constrain the paleogeographic reconstructions. However, it should be noted that paleogeographic reconstructions that incorporate various geological records and interpretations of records may lead to circularity of predictions. Bayesian paleogeographic reconstructions, which could be developed and tested in the future, would circumvent the circularity.

It should be pointed out that in the Article 2, I described the temporal variation in the distribution of continental area with respect to latitude as a bias. However, given that the total area of Earth at each band of latitude also varies through time, the distribution of continents with respect to latitude is not strictly a bias. Therefore, I suggest to use “normalize” instead of “bias” to describe the data processing step, that is, we normalized climate sensitive sediment frequency by continental area while also compensating for the sampling bias introduced by non-random sampling.

In the Article 2, the reconstructions used to analyse paleolatitudinal distributions of lithologies were built mainly based on

paleomagnetic data (i.e. Domeier and Torsvik, 2014; Torsvik and Voo, 2002). However, the reconstruction of Domeier and Torsvik (2014) used fossil data and lithologies as part of the reconstruction process. Therefore, there is some circularity. Ideally, paleomagnetic data should be exclusively used in the reconstructions to avoid such circularity, but this is difficult due to the limited information content in paleomagnetic data to simultaneously constrain relative and absolute plate motions.

2. Importance of digital time-dependent paleogeographic reconstructions

Digital paleogeographic reconstructions are important because they can be linked to other plate tectonic reconstructions and can be tested and expended with incorporation of new data sets (Wright et al., 2013 and Article 1). I made all my digital global paleogeographic maps since the late Paleozoic at both present-day and reconstructed coordinates freely available. They can be attached to different digital plate tectonic reconstructions and be updated when plate motion models are improved, with wider implications for understanding Earth's paleotopography, paleoclimate and ocean circulation, biological radiation and mass extinctions, resource exploration and the role of mantle convection in shaping long-wavelength topography.

Paleogeography can be converted into paleotopography which can be an important initial condition for climate modelling (Salles et al., 2017). Several methods have been attempted to reconstruct paleotopography from paleogeography (e.g. Ziegler et al., 1985; Scotese, 2002; Herold et al., 2008; Verard et al., 2015). In these methods, correlations between paleoenvironments and paleo-elevations are used to estimate paleo-elevations, and relationships between seafloor depth and age are used to estimate paleobathymetry. My paleogeographic maps are the only set of available digital global time-dependent paleogeographic reconstructions extending back to the late Paleozoic. Although global-scale paleotopography reconstructions for the Phanerozoic exist (e.g. Scotese, 2018), they are generally presented as static paleotopographic maps with specific map projections and are tied to different plate motion models. My digital time-dependent paleogeographic reconstructions provide the opportunity for researchers to build flexible paleotopographic reconstructions over deep time using the methods outlined above. Paleobathymetry in deep time is entirely based on synthetic models since no seafloor older than ~200 Ma is preserved (Müller et al., 2008).

3. Combining digital paleogeographic reconstructions, geological databases, plate tectonic reconstructions and mantle flow models

Combining digital global paleogeographic reconstructions, geological observations, plate tectonic reconstructions and mantle flow models can provide insights into understanding mechanisms of continental inundation and distinguishing global or regional sea level change over time. My study (see Article 3) primarily focused on the North and South America continents during the late Paleozoic, as alternative plate reconstructions in these regions result in distinct dynamic topography histories, which can be tested against the geological record of continental flooding. Advances in global plate kinematic models during the Neoproterozoic (e.g., Merdith et al., 2017) make it possible for researchers to extend this approach to Neoproterozoic times in the future by combining paleogeographic reconstructions, eustatic sea level curves and mantle flow models during these times.

4. Future work

Paleogeography plays an important role in understanding the interplay of eustasy and dynamic topography in driving continental flooding. Improving paleogeographic reconstructions by combining other stratigraphic, paleoenvironmental and paleo-lithofacies data is of great importance.

The workflow I developed in Article 1 is useful but some steps are presently still laborious and time-consuming, mainly relating to manual fixes of gaps and overlaps resulting from transferring paleogeographic geometries to a different reconstruction, and to manual modifications of the paleo-coastlines and paleogeographic geometries based on the PBDB test. These steps could be automated in future work.

Climate modelling and landscape evolution modelling require initial topography conditions (e.g., Crowley and Baum, 1992; Goddéris et al., 2014), in addition to other boundary conditions and model parameters such as precipitation, erodibility, sea level variations and dynamic topography magnitude (e.g. Salles et al., 2017). My digital time-dependent global paleogeographic reconstructions could be converted into time-dependent global paleotopography as initial conditions for global/regional modelling of climate and landscape evolution through deep time. However, significant effort is needed to define more detailed type classification for shallow marine environments, land and mountains; each of these environments are not further classified in my paleogeographic reconstructions. A more refined classification of these paleo-environments will be important for providing more precise paleogeographic constraints for studies in diversity and evolution of shallow-sea lives, paleoecology, basin evolution and biogeography (e.g. Pimiento et al., 2016, 2017; Dunhill et al., 2016).

The global sediment data set including coals, evaporites and glacial deposits used in Article 2 can be used to estimate the past climate conditions such as precipitation and rainfall over deep time (Boucot et al., 2013). These estimates can provide constraints to the initial conditions for climate modelling and surface processes' modelling in order to build more robust models. The chemical compositions of these sediments are also thought to be proxies of past climate (e.g. Zigler and Nilsen, 1984; Kump et al., 2000; Warren, 2010; Bahlburg and Dobrzinski, 2011). Comprehensive data gathering and detailed analysis of the geochemistry information recorded in these sediments are needed.

The net rotation of Earth's lithosphere with respect to the underlying mantle is the longest wavelength component of toroidal flow in the mantle and is thought to only be generated in buoyancy driven flows in the presence of lateral viscosity variations (Rudolph and Zhong, 2014). Mantle convection models by Rudolph and Zhong (2014) demonstrated that the differential rotation between the lithosphere and lower mantle induced by plate motions for a plate reconstruction using a hotspot reference frame for the past 100 Myr was significantly larger than the present-day rate of lithospheric net rotation. I investigated two convection models based on two different plate reconstructions (Matthews et al., 2016; Young et al., 2018) as time-dependent surface boundary conditions. The differential rotation between the lithosphere and lower mantle induced by plate motions for each of these two reconstructions remains to be analysed.

Conclusion

This thesis consists of three interrelated studies which together demonstrate that combining digital paleogeographic reconstructions, geological observations, plate tectonic motion models and reconstructions of past mantle flow provides insights into understanding the interaction between surface and deep Earth processes over geological time.

I developed a workflow that can transfer paleogeographic geometries from one plate motion model to another and then using paleoenvironmental information indicated by marine fossil collections from the PBDB to improve the paleo-coastline locations and paleogeographic geometries. This workflow can be applied to other paleogeographic maps. Using this approach, the consistency ratio between the paleogeography and the paleoenvironments as indicated by the marine fossil collections is increased from an average of 75% to nearly full consistency.

I investigated the shifting climatic zones for the last ~400 Myr using a comprehensive database of climate lithologies, plate tectonic reconstructions and novel data analysis approaches. The results suggest that the paleolatitudinal distributions of lithologies have changed through deep geological time, notably a pronounced poleward shift in the distribution of coals at the beginning of the Permian. The distribution of evaporites indicates a clearly bimodal distribution over the past ~400 Myr, as opposed to the previously proposed bimodal or unimodal evaporite patterns. The distribution of glacial deposits is consistent with previous interpretations of the main icehouse and greenhouse periods during the last ~400 Myr.

The comparison between flooding of continents, modelled dynamic topography and published long-term sea level curves indicates that the first-order flooding inundation of North America in the late Paleozoic correlates with eustasy. The flooding lows during the Early Carboniferous and high during the Late Carboniferous for South America are at odds with estimates of eustasy and can be explained by dynamic uplift and subsidence, respectively. Dynamic topography evolution of the reference districts that were used to reconstruct eustatic curves shows that the reference districts in South China and North America were likely affected by mantle flow more than other districts. Dynamic topography should be considered to better understand relative and eustatic sea level changes in the Paleozoic, and for selection of reference districts to build eustatic sea level curves.

References

Bahlburg, H., Dobrzinski, N., 2011. A review of the Chemical Index of Alteration (CIA) and its application to the study of Neoproterozoic glacial deposits and climate transitions. Geol. Soc. London, Mem. 36, 81–92.

Crowley, T.J., Baum, S.K., 1992. Modeling late Paleozoic glaciation. Geology 20, 507–510.

Dunhill, A.M., Bestwick, J., Narey, H., Sciberras, J., 2016. Dinosaur biogeographical structure and Mesozoic continental fragmentation: a network-based approach. J. Biogeogr. 43, 1691–1704.

Goddéris, Y., Donnadieu, Y., Le Hir, G., Lefebvre, V., Nardin, E., 2014. The role of palaeogeography in the Phanerozoic history of atmospheric CO_2 and climate. Earth-Science Rev. 128, 122–138.

Herold, N., Huber, M., Müller, R.D., 2011. Modeling the Miocene climatic optimum. Part I: Land and atmosphere. J. Clim. 24, 6353–6372.

Herold, N., Seton, M., Müller, R.D., You, Y., Huber, M., 2008. Middle Miocene tectonic boundary conditions for use in climate models. Geochem. Geophys. Geosyst. 9, Q10009.

Kump, L.R., Brantley, S.L., Arthur, M.A., 2000. Chemical weathering, atmospheric CO2, and climate. Annu. Rev. Earth Planet. Sci. 28, 611–667.

Merdith, A.S., Collins, A.S., Williams, S.E., Pisarevsky, S., Foden, J.D., Archibald, D.B., Blades, M.L., Alessio, B.L., Armistead, S., Plavsa, D., 2017. A full-plate global reconstruction of the Neoproterozoic. Gondwana Res. 50, 84–134.

Müller, R.D., Sdrolias, M., Gaina, C., Roest, W.R., 2008. Age, spreading rates, and spreading asymmetry of the world's ocean crust. Geochem. Geophys. Geosyst. 9, Q04006.

Pimiento, C., Griffin, J.N., Clements, C.F., Silvestro, D., Varela, S., Uhen, M.D., Jaramillo, C., 2017. The Pliocene marine megafauna extinction and its impact on functional diversity. Nat. Ecol. Evol. 1, 1100–1106.

Pimiento, C., MacFadden, B.J., Clements, C.F., Varela, S., Jaramillo, C., Velez-Juarbe, J., Silliman, B.R., 2016. Geographical distribution patterns of Carcharocles megalodon over time reveal clues about extinction mechanisms. J. Biogeogr. 43, 1645–1655.

Rudolph, M.L., Zhong, S.J., 2014. History and dynamics of net rotation of the mantle and lithosphere. Geochem. Geophys. Geosyst. 15, 1–13.

Salles, T., Flament, N., Müller, D., 2017. Influence of mantle flow on the drainage of eastern Australia since the Jurassic Period. Geochemistry, Geophys. Geosystems 18, 280–305.

Scotese, C.R., 2002. 3D paleogeographic and plate tectonic reconstructions: The PALEOMAP Project is back in town. Houston Geological Society Bulletin 44, 13–15.

Scotese, C.R., Wright, N., 2018. PALEOMAP Paleodigital Elevation Models (PaleoDEMS) for the Phanerozoic PALEOMAP Project. https://www.earthbyte.org/paleodem-resource-scotese-and-wright-2018/.

Vérard, C., Hochard, C., Baumgartner, P.O., Stampfli, G.M., Liu, M., 2015. 3D palaeogeographic reconstructions of the Phanerozoic versus sea-level and Sr-ratio variations. J. Palaeogeogr. 4, 64–84.

Ziegler, A.M., Rowley, D.B., Lottes, A.L., Sahagian, D.L., Hulver, M.L., Gierlowski, T.C., 1985. Paleogeographic interpretation: with an example from the mid-Cretaceous. Annu. Rev. Earth Planet. Sci. 13, 385–428.

Zigler, J.L., Nilsen, T.H., 1984. Geochemistry of Coal from the Ditch Creek Siltstone Member of the Hornbrook Formation, Northern California. Pacific Section SEPM 42, 123–127.

Supplement for Article 1

Improving global paleogeography since the late Paleozoic using paleobiology

Wenchao Cao, Sabin Zahirovic, Nicolas Flament, Simon Williams, Jan Golonka, and R. Dietmar Müller

Correspondence to: Wenchao Cao (wenchao.cao@sydney.edu.au)

I provide two sets of digital global paleogeographic maps during 402-2 Ma: the paleogeography reconstructed using the plate motion model of Matthews et al., (2016) and revised using paleo-environmental information indicated by the marine fossil collections from the PBDB and the original paleogeography of Golonka et al. (2006), an original rotation file of Golonka et al. (2006), a set of paleogeographic maps illustrating the PBDB test and revision of paleo-coastlines and paleogeographic geometries, a set of GeoTiff files of all revised paleogeographic maps, paleobiology data in shapefile format used in this study separated into two sets of consistent marine fossil collections and inconsistent marine fossil collections, an animation for the revised global paleogeographic maps, and a README file outlined the workflow of this study. All supplementary material can be downloaded from the link (*https://www.dropbox.com/s/pwlygntz5mgria5/bg-2017-94-supplement.zip*).

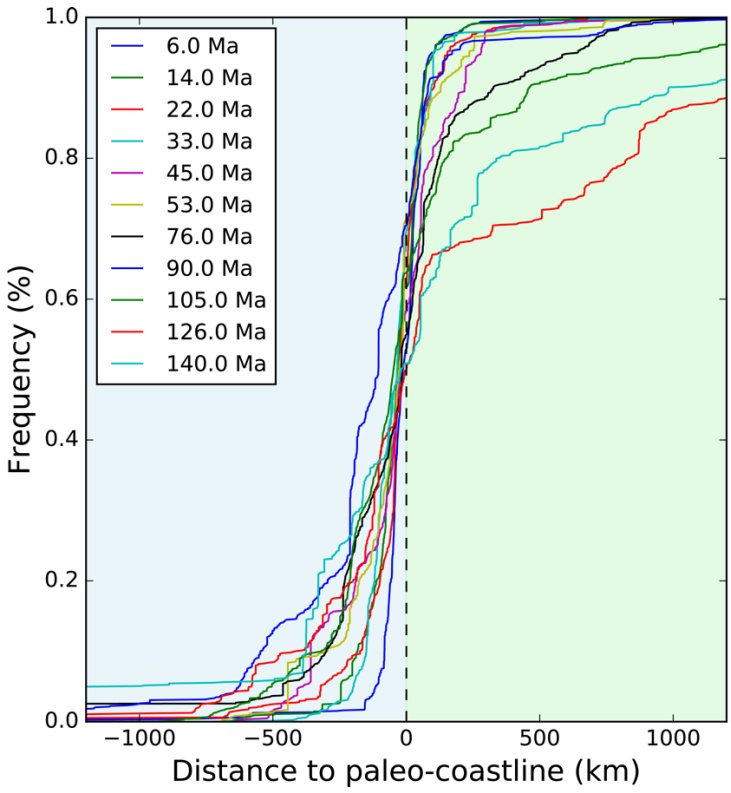

Figure S1. Cumulative frequency of the distance of the marine fossil collections from PBDB to paleo-coastlines derived from the paleogeographic maps of Golonka et al. (2006) since the Cretaceous period. Note that fossil collections located more than ~500 km away from paleocoastlines represent outliers of their distribution.

Supplement for Article 2

Paleolatitudinal distribution of lithologic indicators of climate in a paleogeographic framework

Wenchao Cao, Simon Williams, Nicolas Flament, Sabin Zahirovic, Christopher Scotese, and R. Dietmar Müller

Correspondence to: Wenchao Cao (wenchao.cao@sydney.edu.au)

I provide the lithologic data of coals, evaporites and glacial deposits in shapefile format, three reconstruction models used in this study and an animation demonstrating these three models since the Devonian period, and a PDF file containing two supplementary figures. All the files can be downloaded from the link *https://www.dropbox.com/sh/x1d00ooxu5tikrh/AADq_LsQcX9khzW16EPUbeO6a*. The original lithologic data in tabular format can be found from the link *https://www.researchgate.net/publication/263450893_Phanerozoic_Paleoclimate_An_Atlas_of_Lithologic_Indicators_of_Climate*.

Supplement for Article 3

The interplay of dynamic topography and eustasy on continental flooding in the late Paleozoic

Wenchao Cao, Nicolas Flament, Sabin Zahirovic, Simon Williams and R. Dietmar Müller
Correspondence to: Wenchao Cao (wcao3204@uni.sydney.edu.au)

I provide all the grids of the global continental dynamic topography models in both mantle reference frame and plate reference frame for cases KM16 and AY18. They can be found at http://portal.gplates.org/portal/dt/.